TRIBHUVAN UNIVERSITY

INSTITUTE OF ENGINEERING

PULCHOWK CAMPUS

THESIS NO : M-91-MSMDE-2023-2025

Computational Characteristics of Hydrogen Gas Combustion in Homogeneous Charge Compression Ignition Engine

by

Ghanshyam Aryal

A THESIS

SUBMITTED TO THE DEPARTMENT OF MECHANICAL AND AEROSPACE ENGINEERING IN PARTIAL FULFILLMENT OF THE REQUIREMENTS FOR THE DEGREE OF MASTER OF SCIENCE IN MECHANICAL SYSTEM DESIGN AND ENGINEERING

DEPARTMENT OF MECHANICAL AND AEROSPACE ENGINEERING

LALITPUR, NEPAL

April 18, 2025

COPYRIGHT

TRIBHUVAN UNIVERSITY

INSTITUTE OF ENGINEERING

PULCHOWK CAMPUS

DEPARTMENT OF MECHANICAL AND AEROSPACE ENGINEERING

The undersigned certify that they have read, and recommended to the Institute of Engineering for acceptance, a thesis entitled **"Computational Characteristics of Hydrogen Gas Combustion in Homogeneous Charge Compression Ignition Engine"** submitted by **Ghanshyam Aryal (079MSMDE009)** in partial fulfillment of the requirement for the degree of Master of Science in Mechanical Systems Design and Engineering.

Prof. Dr. Laxman Poudel
Supervisor,
Department of Mechanical and Aerospace Engineering

Asst. Prof. Sudip Bhattrai, Ph.D.
Supervisor,
Department of Mechanical and Aerospace Engineering

Er. Nabin Kumar Shrestha
External Examiner,
Chief Executive Officer,
Precise Hydro Engineering & Construction Pvt. Ltd.,
Tripureshwor, Kathmandu

Tribhuvan University
Institute of Engineering
Department of Mechanical and Aerospace Engineering
Pulchowk Campus

Committee Chairperson,
Asst. Prof. Dr. Sudip Bhattrai
Head of Department,
Department of Mechanical and Aerospace Engineering

Date: April 7, 2025

ABSTRACT

With the trend of limiting carbon emissions, hydrogen gas can be a possible fuel for internal combustion engine to run the transport industry. A 3-dimensional CFD simulation is performed in OpenFoam (Open Field Operation And Manipulation) using engineFoam solver. Turbulence model, combustion model and detailed reaction mechanism are included in this simulation to observe realistic behavior of H_2 gas combustion in internal combustion engine. This work investigates premixed H_2 gas combustion under HCCI environment where premixed H_2 fuel mixture is auto-ignited as temperature surpasses auto-ignition temperature of the fuel mixture during compression stroke. The simulation work is observed between beginning of compression stroke to the end of expansion stroke. Although, pressure and temperature both increases adiabatically during compression stroke, it is unable to ignite the H_2 fuel mixture because of high auto-ignition temperature. As a result, preheating of the H_2 fuel mixture is necessary to achieve H_2 gas combustion near TDC. The variation of mean in-cylinder pressure and temperature against crank angle displacement presents the discontinuities in mean pressure and temperature when the piston is about -10°ATDC because of ignition of premixed mixture at multiple points. Because of reaction, enormous amount of heat is released. As a result, temperature increases which further drives the reaction step forward resulting in further increment in temperature and pressure. The peak mean in-cylinder pressure and temperature for premixed hydrogen fuel is studied for varying value of equivalence ratios which shows peak in-cylinder pressure and temperature also increases with increase in value of equivalence ratios. However, the heat of reaction for premixed H_2 fuel decreases with increase in value of equivalence ratios after one because more fuel is available resulting in incomplete combustion as most of the O_2 is utilized. Furthermore, with increase in engine rpm, the ignition delay period increases as shorter residence time is available for the reacting species. Yet, the peak mean in-cylinder pressure & temperature increases at higher rpm because of faster combustion. On further comparison of mean in-cylinder pressure and temperature between hydrogen and heptane fuel at stoichiometric conditions, it shows significant variation because of one-step reaction mechanism consideration for heptane fuel which oversimplifies the complex chemical and physical process involved.

Keywords: Internal combustion engine, Crank angle displacement, Homogeneous charge compression ignition, Top dead center, Bottom dead center.

ACKNOWLEDGEMENT

The journey of completing this thesis has been one of perseverance, growth, and discovery, and it would not have been possible without the support and encouragement of many individuals.

First and foremost, I extend my deepest gratitude to my supervisors, Prof. Dr. Laxman Poudel and Asst. Prof. Dr. Sudip Bhattrai, whose wisdom, patience, and unwavering support have guided me through every challenge. Their insightful feedback and encouragement have not only refined my research but also shaped my perspective on academic inquiry. I am truly fortunate to have had their mentorship.

I am also profoundly grateful to Department of Mechanical and Aerospace Engineering for providing the resources and a simulation research environment that enabled me to pursue this study. A special appreciation goes to Er. Salim Maharjan, Er. Akin Chhetri and Er. Sandip Gewali whose collaboration, stimulating discussions have enriched my academic research beyond measure.

I also wish to acknowledge Er. Nischal Poudel for his generous support during simulation work.

This thesis is not merely the result of individual effort but a reflection of the collective contributions of those who have supported, inspired, and believed in me. Furthermore, I am very grateful to the classmates of MSMDE batch 2079 for making academic journey, enriching and enjoyable.

CONTENTS

ABSTRACT iii

ACKNOWLEDGEMENT iv

LIST OF FIGURES ix

LIST OF TABLES xi

LIST OF SYMBOLS xii

LIST OF ABBREVIATIONS xvi

1 INTRODUCTION 1

1.1 Background 1

1.1.1 Structure of the IC engine 1

1.1.2 Homogeneous Charge Compression Ignition (HCCI) 2

1.1.3 Working cycles of the HCCI engine 3

1.1.4 Testing and performance of HCCI engines 4

1.1.5 Hydrogen gas as a fuel 5

1.1.6 Challenges of hydrogen as a fuel 7

1.1.7 Hydrogen gas production methods 8

1.2 Motivation 9

1.3 Problem statement 10

1.4 Objective 11

1.4.1 Main objective 11

1.4.2 Specific objectives 11

1.5 Research question 12

1.6 Limitations 12

2 LITERATURE REVIEW 13

2.1 History of hydrogen internal combustion engine 13

2.2 Using hydrogen fuel in HCCI engine 14

3 METHODOLOGY **19**

3.1 Conceptual framework 19

3.2 Literature review 19

3.3 Pre-processing steps 21

3.3.1 Governing equations 21

3.3.2 Thermo-physical properties 22

3.4 Geometrical mesh 24

3.5 Mesh quality 27

3.6 Configuring models 27

3.6.1 Turbulence modeling 27

3.6.2 Chemical kinetics 29

3.6.3 Combustion modeling 30

3.7 Initial boundary conditions & control parameters 32

3.7.1 Initial boundary conditions 32

3.7.2 Simulation control 32

3.8 Simulation & post-processing Analysis 33

3.9 Validation & verification of simulation results 33

3.9.1 Time step sensitivity analysis 33

3.9.2 Mesh independence study 35

3.10 Documentation & reporting 37

3.11 Conclusion & recommendations 37

4 RESULTS AND DISCUSSION **38**

4.1 Variation of thermodynamic properties of premixed hydrogen fuel at stoichiometric mixture 38

4.1.1 Variation of pressure 38

4.1.2 Variation of temperature 40

4.1.3 Actual pressure volume diagram 42

4.1.4 Variation of specific volume 43

4.1.5 Variation of mixture density 44

4.1.6 Heat of reaction 45

4.1.7 Instantaneous power 46

4.1.8 Mass-fraction of species 47

4.2 Variation of thermodynamic properties at varying equivalence ratios of premixed hydrogen fuel 50
4.2.1 Variation of pressure 50
4.2.2 Variation of temperature 51
4.2.3 Variation of heat of reaction 52
4.2.4 Variation of mass-fraction 53
4.3 Variation of thermodynamic properties at different rpm of the engine of premixed hydrogen fuel at stoichiometric conditions 56
4.3.1 Variation of pressure 56
4.3.2 Variation of temperature 57
4.4 Comparison of thermodynamic properties between hydrogen & heptane fuel at stoichiometric conditions 58
4.4.1 Comparison mean pressure variation between hydrogen fuel and heptane fuel 58
4.4.2 Comparison mean temperature variation between hydrogen fuel and heptane fuel 59
4.4.3 Comparison actual pressure volume diagram between hydrogen and heptane fuel 60
4.4.4 Comparison specific volume variation between hydrogen and heptane fuel 61
4.4.5 Comparison mixture density variation between hydrogen and heptane fuel 62
4.4.6 Comparison heat of reaction variation between hydrogen and heptane fuel 63
4.4.7 Comparison instantaneous power variation between hydrogen and heptane fuel 64
4.5 Variation of thermodynamic properties between hydrogen and heptane fuel at same mass flow rate 65
4.5.1 Comparison mean pressure variation at same mass-flow rate . . . 66
4.5.2 Comparison mean temperature variation at same mass-flow rate . 66
4.5.3 Comparison PV diagram at same mass-flow rate 67
4.5.4 Comparison heat of reaction at constant mass-flow rate 69

4.6 Comparing testing parameters between hydrogen and heptane fuel at stoichiometric conditions 69
4.7 Comparing testing parameters between hydrogen and heptane fuel at same mass flow rate 71

5 CONCLUSIONS AND RECOMMENDATIONS 72
5.1 Conclusions 72
5.2 Recommendations 74

REFERENCES 75

APPENDICES 79

LIST OF FIGURES

1.1 Cutaway drawing of Chrysler 2.2-liter displacement four-cylinder spark-ignition engine (Heywood, 2018) 1
1.2 PV diagram of HCCI cycle (Khaliq et al., 2011) 3

3.1 Conceptual Framework 20
3.2 KIVA model of the 4-valve pent roof engine 25
3.3 (a) Cylinder head of the pentroof engine (b) Cylinder liner of the pentroof engine (c) piston of the pentroof engine 26
3.4 Time step sensitivity analysis of mean pressure variation at different CFL number 34
3.5 Time step sensitivity analysis of mean temperature variation at different CFL number 34
3.6 Mean pressure variation at different meshes 36
3.7 Mean temperature variation at different meshes 37

4.1 Variation of mean in-cylinder pressure between -180°CAD to 180°CAD . 39
4.2 Contour showing mean pressure variation at different crank angle position 40
4.3 Variation of mean in-cylinder temperature between -180°CAD to 180°CAD 41
4.4 Contour showing mean temperature variation at different crank angle position 42
4.5 Actual PV diagram between -180°CAD and 180°CAD 43
4.6 Variation of specific volume between -180°CAD and 180°CAD 44
4.7 Variation of mixture density between -180°CAD and 180°CAD 45
4.8 Variation of heat of reaction between -180°CAD and 180°CAD 46
4.9 Instantaneous power between -180°CAD and 180°CAD 47
4.10 Variation of mass fraction of species over CAD 48
4.11 Variation of mass fraction of H_2 over crank angle displacement 48
4.12 Variation of mass fraction of O_2 over crank angle displacement 49
4.13 Variation of mass fraction of H_2O over crank angle displacement 49
4.14 Mean pressure variation at different value of equivalence ratios 50
4.15 Mean temperature variation at different value of equivalence ratios 51
4.16 Comparison heat of reaction at different equivalence ratios 52

4.17 Mass fraction of H_2 variation at different value of equivalence ratios . . . 53
4.18 Mass fraction of O_2 variation at different value of equivalence ratios . . . 54
4.19 Mass-fraction of H_2O variation at different value of equivalence ratios . . 55
4.20 Mean pressure variation at different rpm of engine cycle 56
4.21 Mean temperature variation at different rpm of engine cycle 57
4.22 Variation of mean pressure between two fuels during combustion 59
4.23 Variation of mean temperature between two fuels during combustion . . . 60
4.24 Comparing actual pressure volume diagram between two fuels 61
4.25 Variation of specific volume between two fuels 62
4.26 Variation of mixture density between two fuels 63
4.27 Variation of heat of reaction between two fuels 64
4.28 Comparison instantaneous power between two fuels 65
4.29 Variation of mean pressure between two fuels at same mass flow rate . . 66
4.30 Variation of mean temperature between two fuels at same mass flow rate . 67
4.31 Comparison actual PV diagram between two fuels at same mass flow rate 68
4.32 Variation of heat of reaction between two fuels at same mass flow rate . . 69

LIST OF TABLES

1.1 Comparison of the physicochemical properties of diesel, gasoline, natural Gas and hydrogen fuels (Algayyim et al., 2024) 6

3.1 Thermophysical properties 22
3.2 Engine parameters of kivaTest geometry 25
3.3 Mesh quality statistics 27
3.4 Reduced twelve steps reaction mechanism for H_2 & O_2 (Boivin et al., 2011) 30
3.5 Initial boundary conditions at the -180°crank angle i.e. beginning of compression stroke 32
3.6 Mesh Independence Study 35

4.1 Comparison of performance parameters for hydrogen and heptane fuel at stoichiometric conditions 70
4.2 Comparison of performance parameters for hydrogen and heptane fuel at same mass flow rate 71

LIST OF SYMBOLS

a, b, c, d : Stoichiometric coefficients of the reacting species

A, B, C, D : Reacting species

A_r : Area of the piston

a_i : NASA polynomial coefficients of the species

A_j : Pre-exponential factor for a given reaction step

α : Thermal diffusivity of the mixture

A_s, T_s : Sutherland coefficient

β_j : Temperature exponent for a given reaction step

$C_{\epsilon i}$: Constant term for compression and expansion

C_μ : Model constant

C_p : Specific heat at constant pressure

Cp_s : Molar specific heat of the species

D : Bore diameter of the engine

$\frac{\partial}{\partial t}$: Temporal derivative

D_t : Turbulent diffusion term

D_s : Diffusion coefficient of the species

Ea_j : Activation energy for a given reaction step

ϵ : Dissipation of turbulent kinetic energy

$\bar{}$: Ensemble average

η_{th} : Indicated thermal efficiency

F_i : Body force

h : Specific enthalpy of the mixture

h_s : Specific enthalpy of the species

i, j, k : Cartesian direction components

j : Specified chemical reaction

k : Turbulent kinetic energy of the mixture

K : Constant term for a four-stroke engine

K_c : Thermal conductivity of the mixture

k_{cj} : Equilibrium constant for a given reaction

Kc_t : Turbulent conductivity term

k_{fj} : Forward rate coefficients

k_{rj} : Backward rate coefficients

L_s : Length of the stroke

Le_s : Lewis number of the species

M : Molecular weight of the mixture

$\dot{m}_f$: Mass flow rate supply

$\dot{m}_{C_7H_{16}}$: Mass flow rate of C_7H_{16}

$\dot{m}_{H_2}$: Mass flow rate of H_2

$\dot{m}_{mix}$: Mass flow rate of the mixture

μ : Dynamic viscosity

μ_t : Turbulent viscosity term

n : Number of cylinders

N : Number of species

$\dot{\omega}_s$: Net rate of increase of mass of species due to source term

P : Pressure of the fluid mixture

ϕ_e : Equivalence ratios

P_{imp} : Indicated mean effective pressure

P_r : Prandtl number

Pr_ϵ : Prandtl number for dissipation of turbulent kinetic energy

Pr_k : Prandtl number for turbulent kinetic energy

Pr_t : Turbulent Prandtl number

q_j : Rate of progress variable

r : Compression ratio

R : Universal gas constant

R_ϵ : Reynold's number for turbulent flow

R_{mix} : Specific gas constant

r_p : Pressure ratio

ρ : Density of the mixture

s : Species of the mixture

S : User-specified source term

Sc_s : Species Schmidt number

Sc_t : Turbulent Schmidt number

ψ : Compressibility of the mixture

S_{si} : Source term accounting for spray interactions

S_{ij} : Mean strain rate tensor

S_{rad} : Radiation loss or gain

τ : Viscous stress tensor

τ_C : Characteristic time scale

τ_M : Mixing time scale

T : Temperature of the mixture

t : Time component

$\tilde{}$: Favre average

u : Velocity of the mixture

v'_{ij} : Stoichiometric coefficients of the reactants

v''_{ij} : Stoichiometric coefficients of the products

V_s : Stroke Volume or displacement of the cylinder

W_{net} : Net work done per cycle

X_s : Molar concentration of species

$Y_{C_7H_{16}}$: Mass fraction of C_7H_{16}

Y_{H_2} : Mass fraction of H_2

Y_s : Mass fraction of the species

LIST OF ABBREVIATIONS

ATDC: After Top Dead Center

BDC: Bottom Dead Center

CI: Compression Ignition

CFD: Computational Fluid Dynamics

CFL: Courant Friedrich Lewy

CAD: Crank Angle Displacement

CC: Cubic Centimeter

EGR: Exhaust Gas Recirculation

EV: Electric Vehicle

HCCI: Homogeneous Charge Compression Ignition

IMEP: Indicated Mean Effective Pressure

IP: Indicated Power

ICE: Internal Combustion Engine

LHV: Lower Heating Value

MFLHR: Modified First Law Heat Release

NTP: Normal Temperature Pressure

PaSR: Partially Stirred Reactor

PPM: Parts Per Million

PV: Pressure Volume

PEM: Proton Exchange Membrane

RPM: Revolution Per Minute

SFLHR: Simplified First Law Heat Release

SOE: Solid Oxide Electrolysis

SI: Spark Ignition

SFC: Specific Fuel Consumption

SIO: Specific Indicated Output

SOI: Start of Ignition

SMR: Steam Methane Reforming

TDC: Top Dead Center

TMF: Total Mass Fraction

WHEC: World Hydrogen Energy Conference

CHAPTER ONE: INTRODUCTION

1.1 Background

ICE derives power from the combustion of the fuel with oxygen of the air within the cylinder of the engine. It is a heat engine in which the combustion of a fuel-air mixture takes place within a combustion chamber, a integral part of the working fluid circuit. In an ICE, the expansion of the high-pressure & high temperature gases produced by the combustible mixture applies force to the piston assembly. As a result, this force drives the piston assembly reciprocating within an integral system of the engine. During this process, the chemical energy of the fuel is transformed into kinetic energy which is used to propel the vehicle where the engine is attached with.

1.1.1 Structure of the IC engine

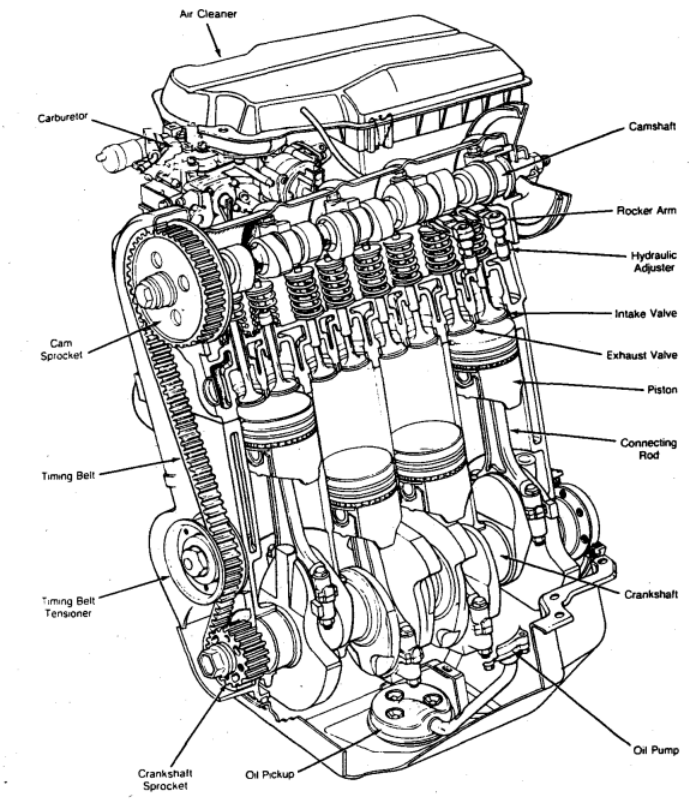

Figure 1.1: Cutaway drawing of Chrysler 2.2-liter displacement four-cylinder spark-ignition engine (Heywood, 2018)

Figure 1.1 illustrates cutaway drawings of a four stroke SI engine. The base of a reciprocating IC engine is the engine block which contain the engine cylinder. The cylinder

contains gas under high pressure and high temperature & also guides the piston. It is a plain cylindrical barrel where the piston slides. The movement of the piston is generally measured in terms of stroke-bore ratio. The upper end consists of a combustion or clearance area in which ignition of the combustible mixture takes place. One end of the cylinder is closed by means of a removable cylinder head which contains both the inlet & exhaust valves. These valves are actuated by means of cam & follower mechanism powered through the engine crankshaft. The inlet & exhaust valves are connected through inlet manifold and exhaust manifold respectively. The main purpose of the cylinder head is to seal the working ends of the cylinder and not to permit entry and exit of the gases without actuation of the engine valves.

The piston is fitted inside the cylinder with a face upward to receive gas pressure & transmit the thrust to the crankshaft via connecting rod. The piston provides tight seal for the gases to prevent escaping from the gap in between the piston and cylinder wall because of the piston rings fitted on the groove of the piston. The thrust on the piston during the power stroke make the piston to slide without tilting because of the skirt i.e. piston wall. The connecting rod transmits the piston load to the crank through the reciprocating motion of the piston assembly into a rotatory motion of the crankshaft as this rotatory motion is required to make the wheel rotates.

1.1.2 Homogeneous Charge Compression Ignition (HCCI)

HCCI is a form of internal combustion where fuel & air are well mixed before combustion starts and it is compressed to the point of auto-ignition during the compression stroke such that it ignites because the temperature surpasses the auto-ignition temperature of the fuel mixture during compression stroke. HCCI has the characteristics both of the conventional gasoline and diesel engine. i.e. it is similar to the spark ignition engine in the sense that both engines utilize premixed charge whereas it is similar to the compression ignition engine as both of them depend on auto-ignition temperature to initiate combustion. During HCCI process, density & temperature both increases because of the compression of the charge as a result the entire mixture reacts spontaneously resulting in auto-ignition of the fuel mixture. HCCI engine produces extremely low level of NOx because the absence of a high-temperature flame front in HCCI combustion which reduces peak temperature

resulting in low NOx formation spontaneously.

1.1.3 Working cycles of the HCCI engine

An internal combustion engine can work as a constant volume, constant pressure or dual combustion cycle mode. Since, HCCI engine works as a constant volume cycle, a detailed explanation of the constant volume cycle is explained below:

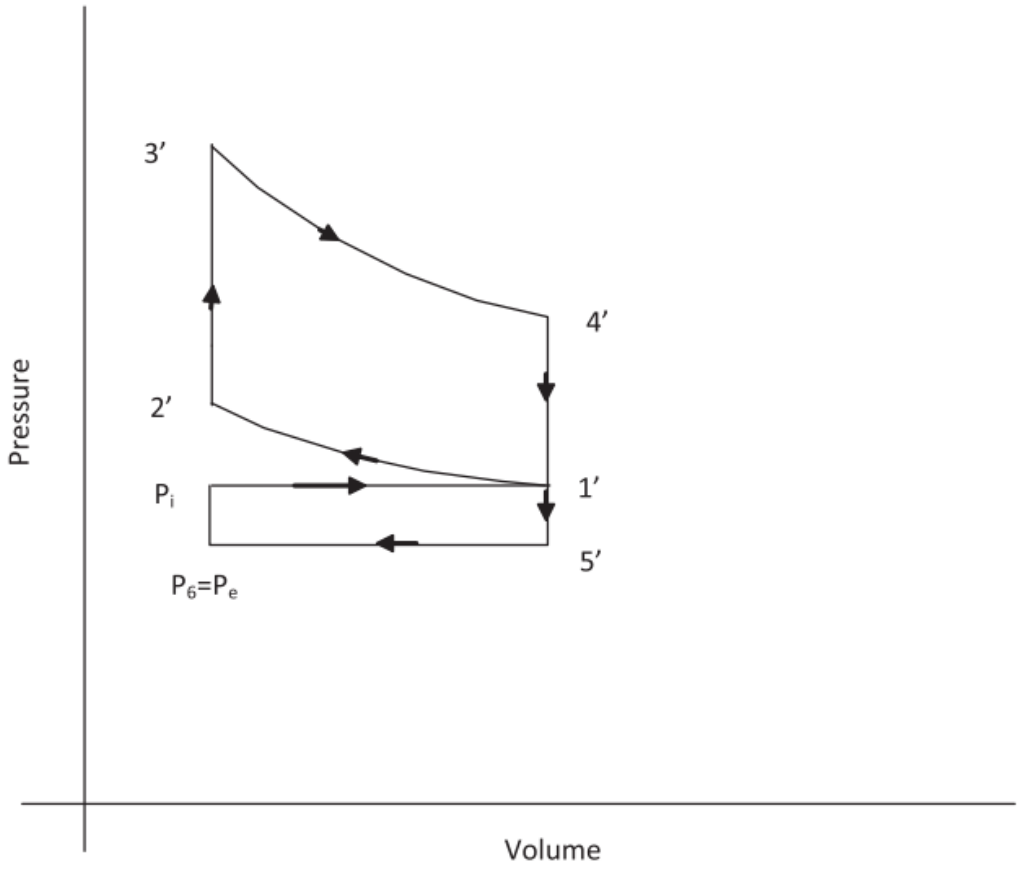

Figure 1.2: PV diagram of HCCI cycle (Khaliq et al., 2011)

Figure 1.2 illustrates various process of the constant volume cycle. Point 1' represents the position of the piston i.e. at the bottom dead center before the cycle starts where the air-fuel mixture is sucked inside the engine cylinder. As the compression stroke begins, the piston moves from position 1' to 2' i.e. from BDC to TDC such that the pressure and temperature increases isentropically. Just before the end of the stroke, the temperature is high enough to ignite the fuel mixture as the temperature at point 2' is greater than the auto-ignition temperature of the fuel mixture. The combustion occurs instantaneously such that the process occurs at the constant volume. Both the inlet and exhaust valves

remain closed during the compression stroke. Due to the ignition of the gases mixture, the thrust produced during the combustion drives the piston from TDC to BDC as a result the work is produced. This expansion stroke begins from point 3' and ends at point 4'. During this stroke, both the valves remain closed, however, when the piston just reaches the BDC, the exhaust valves start to open. The last stroke of the cycle is exhaust stroke which lasts between point 4' and 1' which occurs at constant volume. The removal of burnt gases is accomplished during this stroke as the piston moves from BDC to TDC. As a result, the exhaust gases are driven out from the engine cylinder known as scavenging.

1.1.4 Testing and performance of HCCI engines

The primary task of the new engine is to reduce its capital and running costs. This involves trial of various design concepts. The testing parameters are so enormous and different that it is almost physically impossible to take care of all of them during the engine design. Therefore, it is necessary to conduct the test on the engine and determine the measures which should be taken to improve the engine performance. The nature and the type of the test to be conducted will depend upon a great number of factors such as the degree of development of the particular design, the accuracy acquired, the funds available and the nature of the manufacturing company.

The testing of the engine is necessary to verify the performance of the engine as per the specification. The list of performance parameters are listed below:

- Indicated mean effective pressure
- Indicated Power
- Specific indicated output
- Specific fuel consumption
- Indicated thermal efficiency

Indicated mean effective pressure

Mean effective pressure is defined as hypothetical pressure thought to be acting on the piston assembly throughout the power stroke. If it is based on I.P., it is called indicated mean effective pressure. Since, the power (P) of an engine depends upon the size and speed,

therefore it is not possible to compare engine on the basis of power. Therefore, mean effective pressure is the true indicator of measuring performance of different engines.

Indicated power

The total power developed by the combustible mixture in the combustion chamber is known as indicated power. It is a power that derives the piston inside the engine assembly.

Specific indicated output

It is defined as the indicated power output per unit of piston displacement in an ICE. For engine running at higher speeds, the engine has higher specific indicated output for the same piston displacement.

Specific fuel consumption

It is a parameter that measures mass of fuel consumed per kW power developed per unit hr and it is a criterion of economical power production.

Specific indicated efficiency

It is non-dimensional parameter for comparing the indicated work done by the combustible mixture to the energy supplied by the fuel.

1.1.5 Hydrogen gas as a fuel

Hydrogen is the most abundant chemical element in the universe, being the lightest & probably the most prevalent fuel constitutes approximately 75 % of all normal matter. However, free hydrogen is scarce on the Earth, primarily found in the form of compounds, resulting in a diverse range of molecular configurations. For example: water, organic compounds, natural gas etc. However, the percentage of hydrogen that exists in its compound including diatomic molecules (H_2), atomic hydrogen, and hydrides are very low in the Earth's atmosphere (Armaroli and Balzani, 2011).

Hydrogen is odorless, colorless, tasteless, and non-toxic, although has a low density at NTP but it is highly flammable even at low temperatures. It is highly reactive and easily forms compounds with other elements making it a versatile element suitable for various applications. More importantly, it reacts with oxygen to form water vapor making it a clean-burning fuel and this quality makes it a better fuel in comparison to conventional fossil fuels which emit carbon dioxide and other harmful pollutants.

Physical and chemical properties of hydrogen relevant to fuel

Table 1.1: Comparison of the physicochemical properties of diesel, gasoline, natural Gas and hydrogen fuels (Algayyim et al., 2024)

Properties	Diesel	Gasoline	Natural Gas	Hydrogen
Molar mass (kg/mol)	150-250	60-150	17.3	2
Density(kg/m^3) at 15 °C & 1 atm	840-880	720-780	0.72	0.085
Viscosity (mm^2/s) at 40 °C	1.9-4.1	0.494	-	-
Lower heating value (MJ/kg)	42.8	44	47.5-60	120
Cetane number	51	14.5-20	0	5-10
Research Octane Number (RON)	15-25	95	85-95	>130
Boiling point in C	180-360	38-204	-162	-252.9
Latent heat of vaporisation (kJ/kg)	270	305	509-540	-
Auto-ignition temperature in °C	180-316	258-280	595-650	585
Combustion Energy density (MJ/m^3)	36	42.7	24.6	-
Flame speed(cm/s)	2.0-8.0	37-43	20-38	185-325
Flammability limit (equivalence ratio)	0.6-2	-	-	0.1-7.1
Flammability limit (% volume in air)	0.6-7.5	-	7-21.6	4-75
Adiabatic flame temperature in °C	2054	2150	1810	-
Stoichiometric (air-fuel ratio) mass	14.3	14.6	17.05	34.3

Table 1.1 highlights important properties of hydrogen in comparison to diesel, gasoline, and natural gas. Hydrogen is the smallest, lightest and possesses a very low density in atmospheric conditions. The wider range of flammability limits of hydrogen allows to operate at a broad range of equivalence ratios resulting in efficient combustion across a range of hydrogen concentrations. Secondly, hydrogen requires a notably low ignition energy, i.e. a small fraction of energy is required to start a combustion process. Thirdly,

hydrogen possesses a higher laminar flame speed at stoichiometric ratios in comparison to other fuels, enhancing its ability to approach the thermodynamic ideal engine cycle more closely. Moreover, hydrogen has a high auto-ignition temperature enabling to use of higher compression ratios in hydrogen engines, however because of the high auto-ignition temperature, it is difficult to initiate ignition even at elevated temperatures. Additionally, hydrogen carries the highest stoichiometric ratios among the listed fuels resulting in improved combustion efficiency as more hydrogen is available for the reaction. Similarly, hydrogen possesses the highest lower heating value among the given fuels making it a highly combustible fuel and releasing 120 MJ/kg of energy when ignited in the presence of oxygen molecules.

1.1.6 Challenges of hydrogen as a fuel

Adapting hydrogen as a fuel in internal combustion engines presents a challenge in controlling undesirable phenomena because of low ignition energy, wider flammability range, and rapid laminar flame speed which results in premature ignition and uncontrolled combustion. The challenge lies in reducing these undesirable events while keeping the efficiency and performance better. The solution lies in optimizing engine design, fuel injection strategies, and combustion control mechanisms to mitigate the reactive nature of hydrogen and harness its energy potential effectively (Fayaz et al., 2012).

- **Knocking**: Knocking is a major challenge in hydrogen engines due to the high reactivity and low ignition energy of hydrogen which leads to uncontrolled combustion, damaging the engine and reducing its efficiency. It can be controlled with design modification, exhaust gas recirculation, variable valve timing, and using advanced combustion concept (Fayaz et al., 2012).

- **Backfire**: Backfire, also known as flashback, is an undesirable phenomenon that can occur in hydrogen engines when the flame propagates prematurely back in the inlet manifold, which results in pressure surges, audible noise, and uncontrolled combustion in the intake manifold results in damage or destruction of intake system (Fayaz et al., 2012). It can be prevented using lean air-fuel mixture, early ignition, intake manifold design, intake valve timing and the engine operating conditions (Algayyim et al., 2024).

- **Hydrogen power density**: Due to size and weight constraints in vehicles, hydrogen

must be stored in a small, lightweight system which poses a challenge because hydrogen possesses the lowest energy density by volume among common fuels. Therefore, research are going on to find a safe, reliable, and energy-efficient method of H_2 storage (Durbin and Malardier-Jugroot, 2013). To achieve a reasonable density, it must be stored at a very low temperature using cryogenic storage techniques since at cryogenic conditions, hydrogen is in the liquid state (Kumar et al., 2024).

- **Corrosion**: Hydrogen has been a highly reactive gas, causing corrosion in a variety of engine parts i.e. it reacts with aluminum or cast iron to form aluminum hydride or iron hydride leading to leakage and engine failure due to the brittle nature of hydride. Similarly, hydrogen diffuses through piston ring gaps causing them to swell and become brittle. Moreover, hydrogen reacts with steel valves to form hydrogen embrittlement which is susceptible to cracks. Using corrosion-resistant materials, protective coatings, and hydrogen scavengers, hydrogen corrosion in engine parts can be prevented (Alnaeli et al., 2023; Li et al., 2021).

1.1.7 Hydrogen gas production methods

The main source for hydrogen production is fossil fuels at present, however, it will be necessary to produce it on a large scale using the diminishing amount of fossil sources and also increase the utilization of hydrogen gas (Baykara, 2018). The main methods of hydrogen production are listed below.

- **Steam methane reforming**: Almost 95% of H_2 production is made by using natural gas reforming in large central plants (Boretti and Banik, 2021). In this process, natural gas reacts with steam at high temperatures (700-1000°C) over a catalyst to produce hydrogen and carbon monoxide. Since this reaction is endothermic, heat must be supplied for the reaction to proceed.

- **Partial oxidation**: During this process, methane, natural gas or hydrocarbon is heated in the presence of stoichiometric oxygen to form hydrogen gas has attracted a lot of attention because partial oxidation of methane shows several advantages over steam reforming i.e good response time, compactness and less sensitivity for fuel variation (Freni et al., 2000).

- **Auto-thermal reforming**: It combines both partial oxidation and steam reforming processes for hydrogen production. During this process, oxygen, steam, and methane react together in the presence of a catalyst in a reactor to produce syngas which is the combination of hydrogen, carbon monoxide, steam, and trace gases (Oni et al., 2022).

- **Electrolysis**: Water electrolysis is gaining popularity as a sustainable process for hydrogen production as it involves utilizing renewable energy sources without carbon emission i.e. green hydrogen. It involves splitting water into hydrogen and oxygen using electricity. Alkaline electrolysis, PEM, and SOE cells are the different types depending upon the electrolyte and working temperature used (Sebbahi et al., 2024).

1.2 Motivation

With the overarching goal of the Paris Agreement (2016) - to limit the global average temperature well below 2°C above pre-industrial levels and pursuing efforts for limiting the temperature increase to 1.5°C above pre-industrial levels, intensified research efforts are going on to reduce fuel consumption and mitigating the concentration of harmful exhaust emissions. Concerning the world of transportation, the rapid depletion of conventional fossil fuels has led thrust among researchers for the development and demonstration of alternative energy fuels. Moreover, fluctuation in fuel prices creates uncertainty among manufacturers and customers leading to dilemmas in production and driving behavior, respectively. Additionally, strict Euro emission regulations on regulating substantial reductions in vehicle emissions to combat climate change and improve air quality, pressurize researchers for the advancements in technology, and explore new strategies in developing alternative renewable energy resources and non-conventional fuels. Although, electrification of power trains may have benefited on limiting carbon emissions, internal combustion engines (ICEs) have been the dominant power sources due to high power density, high efficiency, high reliability, and cost-effectiveness. Based on usage and resource availability, the de carbonization method still considers internal combustion engines, especially with the inclusion of zero- and low-carbon fuels.

1.3 Problem statement

The automotive industry faces complex challenges such as depletion of petroleum reserves, skyrocketing in the fuel prices, and strict emission standards. The depletion of petroleum reserves poses a long-term threat, immediate need for alternative and efficient fuel. Concurrently, the fluctuation in fuel prices create uncertainties among manufacturers as well as consumers, which impacts in production cost and driving behavior. In addition, strict emission norms require substantial reductions in vehicle emissions to combat climate change and improve air quality.These requirements confronts need for advancements in technology as well as substantial investment in research and development to cope with reduced fuel consumption, searching for alternative energy resources and mitigation of harmful pollutants in exhaust emissions. Collectively, these challenges are forcing industries to innovate rapidly, transitioning towards sustainable practices and the adoption of electric and hybrid vehicles to ensure future viability and compliance.

However, the degradation of EV batteries overtime affect their driving range and necessitates costly replacements of batteries, which can weaken the initial cost savings from lower fuel and maintenance expenses. This problem creates a significant concern for prospective EV owners, impacting their long-term financial conditions as well as overall satisfaction with the vehicle's performance and its reliability. As a result, ongoing research endeavors focuses on exploring diverse alternative energy sources along with partially or completely replacing fossil fuels, needing to address these challenges and providing sustainable transportation solutions for near future.

With increasing population globally, the world wide demand for energy escalates, which increases energy cost due to imbalance between demand and supply of energy. The current energy demands overwhelmingly dominated by conventional fossil fuels like petroleum crude oil, coal, and natural gas accounts for over 90 percent of global energy demand. This dependency significantly contributes to greenhouse gas emissions and also exacerbates the greenhouse effect. To mitigate these challenges, researchers all around the globe are actively exploring strategies for advancement in technology related to fuel consumption & investment in renewable and non-conventional fuels. A key focus of these efforts is the adoption of renewable alternative fuels such as bio-fuels, methanol, bio-diesel, and

hydrogen gas. These fuels are potential substitutes for diesel in CI engines and gasoline in SI engines.

This thesis work aims to address the computational characteristics of hydrogen gas combustion in homogeneous charge compression ignition engine by applying advanced combustion techniques. This research investigates the development of computational model for combustion of premixed hydrogen fuel mixture including turbulence model, combustion model & detailed reaction mechanism. This research studies variation in thermodynamic properties with crank angle displacement resulting due to combustion phenomena in a premixed hydrogen fuel mixture inside internal combustion engine. This research also compares variation of thermodynamic properties between hydrogen fuel & heptane fuel (a species of diesel fuel) due to combustion inside IC engine to evaluate the performance & efficiency of IC engine to explore and adaptation of hydrogen gas as an alternative fuel.

1.4 Objective

1.4.1 Main objective

- To perform computational characteristics of premixed hydrogen fuel mixture combustion in a homogeneous charge compression ignition engine.

1.4.2 Specific objectives

- To develop a computational model for combustion of premixed H_2 fuel mixture in an internal combustion engine including turbulence model, combustion model & reaction mechanism.
- To observe variation in thermodynamic properties with crank angle displacement resulting due to combustion phenomena in a premixed H_2 fuel mixture.
- To compare variation in thermodynamic properties between hydrogen fuel and heptane fuel (a species of diesel fuel) to evaluate the performance & efficiency of internal combustion engine resulting in the exploration and adaptation of H_2 gas as an alternative fuel.

- To evaluate the testing parameters between hydrogen and heptane fuel at stoichiometric mixture and at same mass flow rate.

1.5 Research question

The following research question would be addressed:
Is the simulation of hydrogen fuel combustion in HCCI engine enough for exploration and adaptation of hydrogen fuel in an IC engine ?

1.6 Limitations

Following are the limitations of the research study:

- This research work is purely simulation based study.
- This simulation study make use of premixed hydrogen fuel and does not consider non-premixed combustion.
- The detailed reaction mechanism of H_2 & O_2 does not consider emission modeling of NO_x.
- To compare hydrogen fuel, this simulation study utilizes the single step reaction mechanism of heptane fuel which is unable to capture complex chemical and physical process involved during combustion.
- This research study treats hydrogen and heptane fuels as standalone fuels and does not take into account dual fuel combustion concepts.

CHAPTER TWO: LITERATURE REVIEW

2.1 History of hydrogen internal combustion engine

Hydrogen internal combustion engine works on the same phenomena as of conventional fossil fuel engines to power vehicles and provides an equivalent amount of drive force. The concept of using hydrogen in internal combustion engines is not new i.e. it is almost as old as that of an internal combustion engine itself. The first mention of hydrogen-powered engines dates back to 1807 when Francois Issac de Rivaz of Switzerland drove an internal combustion engine using a mixture of hydrogen and oxygen (Rațiu, 2003).

In 1860, Jean Joseph Etienne Lenoir patented a gas-driven two-stroke engine powered by hydrogen generated via the electrolysis of water (Fairbanks, 2004). In 1993, Norsk Hydro ran an internal combustion engine using ammonia (Schöffel, 2005). In the year 1933, Erren Engineering company used the first ever hydrogen direct injection engine using pressurized hydrogen into oxygen inside the internal combustion chamber. While injecting hydrogen directly, the system eliminated backfiring and produced higher output and lowered specific fuel consumption (Erren, 1939). In the year 1941, the Russian Boris Shelishch converted 200 GAZ-AA trucks into hydrogen engines which burnt cleaner and worked longer than those powered by gasoline. It was the first installation of a hydrogen-powered internal combustion engine in Russia (Plotnikov and Ulman, 2021). The year 1970 highlighted a significant concern about fuel scarcity and environmental pollution resulting in a new research phase on hydrogen combustion engines, however, initially, hydrogen was explored as a fuel without a sense of urgency and fully relying on the perpetual availability of petroleum products before the World Wars. During World Wars, the perspective of the fuels shifted, highlighting the need for alternative fuels, leading to a renewed interest in hydrogen (Das, 2016).

Between the years 1974-1986, test vehicles with hydrogen combustion engines were developed in Japan at the Musashi Institute of Technology. In year 1974, Musashi used a 4-stroke hydrogen engine & high-pressure storage. Similarly, in the year 1975, Musashi 2 was launched with hydrogen manifold injection on a 4-stroke engine in combination with liquid storage (Furuhama, 1997). Again, in the year 1977, Musashi 3 used a spark-ignited two-stroke engine with hydrogen injection (Furuhama and Kobayashi, 1982). Moreover,

in the year 1984, Musashi-6 came with a late direct injection system with the liquid hydrogen delivery system which was presented at the (5^{th} WHEC, Conference in Toronto (Furuhama et al., 1986).

Therefore, the 20^{th} century has contributed a lot in the field of hydrogen engine technology and shown the possibility of using hydrogen gas in existing internal combustion engines without prior modification. Similarly, in the 21^{st} century, many researches are going on showing interest in using hydrogen gas as an alternative fuel with little modification in engine design.

2.2 Using hydrogen fuel in HCCI engine

Conventional spark ignition engine (SI) is characterized by spark discharge in the premixed mixture, particularly stoichiometric at the constant volume combustion chamber. The major disadvantage of SI engines is low efficiency at partial loads and a limited compression ratio of 8 to 12 because knocking results in low efficiency. Similarly, in conventional diesel combustion, the fuel after leaving the injector nozzles starts to burn including droplet formation, collision, breaking-up, evaporation, and vapor diffusion. The combustion rate is affected by these processes resulting in stratified fuel concentration as part of the fuel will be premixed and a larger proportion of the fuel will take longer time for evaporation as compared to the chemical time scale. As a result, the mixture is divided into high-fuel concentration regions and high-temperature flame regions which implies a large amount of soot formation in the high-fuel concentration region and a great amount of NOx formation in the high-temperature region. Because of low efficiency at partial load in SI engines and large amounts of soot and NO_x emissions in diesel engines, HCCI engines came into practice. HCCI is characterized by fuel and air mixing before combustion starts and the mixtures auto-ignite because of temperature rise in the compression stroke (Yao et al., 2009). In HCCI process, the premixed fuel-air charge is introduced into the combustion chamber at equivalence ratios between 0.15 & 1 (Norbeck et al., 1996).The charge is compressed inside the combustion cylinder. As a result, the auto-ignition temperature of the charge is reached resulting in simultaneous combustion at multiple points inside the cylinder. The process is very fast and it enables all the heat to be released within a shorter time frame of usually 4° crank angle (Tsujimura et al., 2003; Naber and Siebers, 1998).

Stenlåås et al. investigated the potential of using hydrogen as a fuel for homogeneous charge compression ignition engines. They experimented with a highly modified Volvo TD 100 six-cylinder deactivating five-cylinder resulting in a displacement volume of the engine to 1.6 liters. The experiment included variations of parameters such as lambda, engine speed, compression ratio, and intake temperature to explore the efficiency, combustion characteristics, and emission profiles. They observed hydrogen as a possible fuel for an HCCI engine with extremely high heat release between narrow crank angles for lambda ranges from 3-6. Again, the value of lambda was investigated against intake gas temperature and it was observed that the control interval region was narrow when richer mixtures were used. Moreover, the maximum load in HCCI mode for hydrogen was an indicated mean effective pressure of 3.5 bar which was half the load in SI mode and about half of the maximum load in HCCI mode with other fuels which indicated superior thermal efficiency than that of SI. Additionally, it was observed that NOx emissions were found to decrease as expected when lambda increased; however, the concentration of hydrogen was found to be increased in the exhaust with HCCI mode. Nevertheless, emissions of carbon monoxide and hydrogen were detected because of evaporation and partial oxidization of lubricating oil (Stenlåås et al., 2004).

Caton et. al modeled hydrogen HCCI using a single-zone, zero-dimensional model created in Matlab using the geometry of the experimental engine. Thermodynamic calculations were facilitated by Canterrra, an open-source software. Hydrogen combustion simulation used a reaction mechanism developed by Connaire et. al. The model was simulated at a compression ratio of 18 using initial charge temperature (thermal state of reactants), equivalence ratio (compositional state of reactants), and initial pressure (1 atm at BDC). Similarly, the experimental apparatus was built using a single-cylinder cooperative fuels research diesel engine. The rpm was kept at 900 with variable compression ratios, injection timing, and injection amount (diesel fuel). Hydrogen fuel was supplied using a compressed gas cylinder and mass flow rate was controlled using a choke flow orifice. The compression ratios varied between 16.5 to 20, with the intake air temperature at 80 ± 1 °C or 100 ± 1°C at atmospheric pressure. It was found that simulation of hydrogen fuel in HCCI was feasible at a compressible ratio around 18 with an intake heating of 100°C. Similarly, the peak efficiency was obtained at moderate equivalence ratios of 0.2-0.5 with a minimum amount of intake heating. While experimentation, the

hydrogen fuel combustion occurred at intake heating of 80-100°C at an equivalence ratio between 0.15-0.37. The experimental result showed that efficiency decreases at a higher compression ratio larger than 18.5 due to high thermal losses. Similarly, efficiency decreased at a lower compression ratio i.e. lower than 17 due to high chemical and sensible enthalpy losses. Moreover, when compared to conventional diesel combustion, it was observed that the efficiency deficit was around 5 % of the absolute because thermal losses and chemical enthalpy losses were greater resulting in an overall deficit, however, the sensible enthalpy losses were reduced for hydrogen HCCI. Furthermore, NOx emissions were reduced by two orders of magnitude as compared to conventional diesel combustion using hydrogen HCCI. In addition, emissions of unburnt hydrocarbons were found around 100 ppm because of lubricating oil entrainment (Caton and Pruitt, 2009).

Antunes et. al conducted an experimental investigation of hydrogen fuel in HCCI engine using a diesel setup. Factors that were observed were engine efficiency, emissions, and mechanical loads. It was found that high ignition timing control requirements because of high heat release rate. In this experiment, ignition timing was controlled using inlet air heating and satisfactory results were obtained. Although cycle-to-cycle variation was noticeable making it difficult to control ignition timing, it was found that peak in-cylinder pressure and the rate of pressure rise were higher in the HCCI engine than that of conventional diesel engine, limiting HCCI engine to part load operation and potentially requiring design changes to maintain engine reliability. However, the fuel efficiency was significantly higher in comparison to diesel-fuelled engines and higher efficiency was obtained with a very lean mixture. The most useful parameter to control ignition timing was inlet air temperature to ensure auto-ignition. Exhaust emissions were observed and found that negligible amounts of nitrogen oxides were found in comparison to diesel combustion (Antunes et al., 2008).

Guo et. al observed the effect of hydrogen addition on combustion and emission characteristics of n-heptane fuel in HCCI engines using a multi-zone model. It was found that both experimental and calculation models showed that hydrogen addition retards the combustion phasing of n-heptane fuel. The combustion retardation was due to both dilution and chemical effects and more prominent with dilution effects as dilution effect caused n-heptane and oxygen concentration reduction when hydrogen was added. Similarly, the

chemical effect caused H_2 and OH reaction to proceed resulting decrease in hydrogen abstraction from n-heptane fuel. Moreover, hydrogen addition retarded combustion duration at a constant compression ratio due to the chemical effect which intensified reactivity at the high-temperature combustion stage. Furthermore, hydrogen addition increased indicated thermal efficiency at a constant compression ratio because of optimization of combustion phasing. In addition, hydrogen blends brought an increase in unburnt hydrocarbon emission per unit burnt n-heptane mass because hydrogen addition slowed down low temperature kinetics of n-heptane. The oxidation of the remaining hydrocarbon at high temperature was affected by hydrogen addition resulting in competition between key radicals and consequently, more unburnt hydrocarbon were emitted. It was also observed that because of overly retarding combustion phasing due to hydrogen fuel addition, N_2O emissions increased but hydrogen addition moderate the increase in N_2O emissions (Guo and Neill, 2013).

Pachet & his team used HCCI engine to study combined effect of both H_2 & NH_3 under a variable blending ratio of 16:1 for combined heat & power production. A specific focus was kept on maximizing the utilization of ammonia by proportion as well as minimizing the emission of NO_x. A single cylinder having displacement volume of 499 cc was used with inlet pressure varied between 1-1.5 bar; inlet temperature varied between 428 to 473K at constant speed. They observed that stable combustion was achieved with 70% volume of ammonia by proportion with inlet pressure of 1.5 bar and inlet temperature of 473K at an equivalence ratios of 0.28. They also noticed that using 60% ammonia by proportion resulted in lost of combustion efficiency by 0.6 points in comparison to pure hydrogen. They further discovered that NO_x emissions below 6 ppm in case of pure hydrogen whereas for hydrogen-ammonia blended fuel, NO_x emissions were found between 750 to 2000 ppm. Furthermore, with EGR, NO_x emissions were reduced as well as combustion efficiency decreased due to lower in-cylinder temperature. In addition, they found out that the production of significant N_2O for combustion temperature at 1400K. Furthermore, they marked out NH_3 to be an efficient fuel for HCCI condition & circulation of EGR became a promising factor for NO_x reducing mechanism (Pochet et al., 2017).

Wang et. al utilized both experimental & numerical simulation method to observe combustion characteristics of methane hydrogenation homogeneous charge compression igni-

tion using the free piston movement process. They observed parameter such as ignition timing, change of pressure and temperature, & power capability of the device. They found out that the experiment results were basically consistent with the numerical results. They marked out the blending of hydrogen with methane widen the ignition limit of mixture, advancement of ignition timing of the mixture gases and reduced the starting energy required for ignition at an equivalence ratios of 0.5. Additionally, they noticed that blending hydrogen to methane reduced the maximum temperature & pressure within micro-combustion chamber resulting in more stable burning flame & reduced the chances of detonation within combustible fuel mixture. However, they discovered that adding hydrogen to methane resulted in the decrease of the piston free speed, increased in timing of single stroke completion, decreased in the power capacity of the device and also reduced in indicated thermal efficiency (Wang et al., 2019).

CHAPTER THREE: METHODOLOGY

A research methodology is the structural framework under which the entire research is conducted. A research methodology provides a clear road maps for researchers through which researcher design his study so that he can achieve his objectives using the selected techniques and procedures. It includes all the important aspects of research including problem identification, hypothesis formulation, research design selection, data collection & validation tools, interpreting results and drawing conclusions, and also validating the findings with already existing literature or experimental data. Also, research methodology serves as the fundamental steps of any scientific investigation through which researcher achieve his goals by utilizing the available resources.

3.1 Conceptual framework

Figure 3.1 shows a conceptual framework of the research study which employs a computational based methodology to investigate the computational characteristics of hydrogen premixed combustion in an internal combustion engine under HCCI condition. The methodology consists of several key stages such as solver selection, governing equations, physical & chemical properties, mesh definition & quality, turbulence & combustion model implementation, boundary conditions as well as post processing steps which ensures a systematic and reproducible approach to understand hydrogen combustion under HCCI environment and providing insights about it's feasibility through findings.

3.2 Literature review

Literature review provides comprehensive study on the existing research through focusing on research findings, methodologies as well as gap in the existing research. It helps to develop depth understanding on the current subject, finding research problems & also developing methodologies for solving unresolved questions. In this thesis work, literature review extensively focuses on the combustion of premixed hydrogen fuel mixture inside the internal combustion engine. For that purpose, substantial studies are done on the hydrogen fuel, hydrogen-fueled internal combustion engine, HCCI engine, premixed combustion, computational studies, governing equations of fluid flow, impact of turbulence and reaction mechanism to make research work carried out on a smooth and systematic

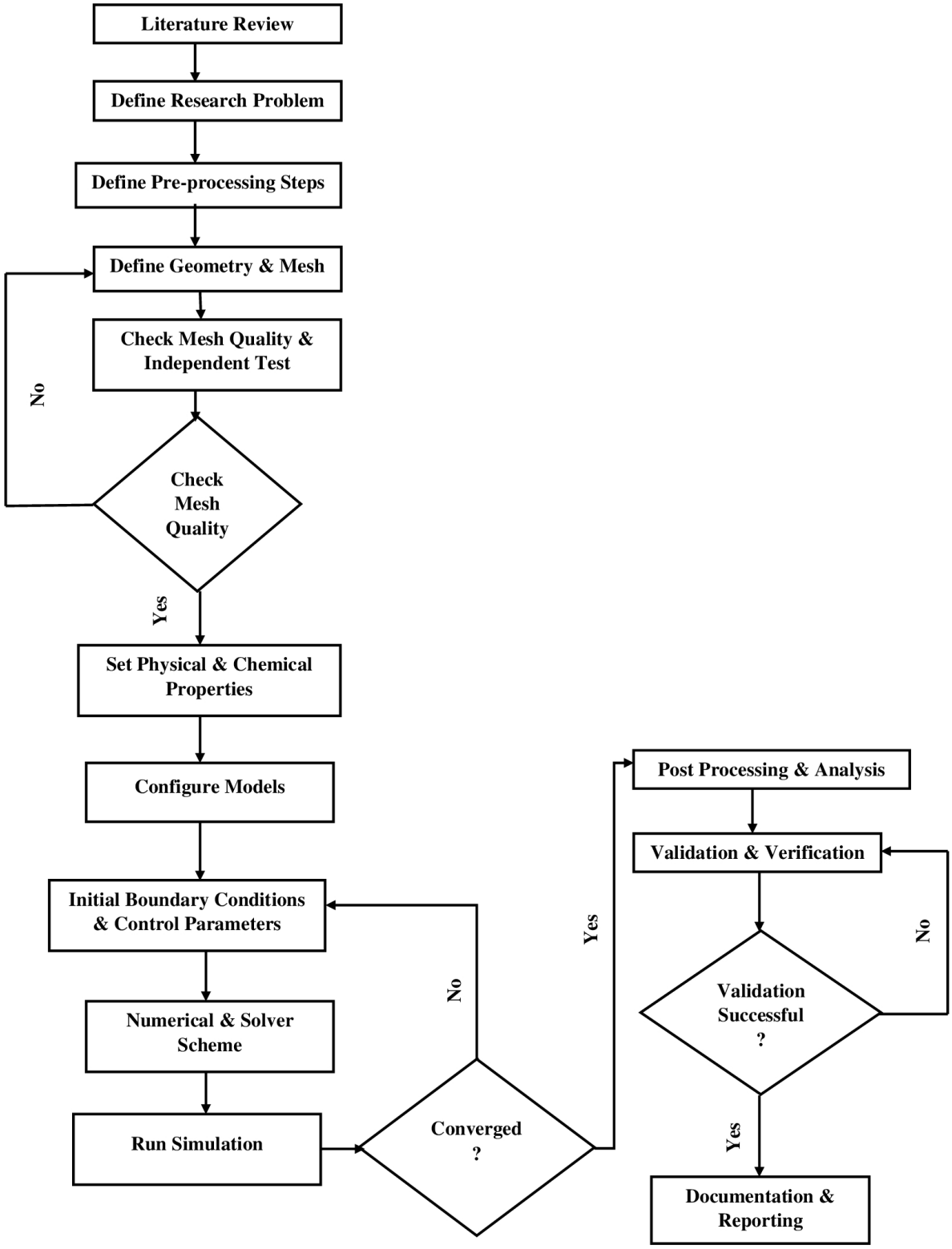

Figure 3.1: Conceptual Framework

way.

3.3 Pre-processing steps

An OpenFoam-based solver, engineFoam which is based on reactingFoam solver was utilized to simulate the combustion of hydrogen gas under HCCI condition. This engineFoam is a transient solver for compressible, turbulent engine flow of reactive or non-reactive flows in internal combustion engine. It includes dynamic mesh handling to model the movement of piston, valves such that it captures the complexities of engine cycle.

3.3.1 Governing equations

The governing equations includes Navier Stokes equation and species mass transport equation for accurate prediction of flow dynamics, heat transfer phenomena and chemical equation.

Continuity equation

$$\frac{\partial \rho}{\partial t} + \frac{\partial (\rho u_i)}{\partial x_i} = 0 \tag{3.1}$$

Momentum equation

$$\frac{\partial \rho u_i}{\partial t} + \frac{\partial \rho u_i u_j}{\partial x_i} = \frac{\partial P}{\partial x_i} + \frac{\partial \tau_{ij}}{\partial x_i} + F_i \tag{3.2}$$

$$\tau_{ij} = \mu \left(\frac{\partial u_i}{\partial x_j} + \frac{\partial u_j}{\partial x_i} - \frac{2}{3}\delta_{ij}\frac{\partial u_k}{\partial x_k} \right) \tag{3.3}$$

Energy equation

The compressible energy equation is given by:

$$\frac{\partial \rho h}{\partial t} + \frac{\partial \rho u_i h}{\partial x_i} = \frac{\partial}{\partial x_i}\left[\frac{\mu}{\mathrm{Pr}}\frac{\partial h}{\partial x_i} + \mu\left(\frac{1}{Sc_s} - \frac{1}{\mathrm{Pr}}\right)\sum_{s=1}^{N} h_s \frac{\partial Y_s}{\partial x_i} \right] + \frac{\partial P}{\partial t} + S_{rad} \tag{3.4}$$

$$\mathrm{Pr} = \frac{\mu C_p}{K_c} \tag{3.5}$$

$$Le_s = \frac{K_c}{\rho C_p D_s} \tag{3.6}$$

$$Sc_s = \frac{\mu}{\rho D_s} \tag{3.7}$$

Species mass transport equation

$$\frac{\partial \rho Y_s}{\partial t} + \frac{\partial \left(\rho u_i Y_s\right)}{\partial x_i} = \frac{\partial}{\partial x_i}\left(\rho D_s \frac{\partial Y_s}{\partial x_i}\right) + \dot{\omega}_s \tag{3.8}$$

3.3.2 Thermo-physical properties

The behavior of chemical species is accounted for changing physical behavior of the flow because of their interaction among themselves. The bulk properties of the flow such as density and dynamic viscosity are calculated in each computational sub domain to determine the physical properties of the flow. The thermo-physical properties used in the simulation is tabulated below:

Table 3.1: Thermophysical properties

Property	**Value**
Thermo type	`hePsiThermo`
Mixture model	`multiComponentMixture`
Transport model	`Sutherland`
Thermo model	`Janaf`
Energy formulation	`SensibleEnthalpy`
Equation of state	`perfectGas`
Specie model	`specie`

Thermophysical type and mixture model

The thermophysical type considered in this simulation is hePsiThermo (fixed composition) based on compressibility ψ. During the simulation, the mixture required by thermophysical models with reactions uses multi-component mixture which are able to interact and

react. Each species has it's own set of library of thermophysical properties such as molecular weight, Janaf coefficients, sutherland coefficients etc.
Mathematically,

$$\psi = \frac{d\rho}{dP} = (RT)^{-1} \tag{3.9}$$

Transport model

The transport model used in this simulation is sutherland where μ as a function of temperature (T) from a sutherland coefficients A_s and T_s which are sutherland coefficients.
Mathematically,

$$\mu = \frac{A_s\sqrt{T}}{1 + \frac{T_s}{T}} \tag{3.10}$$

$$K_c = \frac{\left(C_p + \frac{5}{4}R\right)\mu}{M} \tag{3.11}$$

$$\alpha = \frac{K_c}{\rho C_p} \tag{3.12}$$

Thermodynamic models

The thermodynamic models used in this simulation is Janaf which calculates C_p as a function of temperature which utilizes a set of coefficients taken from Janaf table of thermodynamics. This function is valid between a lower and upper temperature limit. Two sets of coefficients are provided where the first set of coefficients (a_i as i = 1 to 7) are utilized for a upper temperature range whereas second sets of coefficients (a_i as i = 8 to 14) are utilized for below temperature range.
Mathematically,

$$\frac{C_p}{R} = (((a_4T + a_3)T + a_2)T + a_1)T + a_0 \tag{3.13}$$

Equation of state

The fluid inside the internal combustion engine in this simulation is a mixture of H_2, O_2 and N_2 molecules which on combustion produce namely H_2O as by product. This involved molecules are simply diatomic or triatomic molecules which in the normal operating conditions behaves simply as an ideal gases. Therefore, the density of gas is assumed to follow simple perfect gas.

Mathematically,

$$\rho = \frac{P}{RT} \tag{3.14}$$

Selection of energy variable and species

In this simulation, sensible enthalpy is utilized to take into account the energy change due to reactions where heat of formation is not included.
Similarly, species contain the basic thermodynamic properties which are specified for each species from input data such as number of moles, molecular weight of the species etc.

3.4 Geometrical mesh

In this work, the geometrical mesh generated by KIVA model is utilized to simulate the combustion phenomena in an internal combustion engine accurately. It utilizes the kiva-3v solver to generate the combustion system meshes. During mesh processing, the KIVA-3V package utilizes a basic grid generator called K3PREP. The K3PREP uses the block structure grid technology which divides the complex geometry into many simple geometrical areas. Each region generates it's own grid separately and then patches them together to generate the whole domain.

During mesh generation process, these three steps are included. Firstly, the complex geometry is divided into several blocks. Secondly, these blocks are numbered and defined by the structure parameters separately. Finally, the computational domain are generated by patching the block together in a certain order. Before patching, every piece of the grid have their own independent logical coordinates (i,j,k) and physical coordinates (x,y,z). Logical coordinates are used to represent the location of the grid node and the grid cell as well as to establish the logical relationship between them. Similarly, physical coordinates represent the spatial position of each cell. While generating the computational meshes, the preprocessor input data is prepared in file named iprep. This file contains the basic parameters of the engine boundary conditions, the information of each logic block and the block patching commands. The preprocessor generates otape 11 and otape 17 files which are input data to the solver i.e. kiva -3v after renaming respectively to itape11 & itape17. With the run command 'K3VPREP.exe', the mesh is generated by utilizing the input data

from the file named iprep. If the quality of the grid is fine, i.e. no negative grid or inverted grid exist, the mesh can be further used for numerical simulation (Shi et al., 2014).

In this simulation, a geometry from a tutorial case in openFoam called ”kivaTest” is utilized (Kannan and Srivathsan, 2016). It’s a four-valve pent roof engine which uses the real engine geometry with the moving piston as shown in figure 3.2. It consists of cylinder head, cylinder liner and piston with both intake and exhaust valve remains close as a result the working of the valves is not simulated here. This pent roof engine has a pent roof type combustion chamber for faster burning of the air-fuel mixture. The kivaTest engine geometry has the following parameters.

Table 3.2: Engine parameters of kivaTest geometry

Engine Parameter	**Value**
Connecting rod length	0.147 m
Bore diameter	0.092 m
Stroke length	0.08423 m
Clearance length	0.004433 m
Engine speed	1500 rpm

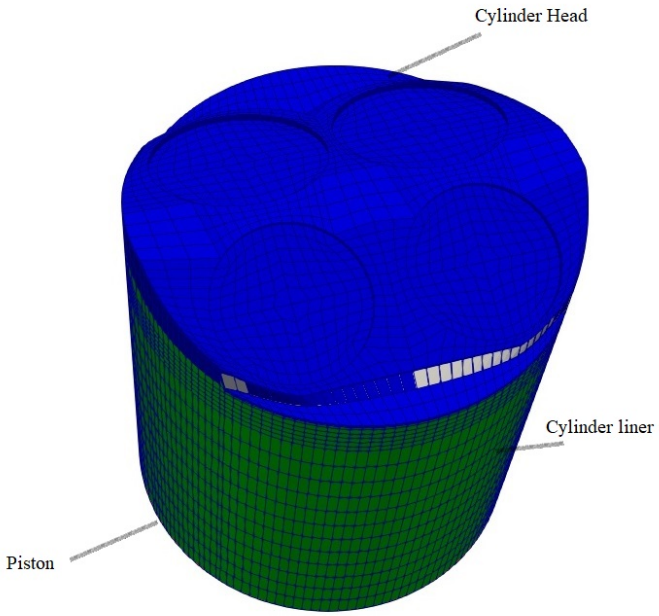

Figure 3.2: KIVA model of the 4-valve pent roof engine

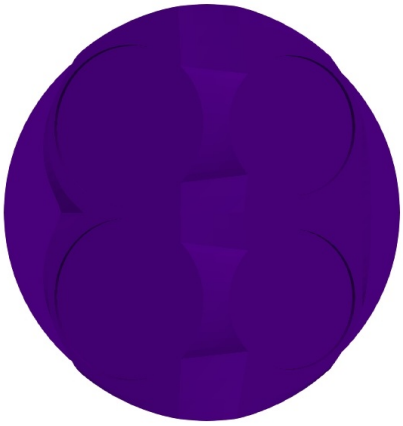

(a)

(b)

(c)

Figure 3.3: (a) Cylinder head of the pentroof engine (b) Cylinder liner of the pentroof engine (c) piston of the pentroof engine

3.5 Mesh quality

The geometrical mesh is checked through checkMesh command. It checks the quality of a computational mesh by providing detail information about the mesh structure, quality metrics, and potential issue that might affects the accuracy and stability of numerical simulation.

Table 3.3: Mesh quality statistics

S.No.	Mesh Stats	Quality
1	Points	30,742
2	Faces	85,742
3	Internal Faces	79,522
4	Cells	27,544
5	Cell Type	Hexahedral
6	Max. Aspect Ratio	34.0317
7	Min. Volume	3.07×10^{-10}
8	Max. Skewness	3.73901

Table 3.3 illustrates the example of mesh quality statistics. It provides information about the mesh structure such as points, faces, cells, cells type etc; quality metrics such as orthogonality, skewness, aspect ratio etc. to minimize potential errors that leads to instability of the numerical study.

3.6 Configuring models

3.6.1 Turbulence modeling

Although, four governing equations represent various physical phenomena happening during the combustion simulation, additional unknown terms will appear when modeling turbulence behavior. A number of different turbulence models were tested during H_2 combustion such as standard k-ϵ, renormalization group k-ϵ, standard $k-\omega$ and $k-\omega$ SST

model. The most consistent and realistic results were obtained with the renormalization group $k-\epsilon$ (RNG $k-\epsilon$) turbulence models with standard coefficients when comparing with both the results of optical measurement of H_2 injection and other metal engine experiments (Babayev et al., 2021). Now, in this model, the turbulence length scale le is given by:

$$le = C_{\mu}^{\frac{3}{4}} \frac{k^{\frac{3}{2}}}{\epsilon} \tag{3.15}$$

The reynolds stress $\tau_{ij}$is given by:

$$\tau_{ij} = 2\mu_t S_{ij} - \frac{2}{3}\delta_{ij}\left(\rho k + \mu_t \frac{\partial \tilde{u_i}}{\partial x_j}\right) \tag{3.16}$$

The turbulence kinetic energy (k) is given by:

$$k = \frac{1}{2}\tilde{u_i'u_i'} \tag{3.17}$$

The turbulent viscosity (μ_t) is given by:

$$\mu_t = C_{\mu}\rho\frac{k^2}{\epsilon} \tag{3.18}$$

The mean strain rate tensor (S_{ij}) is given by:

$$S_{ij} = \frac{1}{2}\left(\frac{\partial \tilde{u_i}}{\partial x_j} + \frac{\partial \tilde{u_j}}{\partial x_i}\right) \tag{3.19}$$

Turbulent diffusion term (D_t) for mass transport and energy transport is given by:

$$D_t = \rho\frac{\mu_t}{Sc_t} \tag{3.20}$$

And, turbulent conductivity term (Kc_t) is defined as:

$$Kc_t = \frac{\rho\mu_t}{Pr_t}Cp \tag{3.21}$$

The transport equation for turbulent kinetic energy k is:

$$\frac{\partial\left(\bar{\rho}k\right)}{\partial t} + \frac{\partial\left(\bar{\rho}\tilde{u_i}k\right)}{\partial x_i} = \tau_{ij}\frac{\partial \tilde{u_i}}{\partial x_j} + \frac{\partial}{\partial x_j}\left(\frac{\mu+\mu_t}{Pr_k}\right)\frac{\partial k}{\partial x_j} - \bar{\rho}\epsilon + \frac{C_s}{1.5}S_s \tag{3.22}$$

The transport equation for dissipation of turbulent kinetic energy ϵ is given by:

$$\begin{aligned}\frac{\partial\left(\bar{\rho}\epsilon\right)}{\partial t} &+ \frac{\partial\left(\bar{\rho}\tilde{u_i}\epsilon\right)}{\partial x_i} \\ &= \frac{\partial}{\partial x_j}\left(\frac{\mu+\mu_t}{Pr_{\epsilon}}\frac{\partial\epsilon}{\partial x_j}\right) \\ &+ C_{\epsilon 3}\bar{\rho}\epsilon\frac{\partial \tilde{u_i}}{\partial x_i} \\ &+ \left(C_{\epsilon 1}\frac{\partial \tilde{u_i}}{\partial x_j}\tau_{ij} - C_{\epsilon 2}\bar{\rho}\epsilon + C_s S_s\right)\frac{\epsilon}{k} \\ &+ S - \bar{\rho}R_{\epsilon}\end{aligned} \tag{3.23}$$

$$R_\epsilon = C_\mu \eta^3 \left(\frac{1 - \frac{\eta}{\eta_o}}{1 + \beta \eta^3} \right) \frac{\epsilon^2}{k} \tag{3.24}$$

$$\eta = \frac{k}{\epsilon} \sqrt{2 S_{ij} S_{ij}} \tag{3.25}$$

$$S_{ij} = \frac{1}{2} \left(\frac{\partial \tilde{u_i}}{\partial x_j} + \frac{\partial \tilde{u_j}}{\partial x_i} \right) \tag{3.26}$$

$$\tilde{u_i} = \frac{\rho \bar{u}_i}{\bar{\rho}} \tag{3.27}$$

$$\tilde{u_j} = \frac{\rho \bar{u}_j}{\bar{\rho}} \tag{3.28}$$

3.6.2 Chemical kinetics

Chemical kinetics deal with rate of chemical reaction where two or more molecules i.e. reactants interact with each other to form products.

For a multi-step reactions, it can be written as:

$$\sum_{s=1}^{N} v'_{sj} X_s \leftrightarrow \sum_{s=1}^{N} v''_{sj} X_s \tag{3.29}$$

The net rate of production of species s is given by:

$$\dot{\omega_s} = \sum_{j=1}^{J} v_{sj} q_j \tag{3.30}$$

$$v_{sj} = v''_{sj} - v'_{sj} \tag{3.31}$$

The rate of progress variable q_j is given by:

$$q_j = k_{fj} \prod_{s=1}^{N} [X_s]^{v_{sj}\prime} - k_{rj} \prod_{s=1}^{N} [X_s]^{v_{sj}\prime\prime} \tag{3.32}$$

$$k_{fj} = A_j T^{\beta_j} exp \left(\frac{-Ea_j}{RT} \right) \tag{3.33}$$

For a reversible reaction at equilibrium condition:

$$aA + bB \leftrightarrow cC + dD \tag{3.34}$$

$$k_{f_j} [A]^a [B]^b = k_{r_j} [C]^c [D]^d \tag{3.35}$$

$$\frac{k_{f_j}}{k_{rj}} = \frac{[C]^c [D]^d}{[A]^a [B]^b} \tag{3.36}$$

$$\frac{k_{f_j}}{k_{r_j}} = k_{c_j} \tag{3.37}$$

Now, rate of change of temperature is given by:

$$\frac{dT}{dt} = \frac{V \frac{\partial P}{\partial t} - \sum_i h_i \dot{\omega_i}}{\sum_i [X_i] C p_i} \tag{3.38}$$

Detailed reaction mechanism of H_2 and O_2

The twelve steps reaction mechanism, a reduced set of twenty one elementary reactions known as San Diego reaction mechanism for describing hydrogen combustion is used in this simulation. It describes accurately premixed and non-premixed combustion as well as auto-ignition and detonations over the whole flammability range from low to very high pressure (Boivin et al., 2011).

Table 3.4: Reduced twelve steps reaction mechanism for H_2 & O_2 (Boivin et al., 2011)

ELEMENTS H O N END SPECIES H_2 H O_2 O OH HO_2 H_2O_2 H_2O N_2 END				
S.NO.	**Reactions**	**Pre-exponential factor**	**Temperature Exponent**	**Activation Energy**
1	H + O_2 = O + OH	3.52E+16	-0.7	1.71E+04
	Reversible reaction	7.04E+13	-0.26	1.43E+02
2	O + H_2 = H + OH	5.06E+04	2.67	6.29E+03
	Reversible reaction	3.03E+04	2.63	4.84E+03
3	OH + H_2 = H + H_2O	2.27E+09	1.3	3.64E+03
	Reversible reaction	1.28E+10	1.19	1.87E+04
4	H + O_2 + M => HO_2 + M	5.75E+19	-1.4	0.00E+00
5	HO_2 + H => OH + OH	7.08E+13	0	2.94E+02
6	HO_2 + H = H_2 + O_2	1.66E+13	0	8.22E+02
	Reversible reaction	2.69E+12	0.36	5.54E+04
7	HO_2 + OH => H_2O + O_2	2.89E+13	0	-4.97E+02
8	H + OH + M = H_2O + M	4.00E+22	-2	0.00E+00
	Reversible reaction	1.03E+23	-1.75	1.19E+05
9	H + H + M = H_2 + M	1.30E+18	-1	0.00E+00
	Reversible reaction	3.04E+17	-0.65	1.04E+05
10	HO_2 + HO_2 => H_2O_2 + O_2	3.02E+12	0	1.39E+03
11	H_2 + HO_2 => H_2O_2 + H	1.62E+11	0.61	2.39E+04
12	H_2O_2 + M => OH + OH + M	8.15E+23	-1.9	4.96E+04
Units are s, mol, cm3□, cal,Kelvin				

3.6.3 Combustion modeling

One of the most important physical phenomena in combustion is turbulent combustion which includes two important aspects i.e. reaction and flow mechanism. The reaction occurs between the two reacting species having certain energies and as a result change

in enthalpy takes place. With the involvement of turbulence, eddies formation take place and these eddies prompt higher mixing of the chemical species. Since, higher mixing induces more reaction resulting in large change in enthalpy, this change in enthalpy affects the buoyancy of the flow, forming more eddies which drive more turbulence. As a result, turbulence affect the mixing time, therefore turbulence combustion must be considered while simulating combustion phenomena. Here, partially stirred reactor mechanism (PaSR) model is included, as PaSR models has shown promising results with the inclusion of multiple reaction mechanism. This combustion model is based on the principle that under turbulent condition, the computation domain is divided into reactive and non-reactive zone. The fraction of reactive cell is determined by a factor λ.

Mathematically,

$$\lambda = \frac{\tau_C}{\tau_C + \tau_M} \tag{3.39}$$

3.7 Initial boundary conditions & control parameters

3.7.1 Initial boundary conditions

Table 3.5: Initial boundary conditions at the -180°crank angle i.e. beginning of compression stroke

Parameters	Internal Field	Piston	Liner	CylinderHead
alphat	0	alphatWallFunction	alphatWallFunction	alphatWallFunction
epsilon	100	epsilonWallFunction	epsilonWallFunction	epsilonWallFunction
k	1	kqRWallFunction	kqRWallFunction	kqRWallFunction
nut	0	nutkWallFunction	nutkWallFunction	nutkWallFunction
H2	0.0285	zeroGradient	zeroGradient	zeroGradient
O2	0.2265	zeroGradient	zeroGradient	zeroGradient
N2	0.745	zeroGradient	zeroGradient	zeroGradient
H2O	0	zeroGradient	zeroGradient	zeroGradient
P	1.00E+05	zeroGradient	zeroGradient	zeroGradient
T	500	433	373	383
Qdot	0	0	0	0
U	(0,0,0)	movingWallVelocity	noSlip	noSlip
Ydefault	0	zeroGradient	zeroGradient	zeroGradient

3.7.2 Simulation control

The simulation is carried out between -180° to 180° crank angle displacement i.e. from the beginning of compression stroke to the end of expansion stroke. The time step taken for each iteration is 0.25°crank angle before the reaction starts and 0.00025 after the reaction has started to keep the maximum courant number less than 0.3. Different discretization schemes are utilized for the different terms in the discretized equations. Time discretization is done using euler, and gradient discretization is done using gauss linear. Similarly, the discretization of divergence term is done using gauss upwind, laplacian term and surface gradient term is done using gauss linear with limited corrector factor of 0.5. Finally, the interpolation scheme is done using a linear scheme.

3.8 Simulation & post-processing Analysis

Once the setup is complete, the respective solver is executed through command window for further post-processing & analysis. The post-processing & analysis are important for interpreting the results through visualizations, extracting numerical data, monitoring convergence and verifying the accuracy of the solution. If the simulation results fail to converge, time steps parameter is modified in control dict file for maintaining stability criterion through monitoring & keeping Courant Friedrich Lewy number (CFL) less than 1. Here, the post-processing is done through paraView to visualize simulation results such as pressure, temperature, mass-fraction, heat of reaction etc.

3.9 Validation & verification of simulation results

The validation & verification of the simulation results is usually done through monitoring the errors in the numerical simulation and also ensuring that the governing equations are properly implemented or not. Generally, the validation & verification is done through time step sensitivity analysis, mesh independence study and experimental results. Here, the verification is done through both time step sensitivity analysis and mesh independence study.

3.9.1 Time step sensitivity analysis

Figure 3.4 and 3.5 illustrates time step sensitivity analysis at diferent CFL numbers of 0.1, 0.2 and 0.3 respectively. Figure 3.4 demonstrates mean pressure variation at different crank angle displacement resulting due to H_2 fuel premixed combustion in internal combustion engine at different CFL number. Similarly, figure 3.5 shows mean temperature variation at different crank angle displacement at different CFL number resulting due to combustion of H_2 premixed fuel mixture in HCCI engine. In both figure, there is no any change in mean pressure and mean temperature plots taken at different CFL number proofs verification of simulation results.

Time step sensitivity analysis for mean pressure variation at different Courant-Friedrichs-Lewy (CFL) number

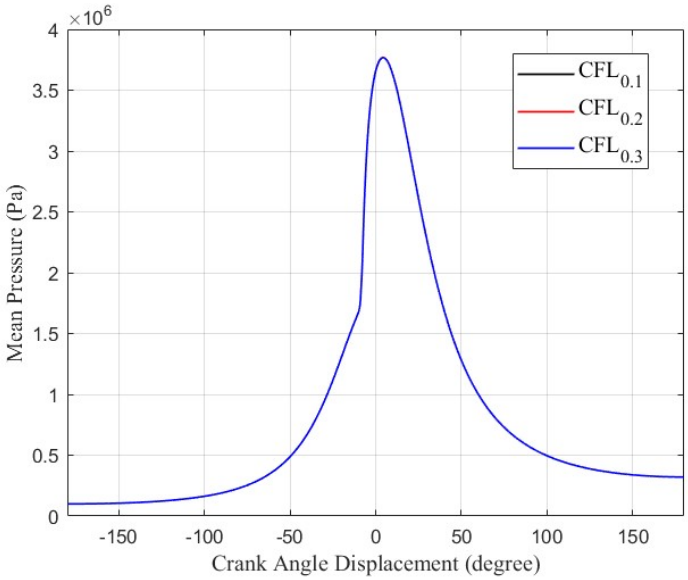

Figure 3.4: Time step sensitivity analysis of mean pressure variation at different CFL number

Time step sensitivity analysis for mean temperature variation at different Courant-Friedrichs-Lewy (CFL) number

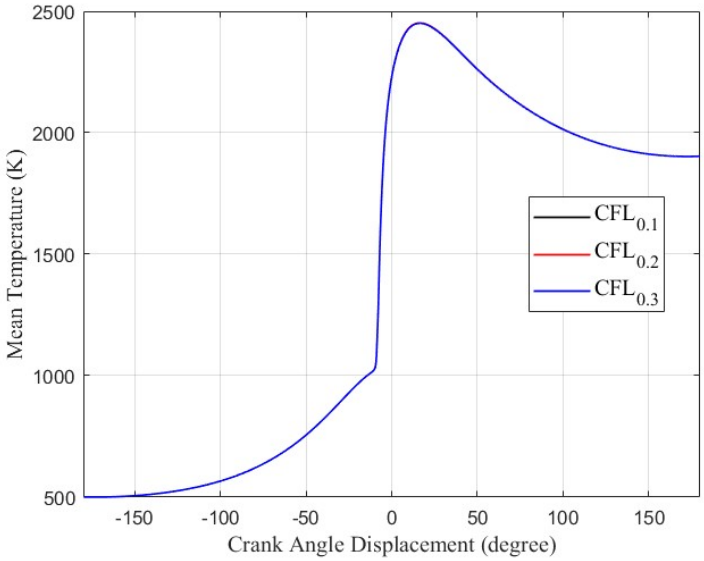

Figure 3.5: Time step sensitivity analysis of mean temperature variation at different CFL number

3.9.2 Mesh independence study

A detailed mesh independence study is performed to ensure accuracy and numerical study of the simulation results. This analysis includes observing variation in thermodynamic properties with crank angle revolution with different cell number to determine the concept such that further refinement not only has a negligible change on the results but also save computational time and resources.

Table 3.6: Mesh Independence Study

S.no.	Grid type	No. of Cells	Cell types	Pmax (bar)	Tmax (K)
1	Mesh I	27544	Hexahedral	37.7	2451
2	Mesh II	55088	Hexahedral	38.0	2488
4	Mesh III	220352	Hexahedral	38.0	2498

Table 3.6 illustrates peak mean pressure and peak mean temperature variation at different cell number. Mesh I has 27544 hexahedral cells which has peak mean in-cylinder pressure and temperature value of 3.77 bar and 2451 K respectively. Similarly, mesh II has 55088 hexahedral cells having peak mean in-cylinder pressure and temperature value of 3.8 bar and 2488 K respectively. In addition, mesh III has 220352 hexahedral cells having peak mean in-cylinder pressure and temperature value of 3.8 bar and 2498 K respectively. Since there is no significant difference in peak in-cylinder pressure and temperature, mesh I is considered for computational analysis in order to save computational time.

Mesh independence study for mean pressure variation

Figure 3.6 illustrates mean in-cylinder pressure variation for different type of mesh size. Since there is no significant variation of mean in-cylinder pressure along CAD for all three meshes. Here, mesh I has peak in-cylinder pressure value of 3.7 bar whereas mesh II and mesh III has both peak in-cylinder pressure value of 3.8 bar at around 10°ATDC. Furthermore, all the three meshes of different mesh sizes follow the same path of mean pressure variation along CAD showing consistence results of mean pressure.

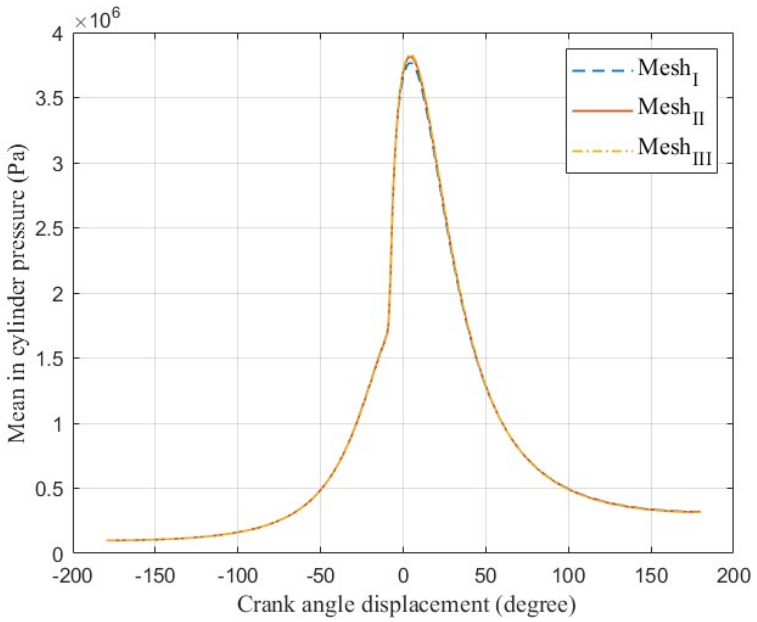

Figure 3.6: Mean pressure variation at different meshes

Mesh independence study for mean temperature variation

Figure 3.7 illustrates mean in-cylinder temperature variation for different mesh sizes. Since there is no significant variation of mean in-cylinder temperature along CAD for all three meshes. Here, mesh I has peak in-cylinder temperature value of 2450 K whereas mesh II and mesh III has both peak in-cylinder temperature value of 2488 K and 2498 K respectively at around 10°ATDC. In addition, all the three meshes follow the same path of mean temperature variation with CAD which shows consistence results.

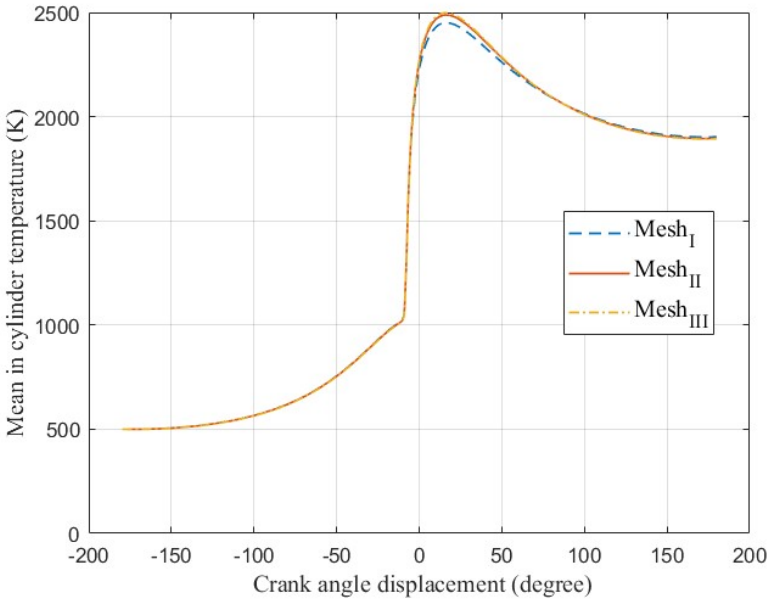

Figure 3.7: Mean temperature variation at different meshes

3.10 Documentation & reporting

The findings of the research work will be documented systematically and will be submitted to the respective Department as the thesis work as per the requirements of the Department of Mechanical & Aerospace Engineering.

3.11 Conclusion & recommendations

The conclusion of the research work on the combustion of the premixed hydrogen fuel mixture will be documented & further recommendation will be provided for the continuation of research on hydrogen combustion for the development of alternative fuel. The recommendations will be drawn from the learning experiences the author has gained while doing simulation of hydrogen gas premixed combustion in homogeneous charge compression ignition engine. Alongside the conclusion & recommendation, the research work will also attempt in serving it's purpose of identifying alternative fuel through observation of thermodynamic properties that assists in the development of fuel combustion lab in IOE, Pulchowk campus in near future.

CHAPTER FOUR: RESULTS AND DISCUSSION

In this simulation, 4-valve pent roof engine is observed between the beginning of compression stroke until the completion of expansion stroke. During this process, premixed hydrogen gas in presence of air at stoichiometric condition is compressed such that H_2 auto-ignites because of increase in mean in-cylinder pressure and temperature. The premixed hydrogen gas is kept at 1 bar at 500 K at the beginning of compression stroke. During compression stroke, pressure and temperature increases adiabatically such that it reaches around 17 bar at 1100 K when the piston is at -10°ATDC. As a result reaction occurs between reacting species i.e. H_2 and O_2 resulting in increase in peak mean pressure and temperature reaching about 37 bar at 2450 K and H_2O is formed as by product. Furthermore, the thermodynamic properties of hydrogen premixed fuel is compared with heptane fuel at stoichiometric conditions as well as testing parameters are calculated for both fuels in order to establish hydrogen as an alternative fuel. Again, the thermodynamic properties and the testing parameters of both the fuels are compared at the same mass flow rate during combustion in an internal combustion engine in order to demonstrate the fuel economy of hydrogen gas.

4.1 Variation of thermodynamic properties of premixed hydrogen fuel at stoichiometric mixture

4.1.1 Variation of pressure

- Graphical representation of mean pressure variation:

  Figure 4.1 illustrates the mean pressure variation for stoichiometric premixed hydrogen fuel mixture over the crank angle displacement of -180°CAD to 180°CAD. Initially, the pressure rises because of compression up to -10°ATDC. After -10°ATDC the mean pressure increases because of reaction between reacting species resulting in spontaneous increase in mean pressure reaching a value of 37 bar. The ignition delay can be clearly seen in figure 4.1 as ignition starts at about -10°ATDC as the temperature is not sufficient enough to ignite the fuel mixture before -10°ATDC. With SOI, the fuel mixture ignites spontaneously at multiple points resulting in increase in mean pressure steadily. B.T. Kannan & P.S. Srivathsan performed numerical simulation of iso-octane fuel in SI engine using spark ignition in openFoam. They considered the same KIVA geometry

for the simulation & the simulation were carried out with ignition on & off in the iso-octane fuel mixture. They simulated average pressure and temperature variation with CAD from -180° to 60° with combustion process initiation and observed both pressure and temperature rise with crank angle displacement. The nature of the curve for both the mean pressure and temperature variation is similar as obtained in figure 4.1 and 4.3 (Kannan and Srivathsan, 2016).

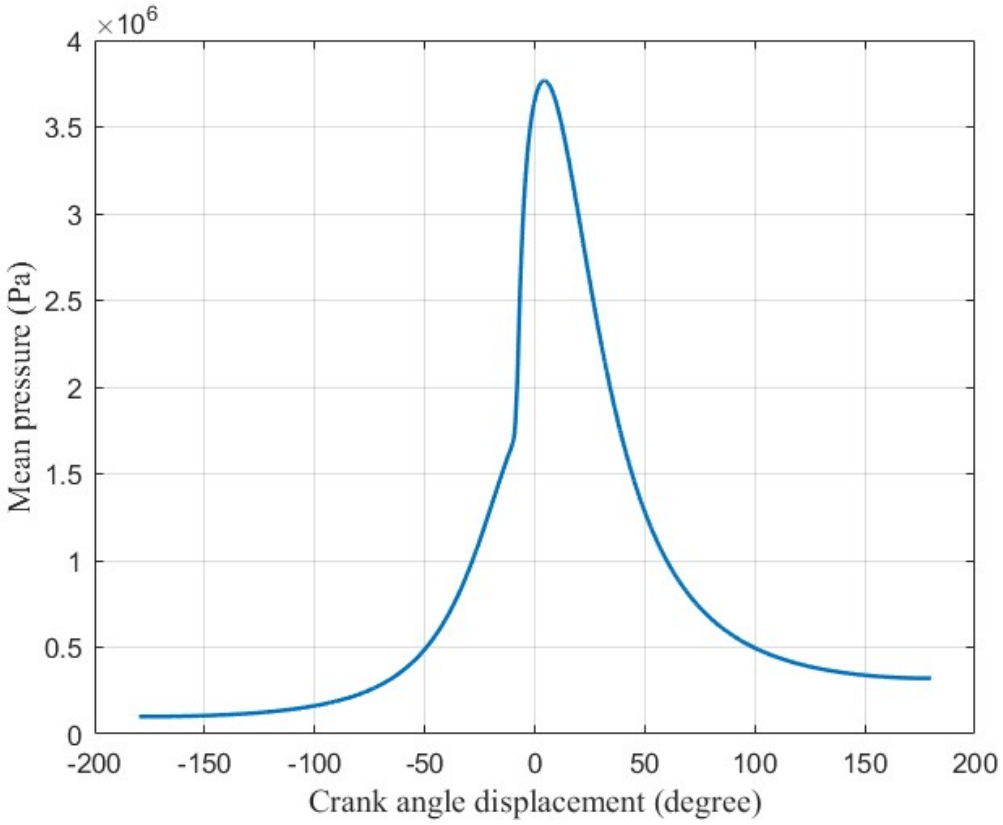

Figure 4.1: Variation of mean in-cylinder pressure between -180°CAD to 180°CAD

- Contour plot of variation of pressure:

  Figure 4.2 illustrates contour plot of the mean pressure variation of premixed hydrogen fuel mixture at stoichiometric values over the crank angle displacement of -180°CAD to 180°CAD. Initially, the pressure reading is 1 bar inside internal volume of the cylinder i.e. at the beginning of compression stroke. As the compression phenomena goes on, the mean pressure rises reaching a value of 17 bar at position of -10°ATDC before the reaction takes place. After -10°ATDC, the mean pressure increases steadily because of initiation of reaction between reacting species and also as the ignition goes on, the mean pressure value reaches a peak value of 37 bar. Similarly, the mean pressure decreases

during expansion stroke as the work is done by the gases pushing the piston towards BDC reaching a value of 3.2 bar at the end of expansion stroke. Here, the pressure contour at three different positions is shown.

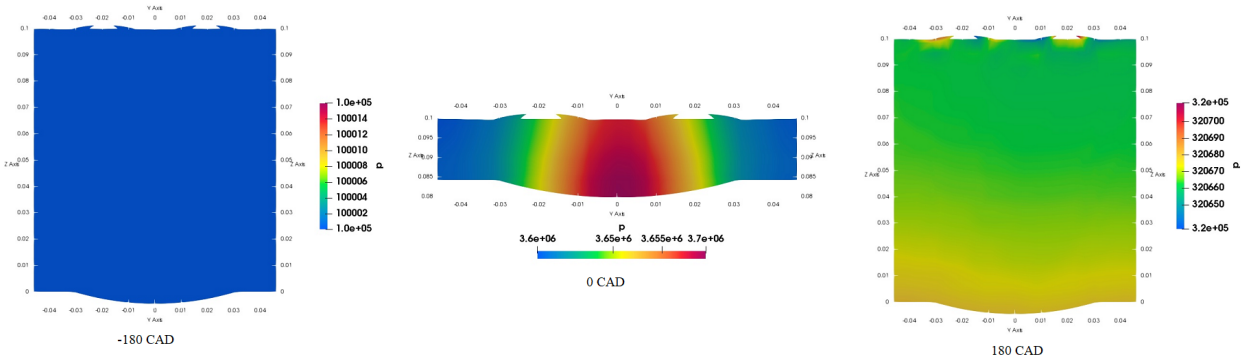

Figure 4.2: Contour showing mean pressure variation at different crank angle position

4.1.2 Variation of temperature

– Graphical representation of the mean temperature variation:

  Figure 4.3 illustrates the mean temperature variation for premixed hydrogen fuel mixture at stoichiometric condition over the crank angle displacement between compression stroke to the expansion stroke. Initially, the temperature rises because of compression as the work is done on the gases mixture i.e. up-to -10°ATDC. After -10°ATDC, the mean temperature increases because of the ignition of the reacting mixture reaching a peak mean value of 2450 K. In addition, the mean temperature decreases during the expansion stroke as the reacting gases does positive work on the piston assembly. Similarly, the ignition delay can also be seen in figure 4.3 as ignition starts after -10°ATDC. K.S. Kolambe & S.L. Borse presented numerical investigation of SI engine using an open source CFD tool- openFoam. The geometry including cylinder head, piston, liner and combustion domain was created by using blockMesh command using the engine dimension as that of KIVA test. In this work, the combustion behavior inside the cylinder of SI engine with different spark plug position were observed. Similarly, the incylinder pressure and temperature were observed with the post-processing tool Paraview. The nature of in-cylinder pressure and temperature variation with crank angle displacement shows similar trends as observed in figure 4.1 and 4.3 (Kolambe and Borse, 2016).

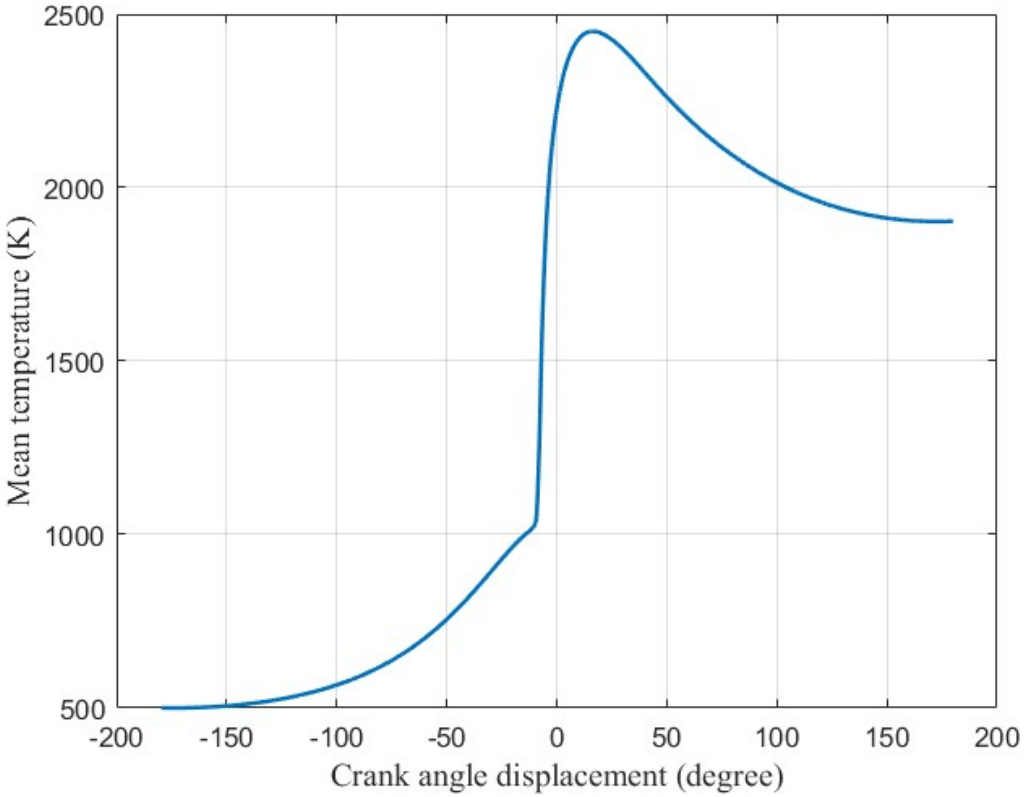

Figure 4.3: Variation of mean in-cylinder temperature between -180°CAD to 180°CAD

– Contour plot of variation of temperature:

  Figure 4.4 illustrates contour plot of the mean temperature variation for stoichiometric premixed hydrogen fuel mixture over the crank angle displacement of -180°CAD to 180°CAD. Initially, the mean temperature reading is 500 K as the compression phenomena goes on, the temperature increases because of compression stroke. As the mean temperature exceeds auto-ignition temperature of the fuel mixture, the fuel mixture get ignited as a result of which the mean temperature increases reaching a maximum peak value of 2500 K at most section inside the combustion chamber at around 0°crank angle position. After 0°crank angle, the temperature decreases due to adiabatic expansion as the work is done by the reacting gases on the piston surface reaching a mean value of around 1800 K. The contour plot of temperature variation at different position of CAD is shown here:

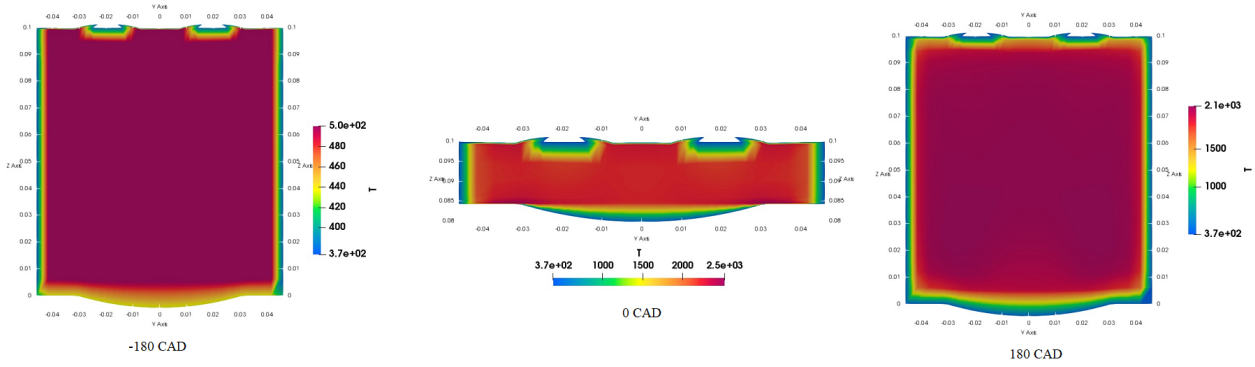

Figure 4.4: Contour showing mean temperature variation at different crank angle position

4.1.3 Actual pressure volume diagram

Figure 4.5 illustrates actual PV diagram of premixed hydrogen fuel combustion in HCCI engine. The compression process 1-2 occurs adiabatically as the volume decreases during this process because the piston moves from BDC to TDC as a result the work is supplied on the reacting gases during this process. The process 2-3 is at constant volume process where heat is released because of ignition of the reacting mixture as the compression temperature surpasses auto-ignition temperature of the fuel mixture. Similarly, the expansion process 3-4 occurs adiabatically and also the work is done by the reacting gases on the piston surfaces in order to obtain positive work-done. The workdone during the process 1-2 is negative whereas the workdone during the process 3-4 is positive. By subtracting the negative workdone from the positive workdone, the net work done per cycle is obtained. The nature of the PV diagram obtained in this simulation work is similar to the nature of the PV diagram as presented in his thesis work by Philip S. Zoldak (Zoldak, 2005). In addition, the actual indicator diagram is nearer to the ideal engine cycle because of higher laminar flame speed and as a result higher thermodynamic efficiency is achieved (Albayrak, 2012).

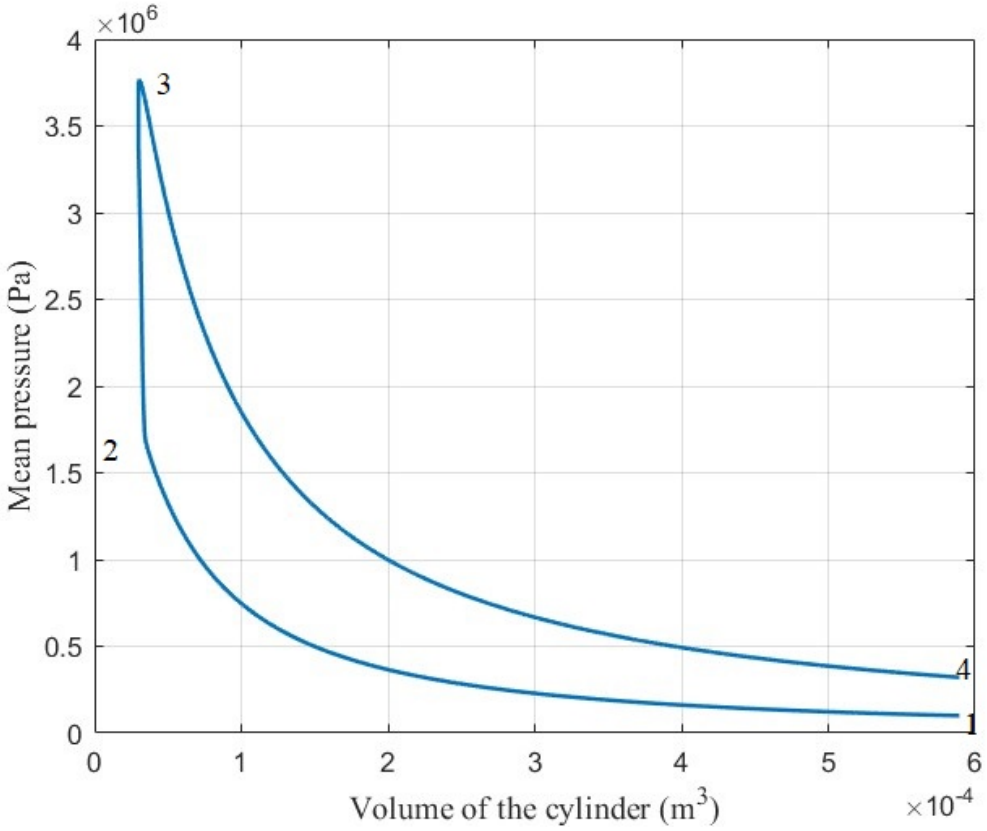

Figure 4.5: Actual PV diagram between -180°CAD and 180°CAD

4.1.4 Variation of specific volume

Figure 4.6 illustrates the variation of specific volume of premixed hydrogen fuel mixture inside the internal combustion engine with respect to crank angle movement. It is assumed that the gas mixture follows perfect gas law. During compression stroke, pressure increases because of compression and as soon as the heat addition takes place, the specific volume decreases from 1.9 m^3/kg reaching a minimum of 0.2 m^3/kg. Similarly, during expansion stroke, mean pressure decreases because of the work done by the reacting gases,however the specific volume increases reaching a maximum value of 1.7 m^3/kg. The nature of specific volume curve is U-shaped curve i.e. initially decreases reaching minimum value and then increases.

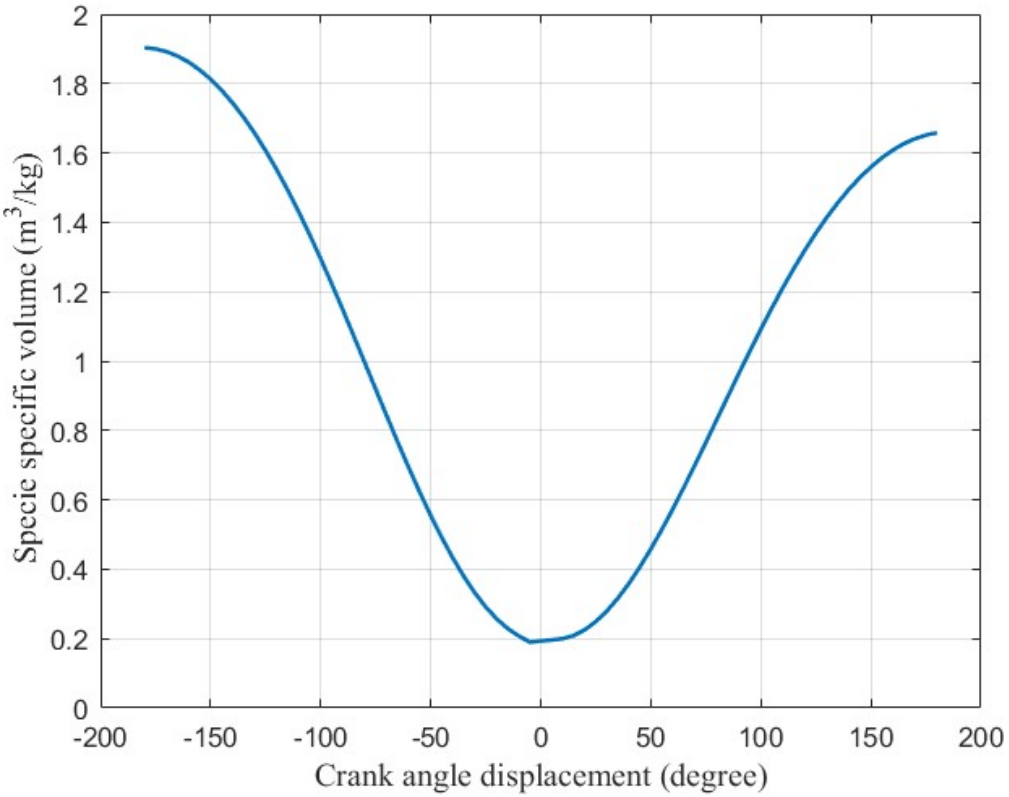

Figure 4.6: Variation of specific volume between -180°CAD and 180°CAD

4.1.5 Variation of mixture density

Figure 4.7 illustrates variation of mixture density over crank angle displacement of -180°CAD to 180°CAD. Initially because of compression of the gases mixture, the pressure increases as a result mixture density also increases using the relation of perfect gas. Similarly, during ignition of the gases mixture, the pressure increases steadily and also the density increases reaching a maximum value of 5.3 kg/m^3. Furthermore, the pressure decreases because of expansion stroke as the work is done by the reacting gases and so does the mixture density reaching a minimum value of 0.6 kg/m^3.

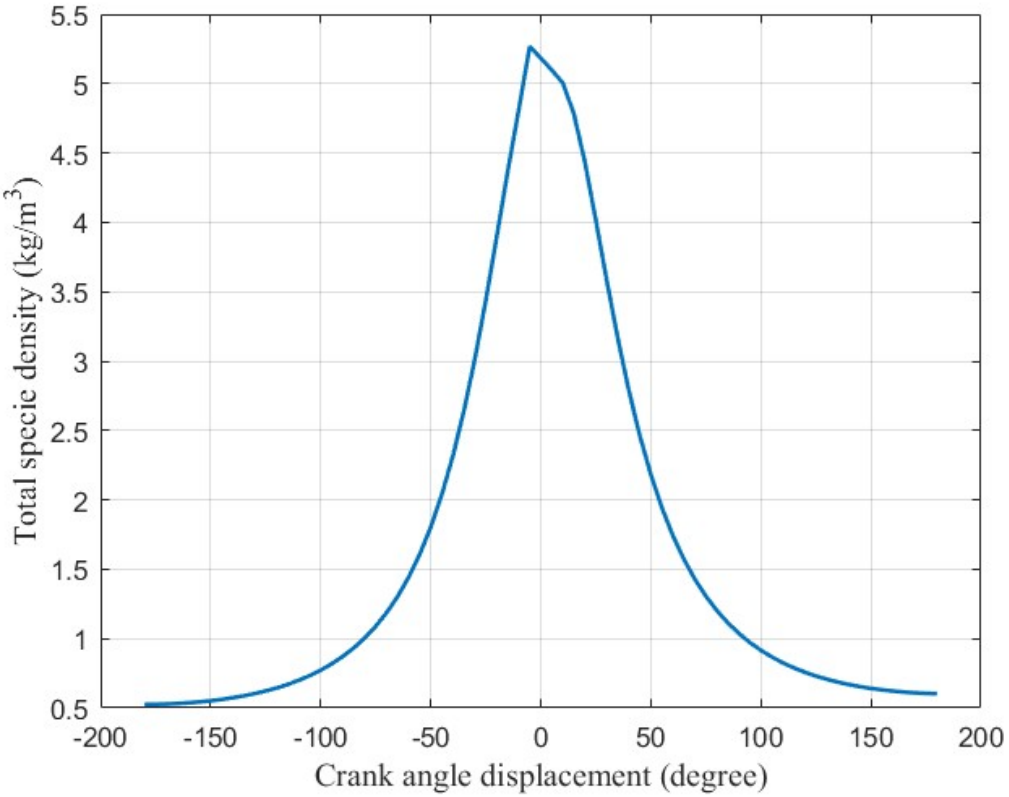

Figure 4.7: Variation of mixture density between -180°CAD and 180°CAD

4.1.6 Heat of reaction

Figure 4.8 shows heat of reaction of premixed hydrogen fuel combustion inside IC engine. Initially, the reaction does not occur because the temperature and pressure both are significantly low for the reaction to initiate. However, during compression stroke, the pressure and temperature both increases, as a result intra-molecular bonds start to break down and new inter-molecular bonds start to form. During this process, the heat is generally consumed to increase the activation energy of the reacting molecules. In addition, due to increase in temperature, the activation energy of the reacting mixture increases, as a result the reacting molecules are able to cross the energy barrier. Therefore, the older bonds break down and new bonds between the reacting molecules are formed. During this process, the enormous amount of heat is released known as heat of reaction or heat of combustion. Here, the peak heat released rate per unit volume is near about $11.5 * 10^9 Watt/m^3$. This heat of reaction is obtained in the narrow range as the ignition starts at several region within the combustion chamber in

HCCI engine. Fathi and his team presented SFLHR & MFLHR models for accurate prediction of gross heat release in HCCI engines during combustion which results in high heat release rate over a short combustion duration and it showed similar nature as present in figure 4.8 (Fathi et al., 2010).

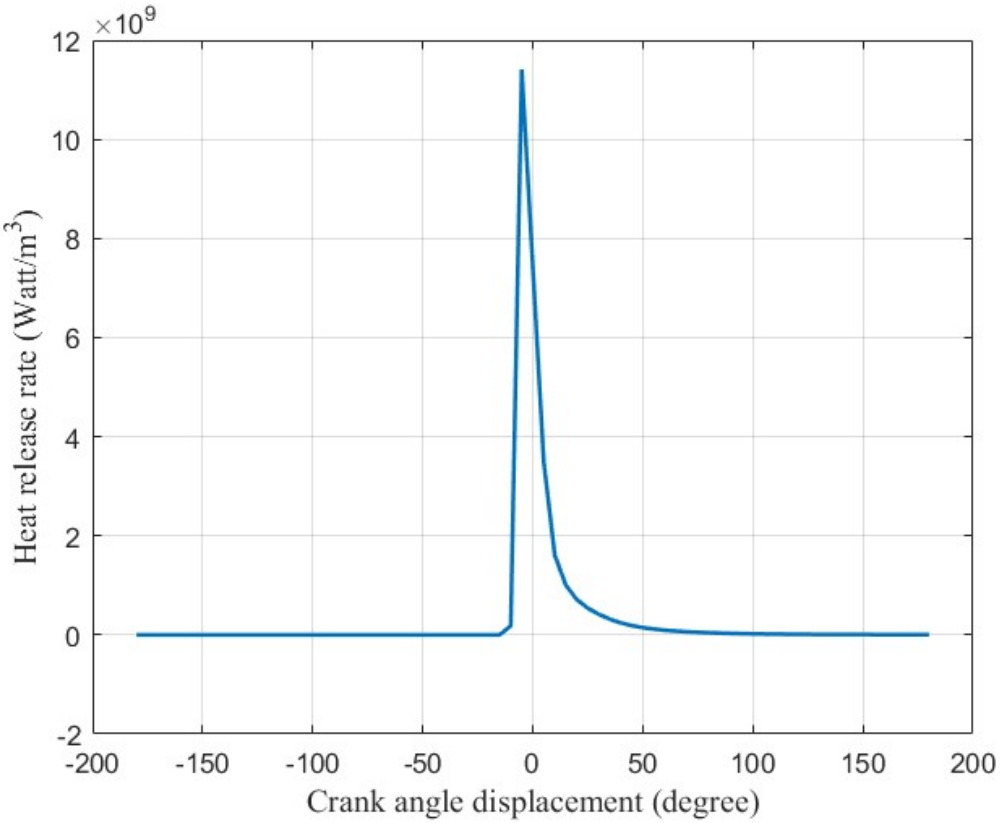

Figure 4.8: Variation of heat of reaction between -180°CAD and 180°CAD

4.1.7 Instantaneous power

Figure 4.9 illustrates instantaneous power plotted against a CAD for an HCCI engine using hydrogen premixed fuel. Initially the power is negative indicating that the work is done on the fuel mixture upto near TDC. As the piston moves near TDC, a sharp increase in power occurs due to the combustion of hydrogen fuel as the temperature exceeds auto-ignition temperature of the fuel mixture. The maximum power is achieved between 0°and 25°ATDC due to the force applied by the combustion gases during the expansion stroke. Similarly, the notch is seen before 0°CAD because of brief delay between ignition and the rapid pressure rise after combustion. Although, pressure starts to build up inside combustion chamber but it has not reached a level

to produce a strong positive power output, as a result notch is seen which causes a momentary reduction in power output.

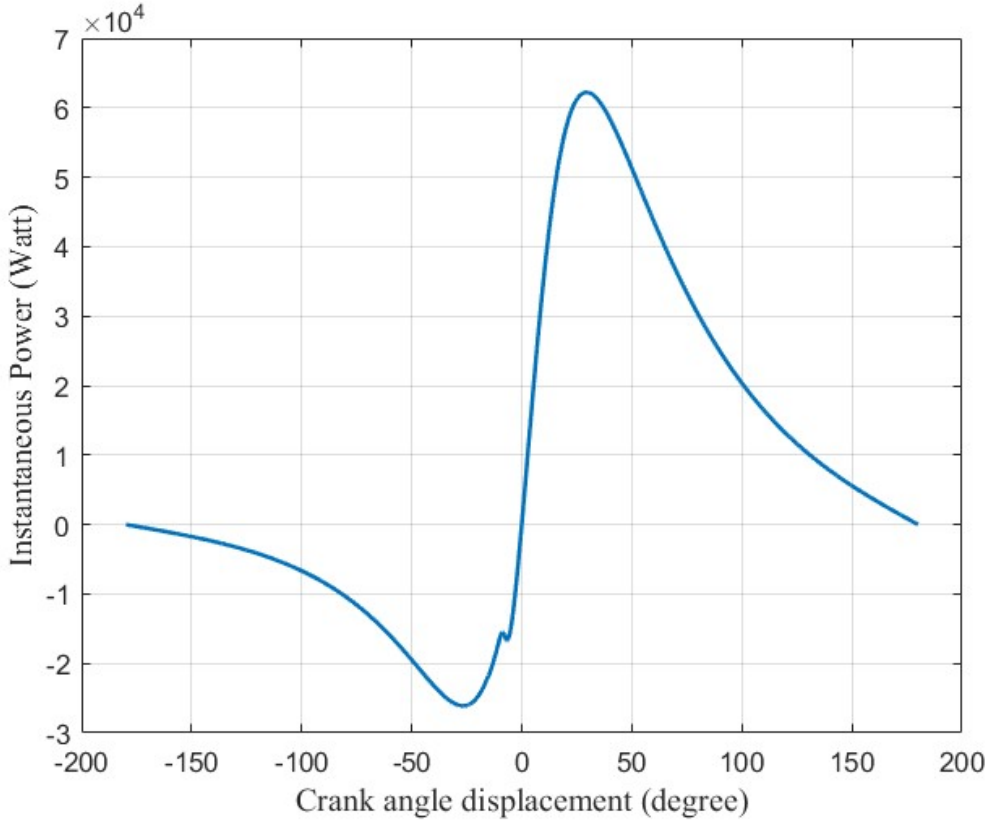

Figure 4.9: Instantaneous power between -180°CAD and 180°CAD

4.1.8 Mass-fraction of species

∗ Graphical representation of mass-fraction of species

Figure 4.10 represents how mass fraction of the species varies over crank angle displacement. Initially, the mass fraction of H_2, O_2 and N_2 is taken 0.0285, 0.2265 and 0.745 respectively. However, the mass fraction of other species is taken zero. With reaction proceedings, the mass fraction of H_2 and O_2 decreases whereas the mass fraction of H_2O increases over time and reaching a value of 0.25. However, the total mass fraction of the species remains constant i.e. equal to 1. In addition, this reduced twelve steps reactions mechanism does not consider emission modeling of NO_x i.e. N_2 dissociation over time. Different color codes are given for different species. Their utilization and formation over crank angle displacement is shown in figure 4.10.

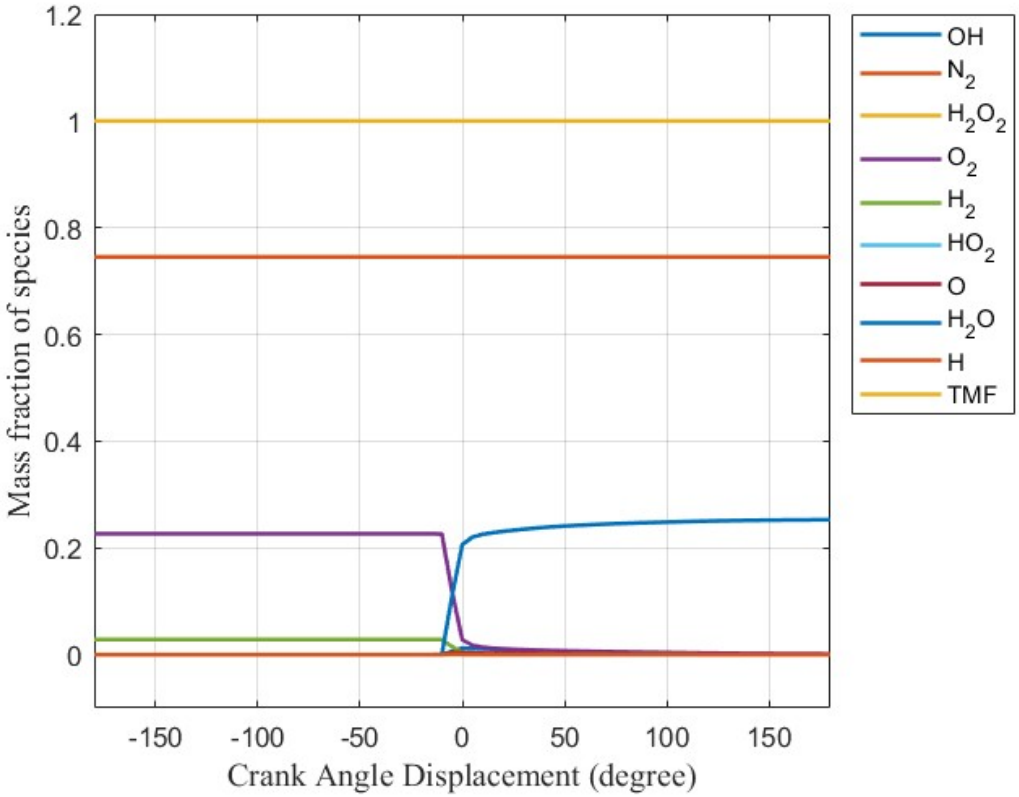

Figure 4.10: Variation of mass fraction of species over CAD

* Variation of mass-fraction of H_2

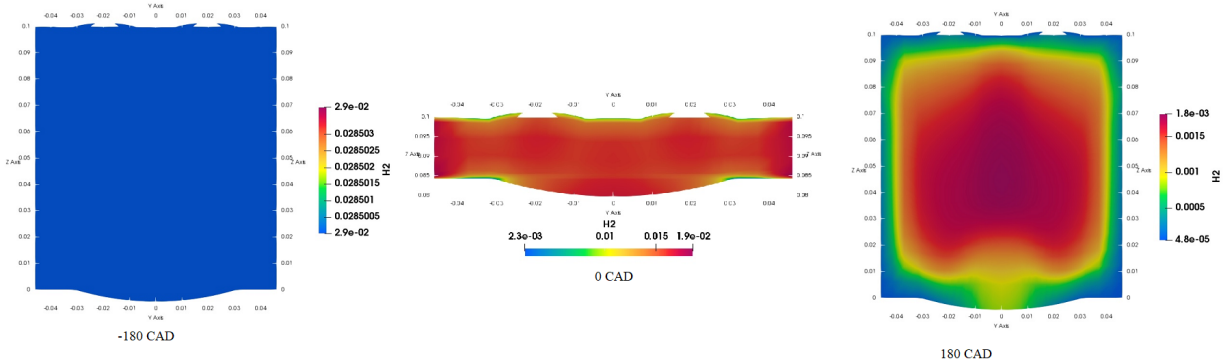

Figure 4.11: Variation of mass fraction of H_2 over crank angle displacement

* Variation of mass-fraction of O_2

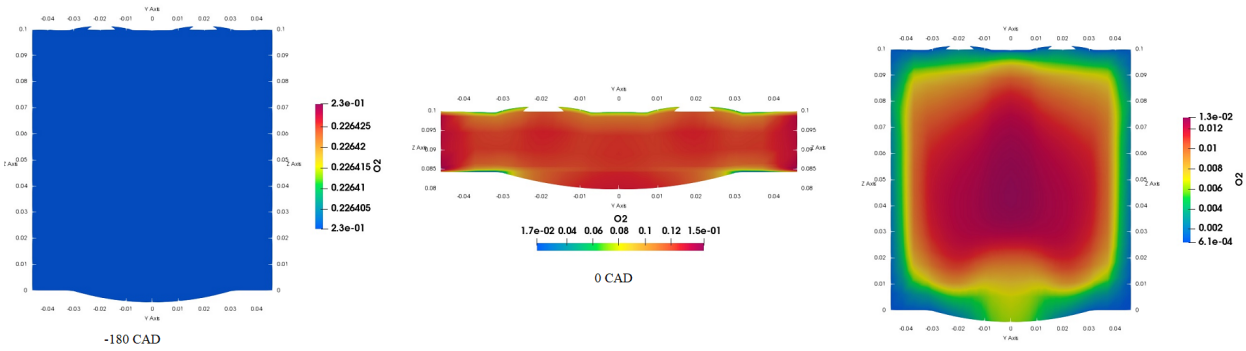

Figure 4.12: Variation of mass fraction of O_2 over crank angle displacement

∗ Variation of mass-fraction of H_2O

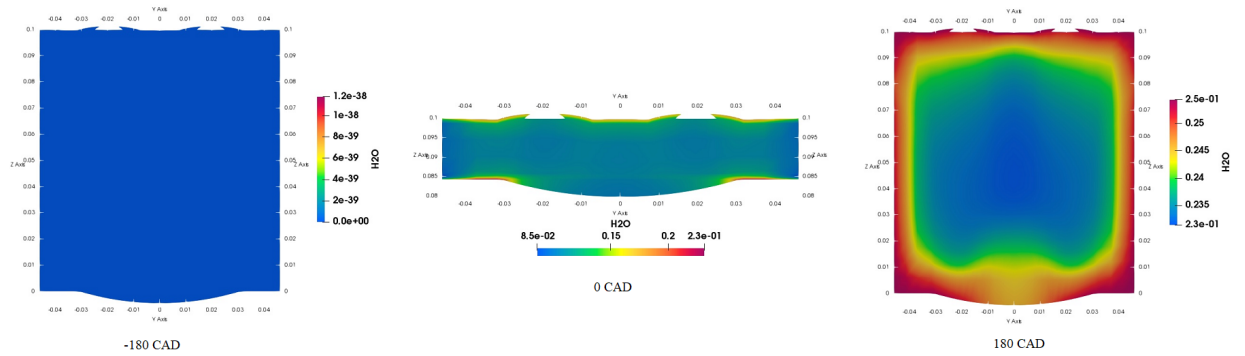

Figure 4.13: Variation of mass fraction of H_2O over crank angle displacement

Figure 4.11, 4.12, and 4.13 demonstrates contour plots of how mass fraction of different species like H_2, O_2, and H_2O varies along the crank angle displacement. Initially, the mass fraction of H_2 taken is 0.0285 i.e. at 180°CAD. With the revolution of engine cycle, the mass fraction of H_2 decreases and reaches a value of $1.8e^{-03}$ as shown in figure 4.11. Similarly, the mass fraction of O_2 decreases from 0.2265 to $1.3e^{-02}$ with crank displacement of -180°CAD to 180°CAD as shown in figure 4.12. However, the mass fraction of H_2O increases from 0 to 0.25 with engine revolution between compression to expansion stroke as shown in figure 4.13. Likewise, the mass fraction of intermediate species such as OH, H_2O_2, HO_2, O and H increases and decreases as the reaction progress with engine revolution.

4.2 Variation of thermodynamic properties at varying equivalence ratios of premixed hydrogen fuel

4.2.1 Variation of pressure

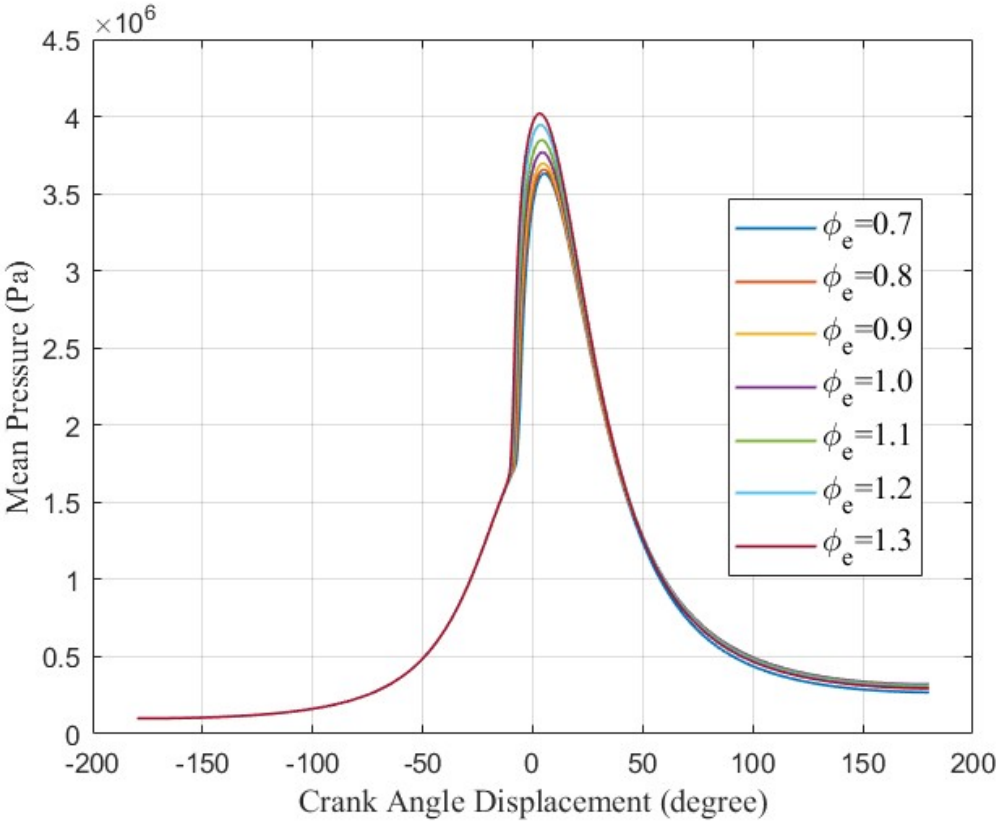

Figure 4.14: Mean pressure variation at different value of equivalence ratios

Figure 4.14 illustrates variation of mean pressure over CAD between -180°to 180°for varying values of ϕ_e. With increase in mass-fraction of H_2 due to increase in ϕ_e, the maximum mean pressure increases because of increase in reaction rate which results due to increase in frequency of collisions between reacting species. Additionally, the increase in the value of ϕ_e, the ignition delay period decreases because of the increase in collision frequency of the reacting species. The maximum value of mean pressure is achieved with equivalence ratios of 1.3 and the value is around 40 bar. Similarly, the peak mean pressure decreases with decreasing in ϕ_e. The minimum value of peak mean pressure is achieved with ϕ_e is equal to 0.7 and the value is around 36 bar. This figure 4.14 also illustrates wider flammability limits of hydrogen fuel mixture with minimum amount of mean pressure drop.

4.2.2 Variation of temperature

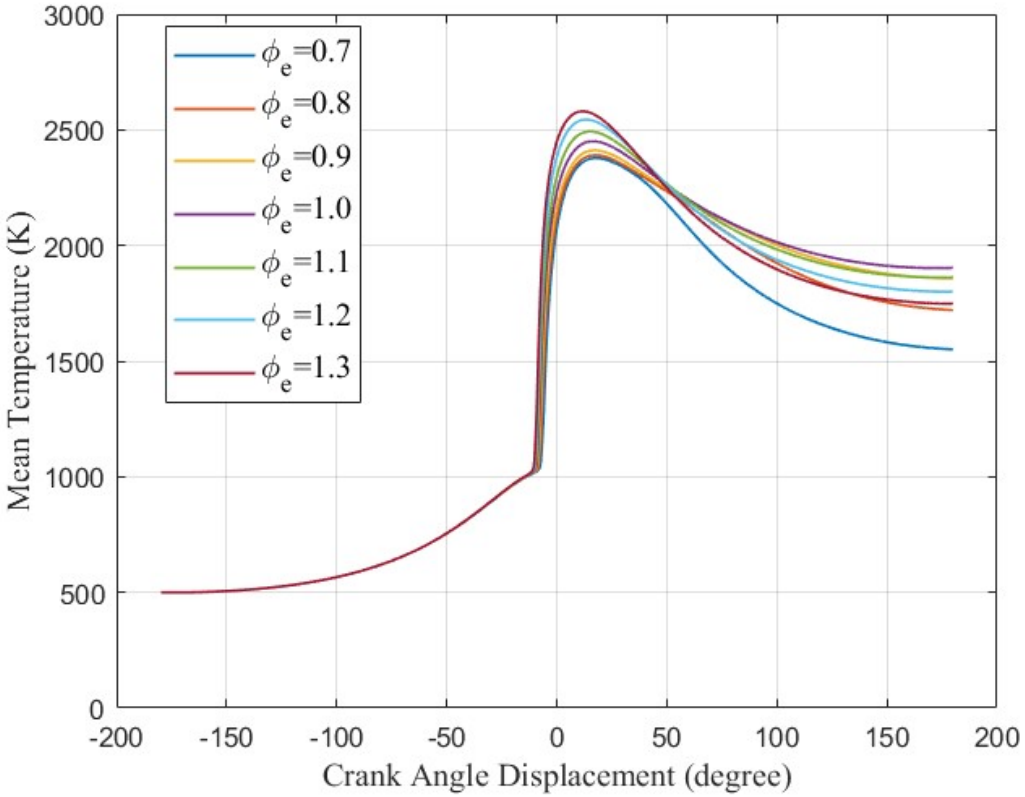

Figure 4.15: Mean temperature variation at different value of equivalence ratios

Figure 4.15 illustrates mean temperature variation over CAD between -180°to 180°i.e. between compression stroke to the end of expansion stroke for different values of ϕ_e. Likewise in mean pressure variation, mean temperature varies in a similar pattern as increase in mass-fraction of hydrogen fuel increases the rate of reaction between the colliding mixture. The peak mean temperature of 2600 K is obtained at maximum value of ϕ_e i.e. 1.3. Similarly, the minimum value of peak mean temperature achieved value is around 2400 K and it is obtained at minimum value of ϕ_e i.e. 0.7. With increase in mass-fraction of H_2, the ignition of the fuel starts early as shown in figure 4.15. The ignition of the fuel starts at -10.82°ATDC when the ϕ_e is equals to 1.3 whereas the ignition of the fuel starts at -7.69°ATDC when the ϕ_e is 0.7.

4.2.3 Variation of heat of reaction

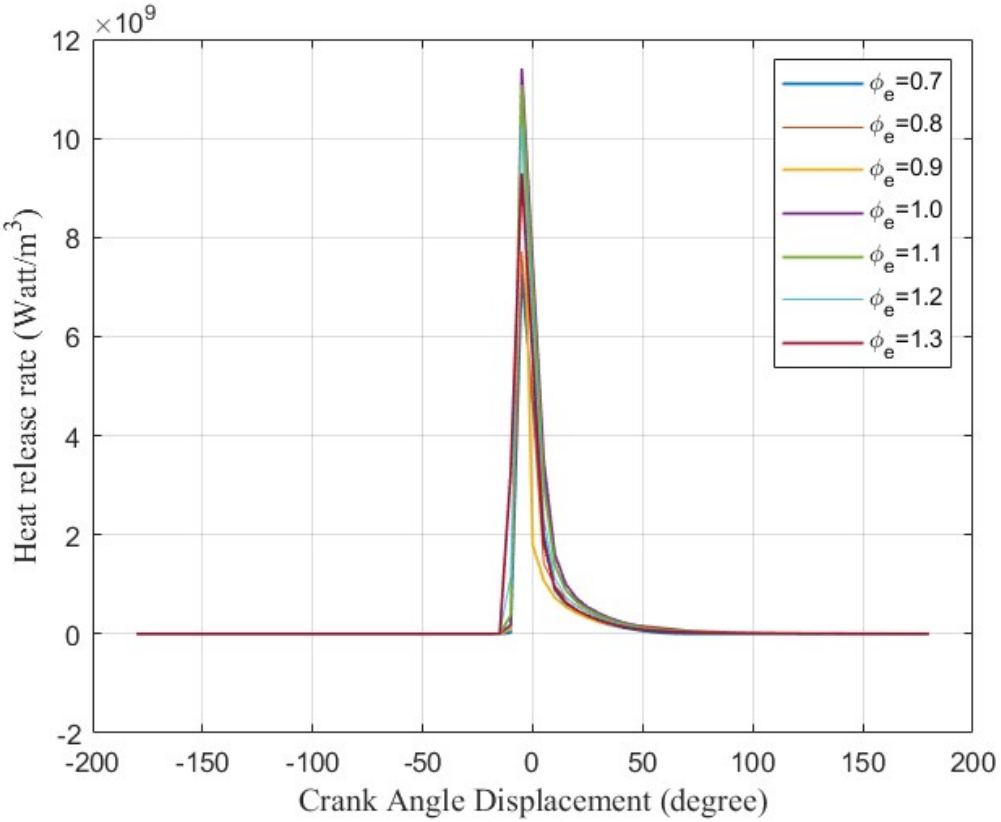

Figure 4.16: Comparison heat of reaction at different equivalence ratios

Figure 4.16 illustrates heat of reaction at different value of ϕ_e . The heat of reaction is maximum in case of ϕ_e is equal to 1.0 whereas heat of reaction is minimum in case of ϕ_e equals to 0.7. The heat released rate per unit volume decreases with increase in value of ϕ_e after ϕ_e is equal to 1 because large amount of fuel is available resulting in incomplete combustion and almost all the mass-fraction of O_2 is utilized during the reaction. Similarly, at ϕ_e less than 1, the heat of reaction decreases because less amount of fuel is available and almost all the fuel is consumed during the reaction resulting in lower rate of heat released per unit volume.

4.2.4 Variation of mass-fraction

Mass-fraction variation of H_2 at different values of equivalence ratios

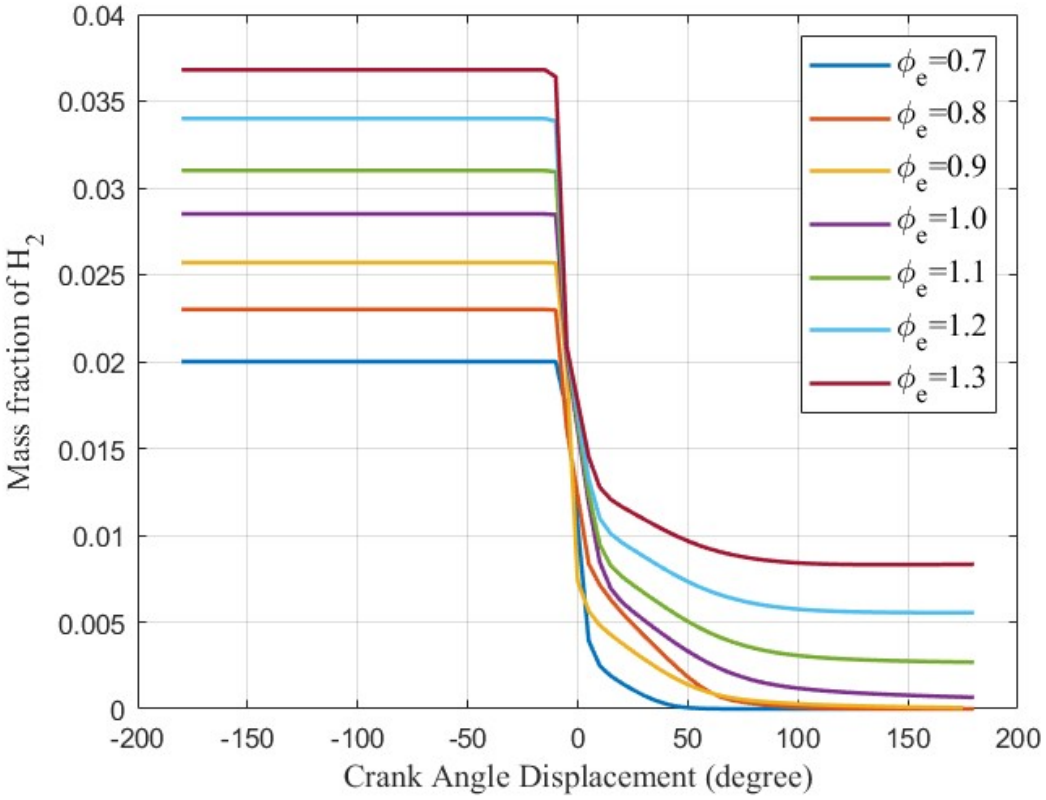

Figure 4.17: Mass fraction of H_2 variation at different value of equivalence ratios

Figure 4.17 illustrates variation of mass-fraction of H_2 over CAD between -180 to 180 at different value of ϕ_e between 0.7 to 1.3. With increase in ϕ_e initially, the remaining mass-fraction of H_2 after the completion of expansion stroke increases. Similarly, with decrease in ϕ_e at the beginning, the remaining mass-fraction of H_2 decreases with the end of expansion stroke i.e. minimum amount of H_2 at ϕ_e of 0.7 at the end of expansion stroke. At each case, the mass-fraction of H_2 decreases because of reaction between H_2 and O_2 inside internal combustion engine.

Mass-fraction variation of O_2 at different values of equivalence ratios

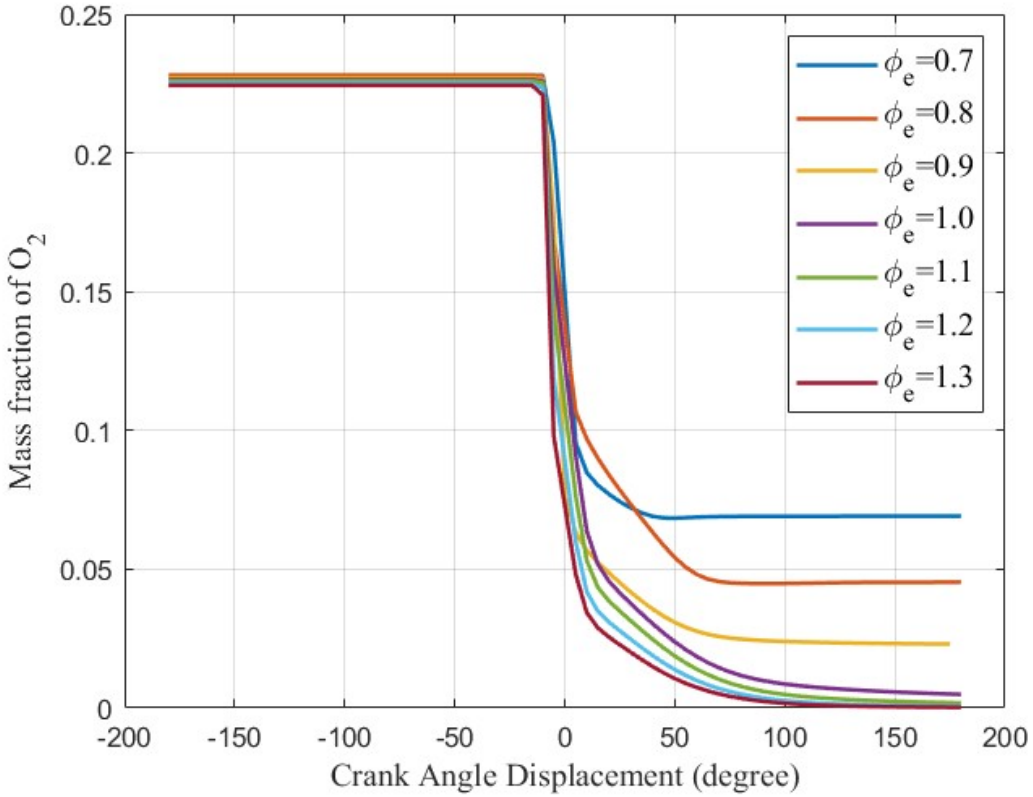

Figure 4.18: Mass fraction of O_2 variation at different value of equivalence ratios

Figure 4.18 shows variation of mass-fraction of O_2 with different values of ϕ_e ranging from 0.7 to 1.3. With higher value of ϕ_e initially, the mass-fraction of O_2 with the completion of expansion stroke decreases with minimum value at ϕ_e equals to 1.5. The mass-fraction of O_2 is consumed during chemical reaction at each value of ϕ_e as temperature surpasses auto-ignition temperature of hydrogen fuel during compression stroke, as a result old bonds are broken out and new bonds are formed which produces H_2O as by product.

Mass-fraction variation of H_2O at different values of equivalence ratios

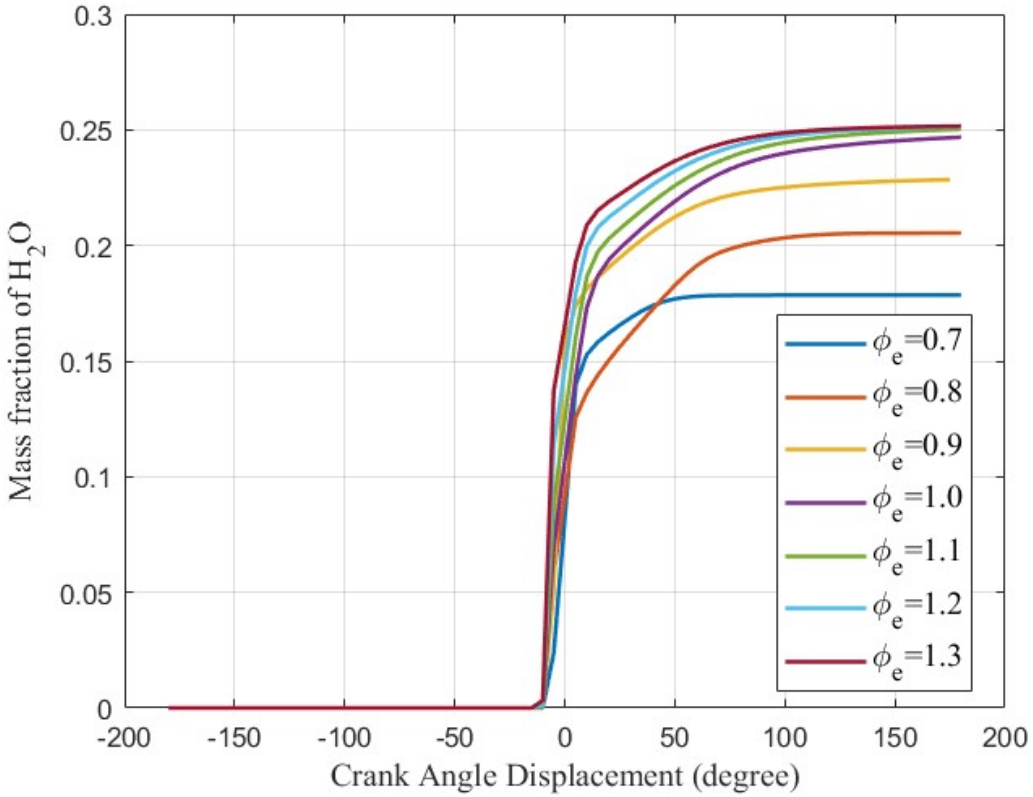

Figure 4.19: Mass-fraction of H_2O variation at different value of equivalence ratios

Figure 4.19 illustrates the variation of mass-fraction of H_2O at varying value of ϕ_e between 0.7 to 1.3 at different CAD. Initially, the mass-fraction of H_2O is zero because no reaction occurs at initial condition as the temperature is not sufficient enough to break the old H_2 & O_2 bonds. As the temperature is large enough to initiate reaction because of high increase in activation energy, mass-fraction of H_2O starts increasing with a maximum value of 0.25 around ϕ_e ranges between 1.0-1.3. However, at lower value of ϕ_e between 0.7-0.9, the mass-fraction of H_2O formed is quite less in-comparison to the H_2O formation at higher values of ϕ_e because at lower value of ϕ_e most of the mass-fraction of H_2 is consumed.

4.3 Variation of thermodynamic properties at different rpm of the engine of premixed hydrogen fuel at stoichiometric conditions

4.3.1 Variation of pressure

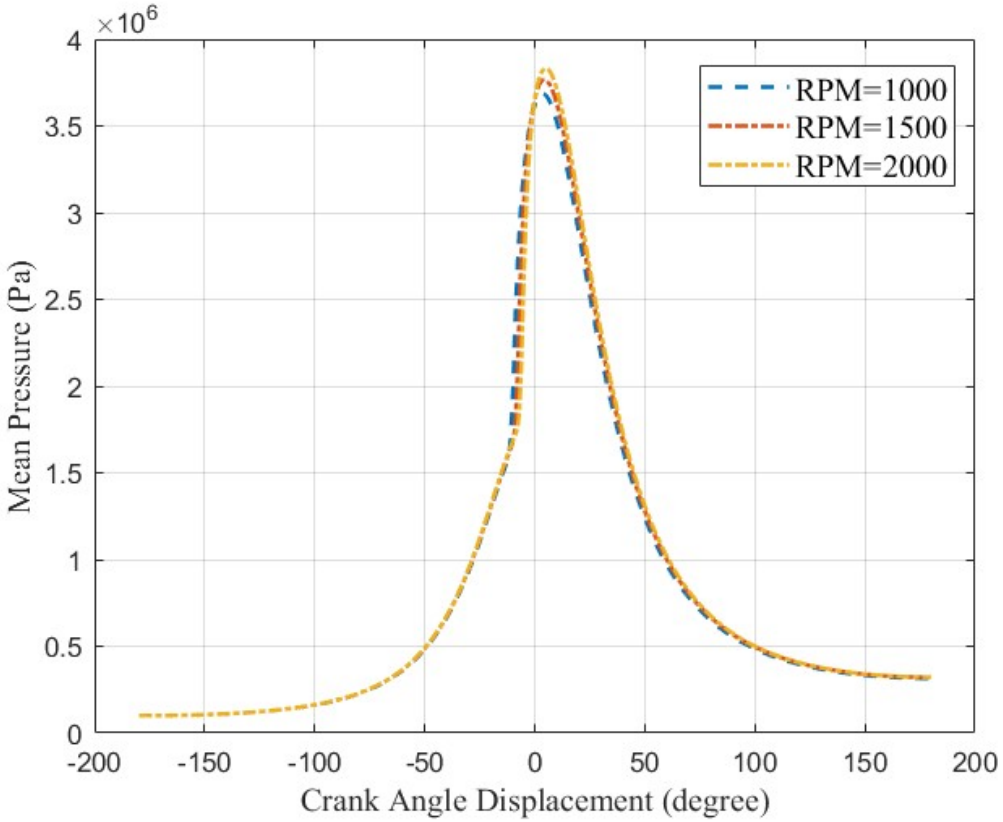

Figure 4.20: Mean pressure variation at different rpm of engine cycle

Figure 4.20 illustrates variation of mean in-cylinder pressure at different rpm of the engine plotted against CAD. Initially, the increase in mean pressure during compression stroke do not show any variation when plotted at different engine speed. However, with the initialization of reaction between reacting species, the mean in-cylinder pressure increases with increase in engine rpm because of faster combustion which results in rapid energy released . Also, the ignition delay increases with increase in engine rpm because of shorter residence time available for the reacting species. Although, there is no significant difference in maximum mean in-cylinder pressure when observed at different rpm, but the maximum mean in-cylinder pressure is obtained at 2000 rpm because of faster reaction rates.

4.3.2 Variation of temperature

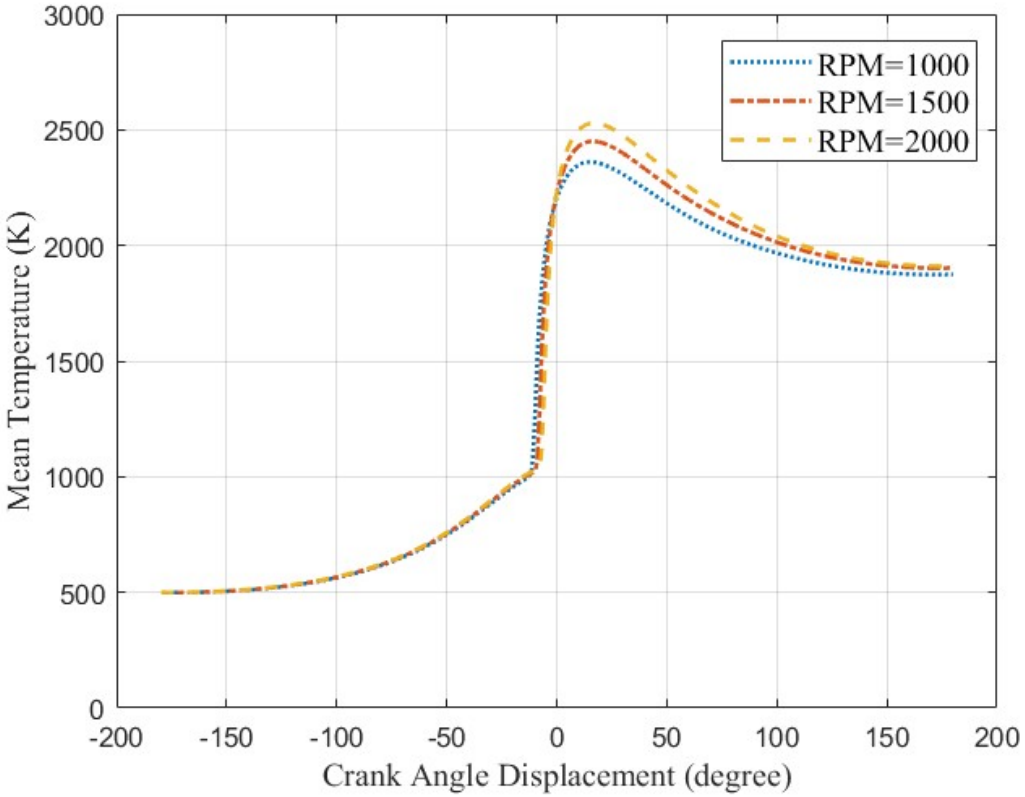

Figure 4.21: Mean temperature variation at different rpm of engine cycle

Figure 4.21 illustrates mean in-cylinder temperature variation at different rpm of engine plotted against CAD. As explained earlier, initially the increase in mean in-cylinder temperature is because of compression stroke at all engine rpm. As the temperature exceeds auto-ignition temperature of the reacting mixture, the H_2 fuel mixture ignites immediately resulting in intensive increase in peak mean temperature as a result the maximum mean in-cylinder temperature is achieved with higher engine rpm i.e. 2000. Similarly, the minimum peak mean in-cylinder temperature is observed at lower rpm i.e. 1500 because of lower combustion rates at lower engine speed.

4.4 Comparison of thermodynamic properties between hydrogen & heptane fuel at stoichiometric conditions

The thermodynamic properties such as mean in-cylinder pressure, mean in-cylinder temperature, specific volume, specific density, Heat of reaction and PV diagram is compared between H_2 & C_7H_{16} in order to establish hydrogen gas as an efficient fuel. All these properties are observed at stoichiometric mixture of respective fuel and keeping all the parameters same except initial fuel temperature to prevent heptane fuel from early combustion.

4.4.1 Comparison mean pressure variation between hydrogen fuel and heptane fuel

Figure 4.22 shows the mean in-cylinder pressure variation between H_2 and C_7H_{16} fuel mixture inside HCCI engine. Here, the mean pressure value consideration inside cylindrical volume is 1 bar. As the compression process goes on, the mean in-cylinder pressure increases adiabatically. As the temperature reaches about auto-ignition temperature of the fuel mixture, the fuel mixture ignites as a result the mean pressure increases steadily. In comparison to hydrogen fuel, the heptane fuel ignites early resulting in increase in mean pressure as the engine cycle progress. The early ignition of the heptane fuel indicates it's lower auto-ignition temperature in comparison to hydrogen fuel mixture. In comparison to mean pressure curve, the maximum mean pressure value of heptane fuel dominates the mean maximum pressure of hydrogen fuel because the single step reaction of heptane fuel results in the complete combustion of the fuel mixture as a results it over predicts the heat release rate.

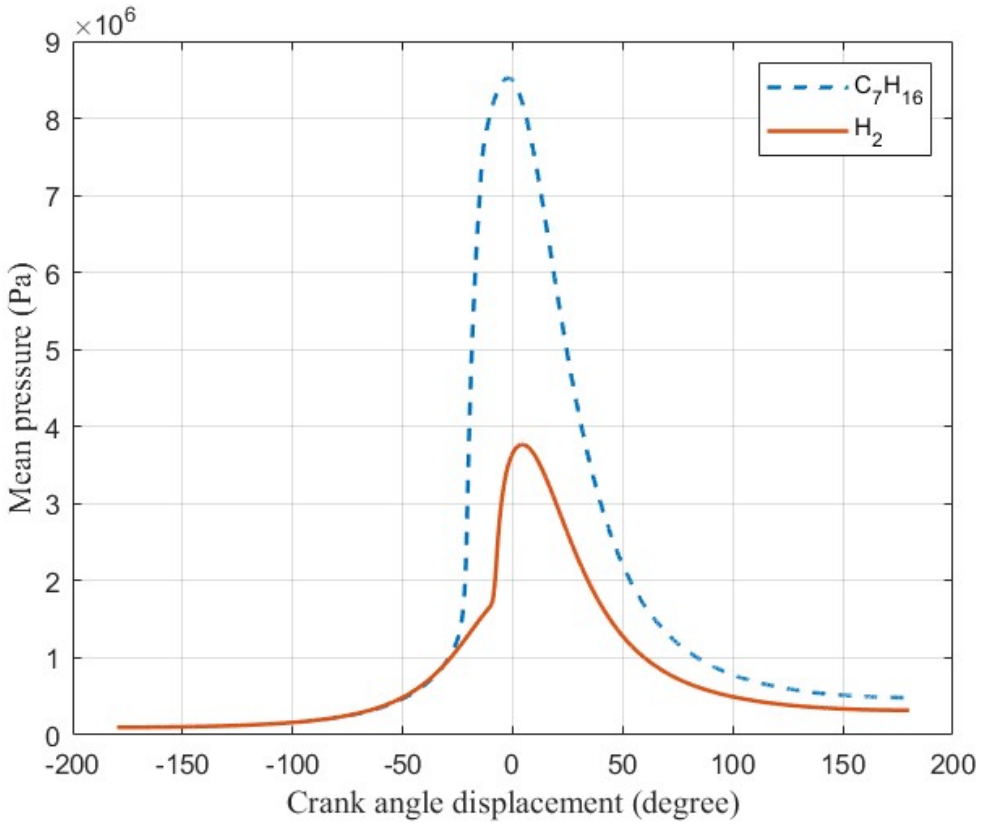

Figure 4.22: Variation of mean pressure between two fuels during combustion

4.4.2 Comparison mean temperature variation between hydrogen fuel and heptane fuel

Figure 4.23 illustrates the mean temperature variation between hydrogen fuel and heptane fuel mixture while simulating in internal combustion engine between compression stroke and expansion stroke. Here, the initial temperature of heptane fuel mixture is taken $400K$ (to prevent early ignition) whereas the initial temperature of hydrogen fuel mixture is taken $500K$ for making the hydrogen fuel to auto-ignite during compression stroke. During compression stroke, the temperature increases according to adiabatic process and reaches auto-ignition point. At auto-ignition point, the fuel mixture reacts because of increase in activation energy of the reacting mixture and ignition occurs resulting in increase in mean temperature steadily. Figure 4.23 compares the mean in-cylinder temperature of both the fuel mixtures. The difference in maximum mean temperature results due to complete combustion of the heptane fuel in comparison to hydrogen fuel mixture because of the simpler reaction mecha-

nism consideration in case of heptane fuel. This figure also compares ignition delay between both the fuel mixture. The ignition delay is seen less in heptane fuel mixture in comparison to hydrogen fuel.

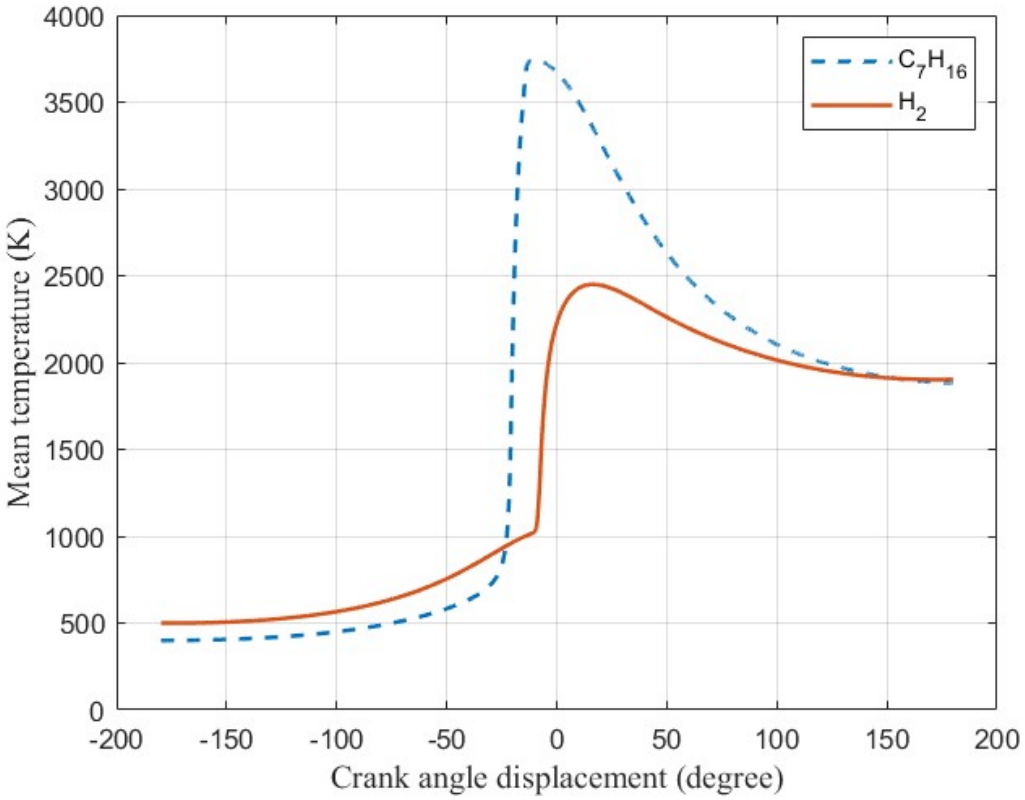

Figure 4.23: Variation of mean temperature between two fuels during combustion

4.4.3 Comparison actual pressure volume diagram between hydrogen and heptane fuel

Figure 4.24 demonstrates comparison of actual pressure volume diagram between heptane fuel and hydrogen fuel mixture. Points 1, 2, 3 and 4 represents work cycle for hydrogen fuel whereas points 1, 2', 3' and 4' represents work cycle for heptane fuel. Process 1-2 and 1-2' shows adiabatic compression process for hydrogen fuel and heptane fuel respectively. Similarly, process 2-3 and 2'-3' shows constant volume combustion for hydrogen fuel and heptane fuel respectively. In addition, process 3-4 and 3'-4' represents adiabatic expansion process for hydrogen and heptane fuel respectively. For both the cases, the process is observed between -180°CAD to 180°CAD as a result the cycle is not closed at the ends. This figure 4.24 illustrates

actual net work done per cycle obtained for both hydrogen and heptane fuel. It shows more positive work obtained in case of heptane fuel because of complete combustion of heptane fuel.

However, the negative workdone is observed around TDC in case of heptane fuel. It results in efficiency drop due to early start of combustion which causes the piston to experience increased cylinder pressure on the upward stroke towards TDC. This causes extra disadvantages work into the compression stroke causing a negative area in the PV diagram of the HCCI engine (Tóth-Nagy, 2024).

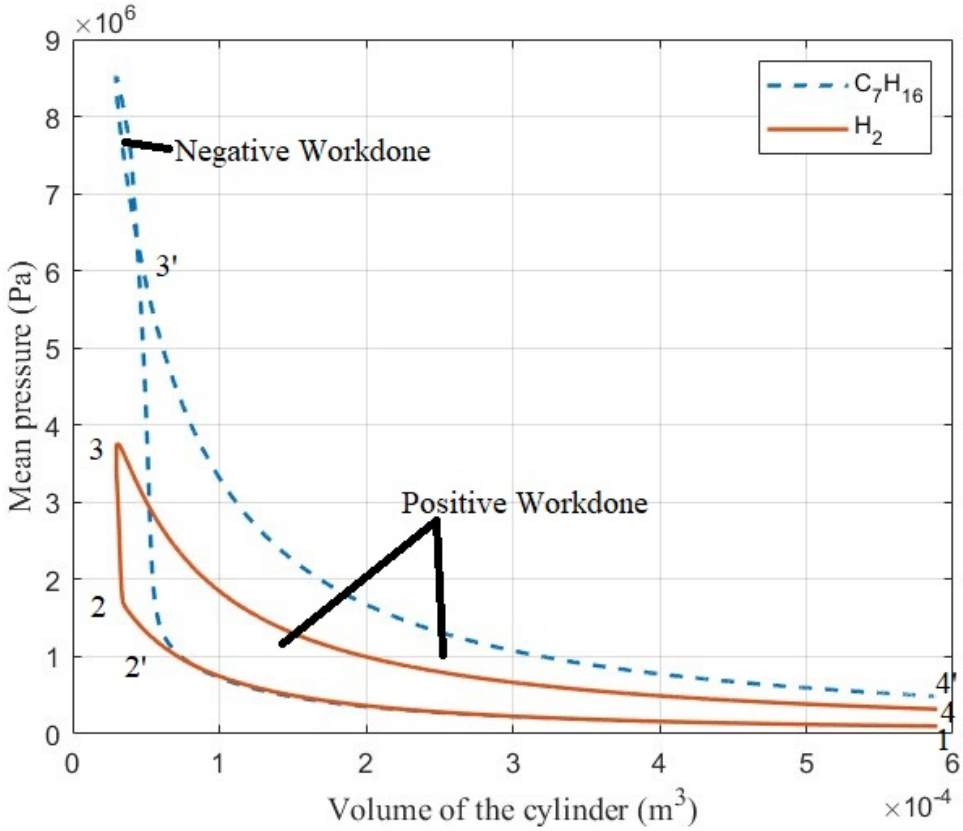

Figure 4.24: Comparing actual pressure volume diagram between two fuels

4.4.4 Comparison specific volume variation between hydrogen and heptane fuel

Figure 4.25 illustrates variation of specific volume with crank angle displacement in internal combustion engine between hydrogen and heptane fuel. At initial condition, due to H_2 lower molecular weight, the specific volume of H_2 gas is more as a result it occupies more space inside internal combustion engine. However, with the increase

in mean pressure and temperature because of both compression and heat addition, the specific volume of both fuels decreases when the piston moves from BDC to TDC reaching a minimum value at TDC. The dominance of mean pressure to temperature ratios is higher in case of heptane fuel in comparison to hydrogen fuel as a result the value of specific volume is lesser for heptane fuel during crank angle movement reaching minimum value of about 0.15 m^3/kg. However, the specific volume of both the gases fuel increases with the increase in crank movement after TDC as mean pressure and temperature both decreases during expansion stroke.

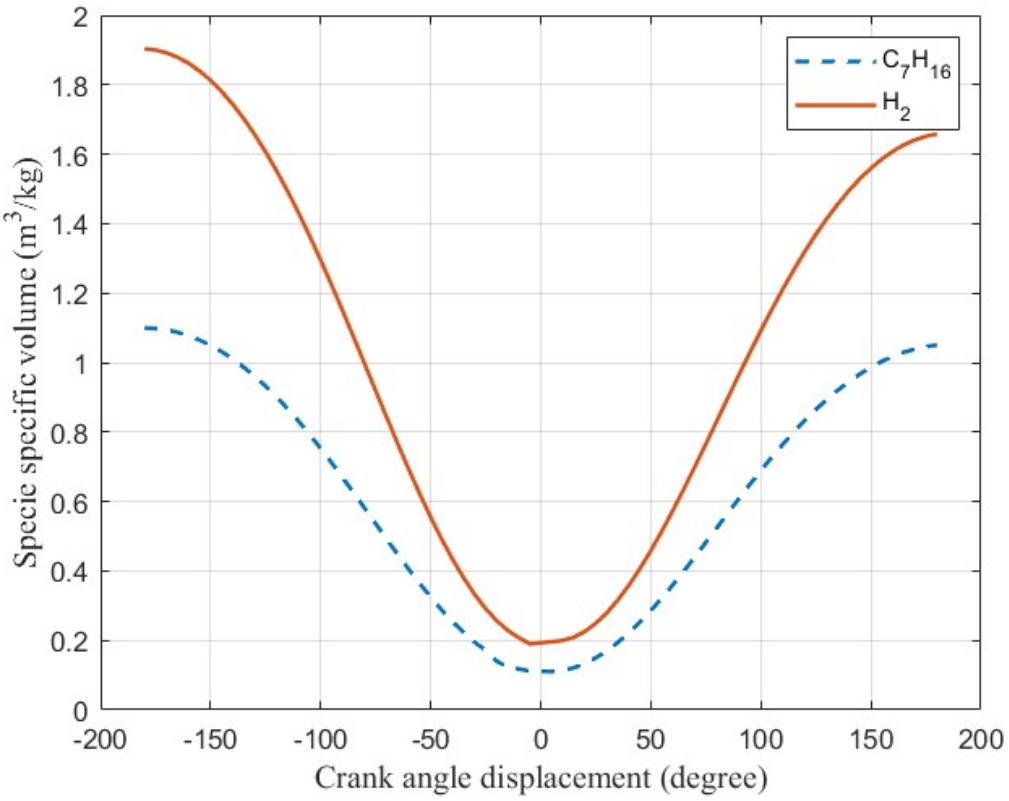

Figure 4.25: Variation of specific volume between two fuels

4.4.5 Comparison mixture density variation between hydrogen and heptane fuel

Figure 4.26 illustrates the variation of mixture density of two fuels H_2 & C_7H_{16} with crank angle movement between -180°CAD to 180°CAD. The mixture density of both the fuels increases with crank displacement from BDC to TDC because pressure increases during compression and heat addition stroke as mixture density has direct re-

lation with pressure to temperature ratios. Similarly, mixture density decreases during expansion stroke as pressure and temperature both decreases during expansion stroke due to work-done by the gases on the piston surface. Since pressure increases rapidly during heat addition process for heptane fuel, the mixture density increases rapidly too in comparison to hydrogen fuel. The supremacy of mean pressure to temperature ratios is significant in case of heptane fuel as a result density of the mixture has a higher value through out the crank angle displacement with a peak value around 9 kg/m^3.

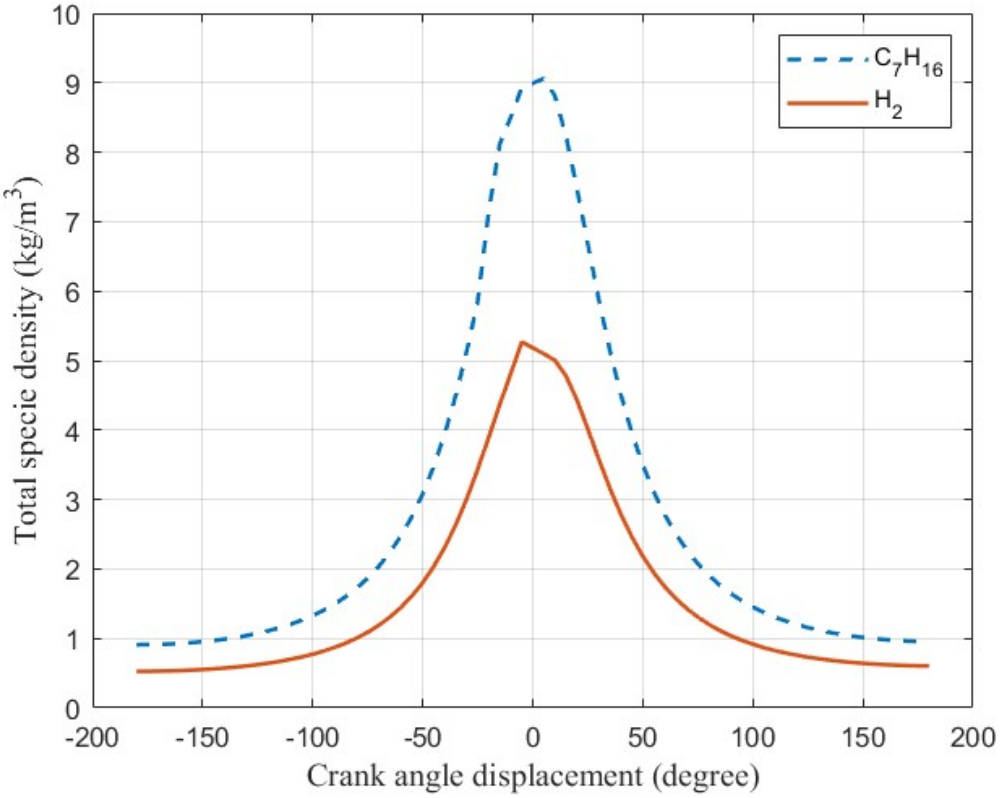

Figure 4.26: Variation of mixture density between two fuels

4.4.6 Comparison heat of reaction variation between hydrogen and heptane fuel

Figure 4.27 illustrates comparison of heat of reaction between hydrogen and heptane fuel mixture. Heat of reaction or heat of combustion generally refers to the heat released when reactants are burnt to form product. Here, the heat release rate per unit volume of heptane fuel is significantly high in comparison to the hydrogen fuel due

to complete combustion of heptane fuel mixture. From figure, the peak heat release rate per unit volume of heptane fuel is $2.75 * 10^{10} Watt/m^3$ whereas the peak heat release rate per unit volume of hydrogen fuel is $11.5 * 10^9 Watt/m^3$. This figure 4.27 also demonstrates the early ignition and rapid energy rate release for heptane fuel in comparison to hydrogen fuel because of simpler reaction mechanism consideration in case of heptane fuel which results in complete combustion.

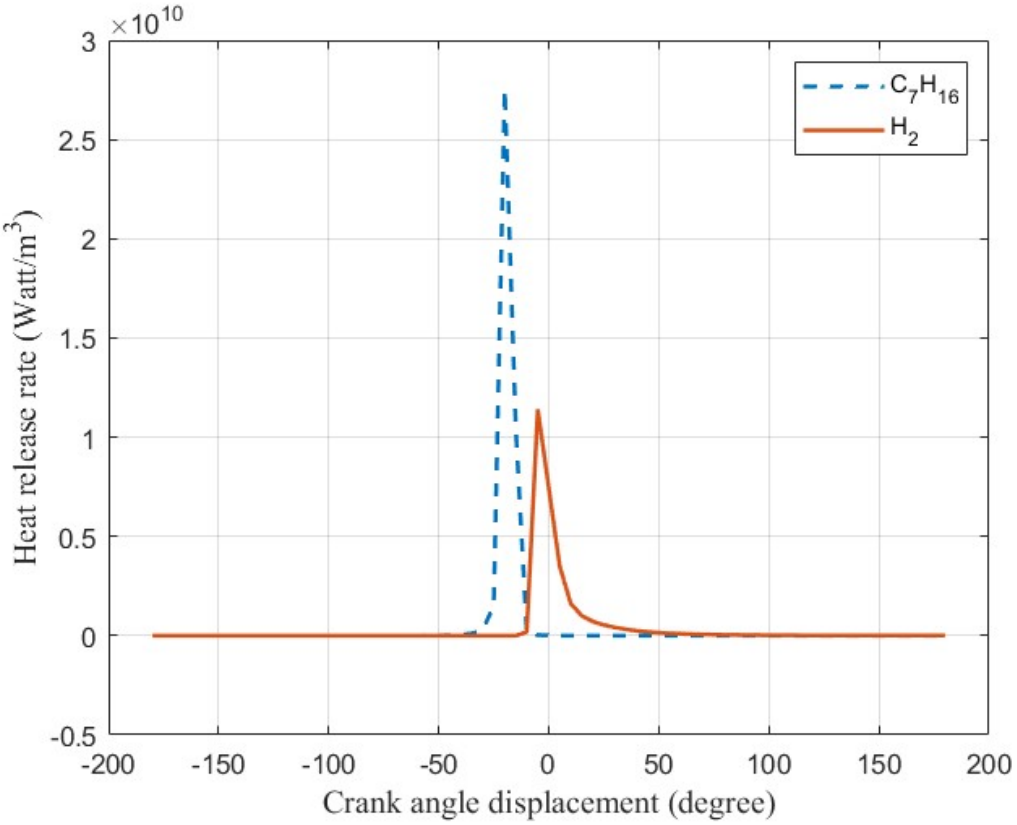

Figure 4.27: Variation of heat of reaction between two fuels

4.4.7 Comparison instantaneous power variation between hydrogen and heptane fuel

Figure 4.28 illustrates instantaneous power variation between hydrogen fuel and heptane fuel plotted against CAD. Initially, the power is consumed during compression stroke to compress the gaseous mixture in both the fuels. However, the power consumed by the heptane fuel is more during compression stroke, but also the power developed by the heptane fuel is significant in comparison to hydrogen fuel mixture. This is because of complete combustion of heptane fuel mixture as a result more in-

stantaneous power is obtained. Here also, when the piston is at near TDC, the peak power is achieved due to combustion of fuels in multiple points inside HCCI engine results in rapid increase in instantaneous power. The nature of the plot is similar in both the fuels; however, the area under the curve is more in case of heptane fuel which signifies burning characteristics of the heptane fuel because of consideration of simple one-step reaction mechanism.

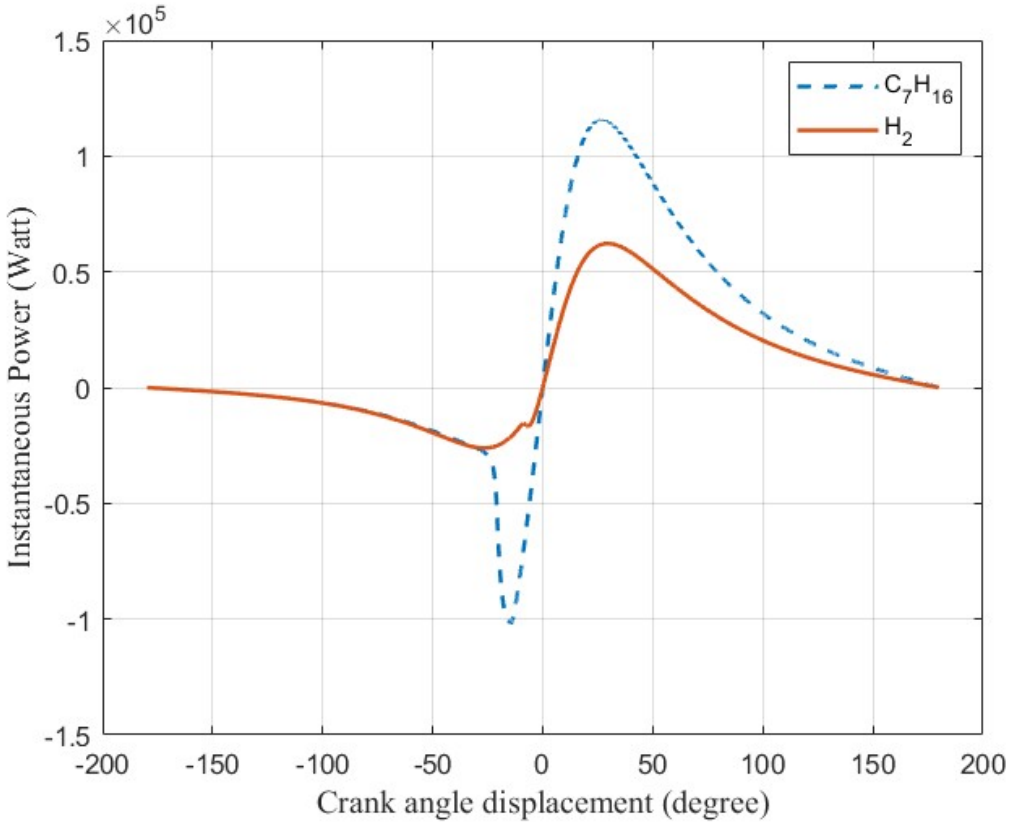

Figure 4.28: Comparison instantaneous power between two fuels

4.5 Variation of thermodynamic properties between hydrogen and heptane fuel at same mass flow rate

In this study, the mass flow rate of hydrogen and heptane fuel is kept same to observe variation in thermodynamic properties against CAD. The mass flow rate of both the fuels is considered as $1.0035 * 10^{-04} kg/s$ and the other parameters are kept unchanged.

4.5.1 Comparison mean pressure variation at same mass-flow rate

Figure 4.29 illustrates mean in-cylinder pressure variation between hydrogen and heptane fuel at same mass flow rate. Although, the peak mean in-cylinder pressure for heptane fuel is more in comparison to peak mean in-cylinder pressure for hydrogen fuel but comparable in range.The peak mean in-cylinder pressure of hydrogen fuel is 38 bar whereas the peak mean in-cylinder pressure of heptane fuel is 40 bar. For both the fuels, initially the pressure rises because of compression stroke. After the ignition, mean pressure increases tremendously because of ignition at multiple points in both the fuel mixture. Due to low auto-ignition temperature of heptane fuel, which shows early start of combustion phase.

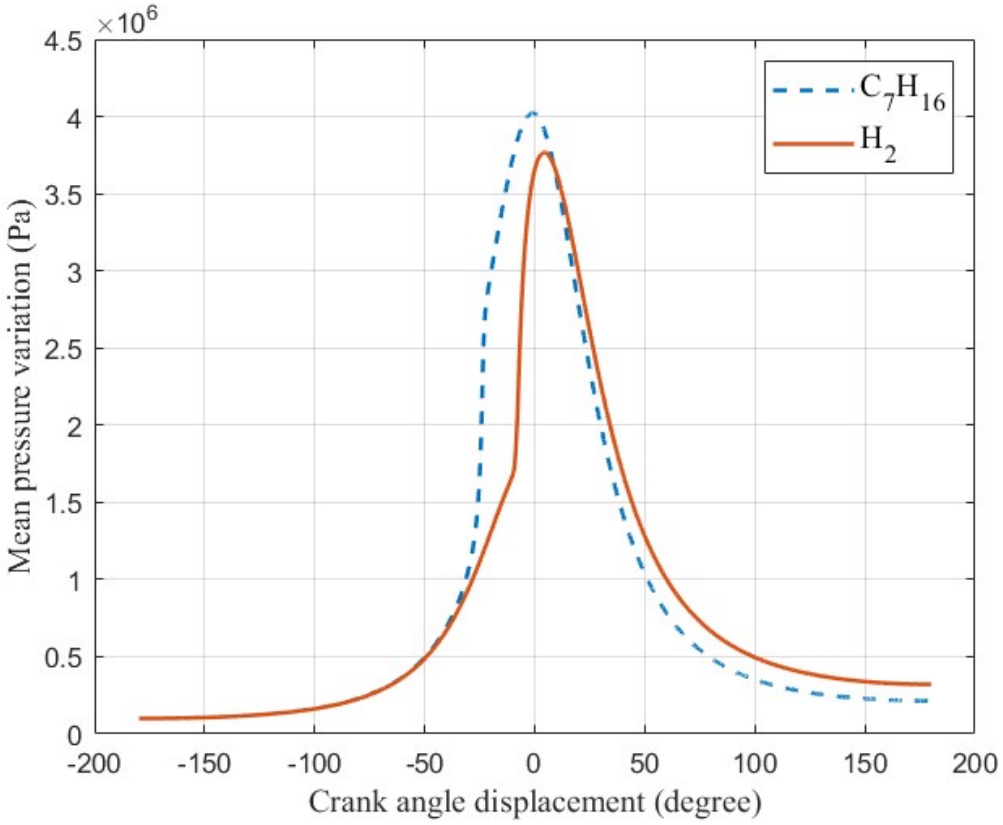

Figure 4.29: Variation of mean pressure between two fuels at same mass flow rate

4.5.2 Comparison mean temperature variation at same mass-flow rate

Figure 4.30 illustrates mean temperature variation between hydrogen and heptane fuel taken at same mass flow rate. The peak in-cylinder temperature of hydrogen fuel is near about 2500 K whereas the peak in-cylinder temperature of heptane fuel is at

about 1800 K when same mass flow rate of the fuels is considered. The lower peak mean in-cylinder temperature of heptane fuel is because of dilute concentration of fuel mixture in comparison to hydrogen fuel.

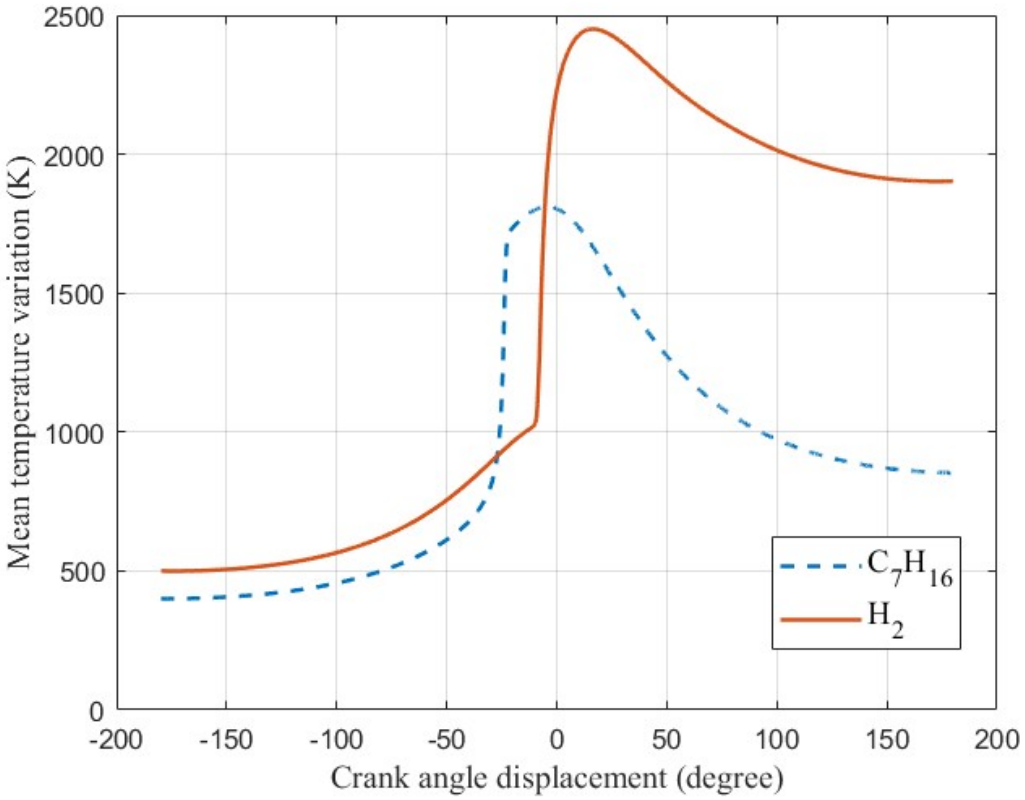

Figure 4.30: Variation of mean temperature between two fuels at same mass flow rate

4.5.3 Comparison PV diagram at same mass-flow rate

Figure 4.31 illustrates PV diagram between hydrogen and heptane fuel considering same mass-flow rate. Here, the negative work done due to early combustion of heptane fuel is also seen around the TDC which results in efficiency drop. The heat addition takes place at constant volume process under HCCI condition. The area covered under PV diagram is more in case of hydrogen fuel in comparison to heptane fuel which results more net work done per cycle at the same mass flow rate. For the same mass flow rate, because of net work done per cycle is higher in case of hydrogen fuel which also illustrated more indicated power output in comparison to heptane fuel.

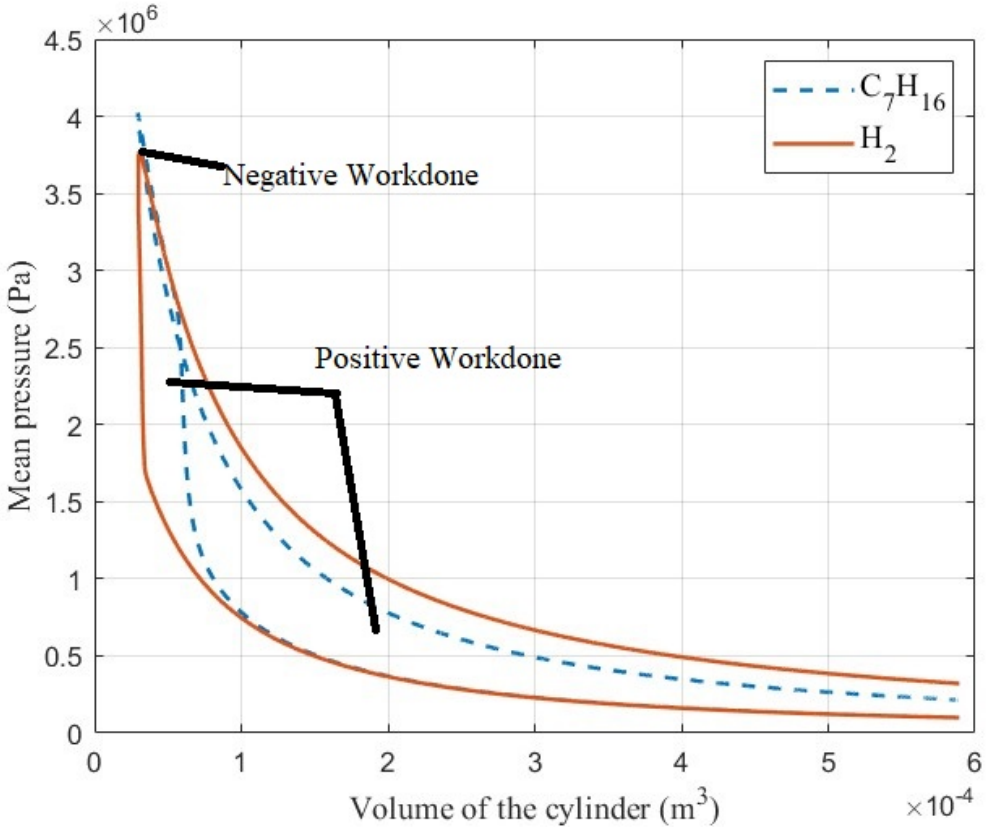

Figure 4.31: Comparison actual PV diagram between two fuels at same mass flow rate

4.5.4 Comparison heat of reaction at constant mass-flow rate

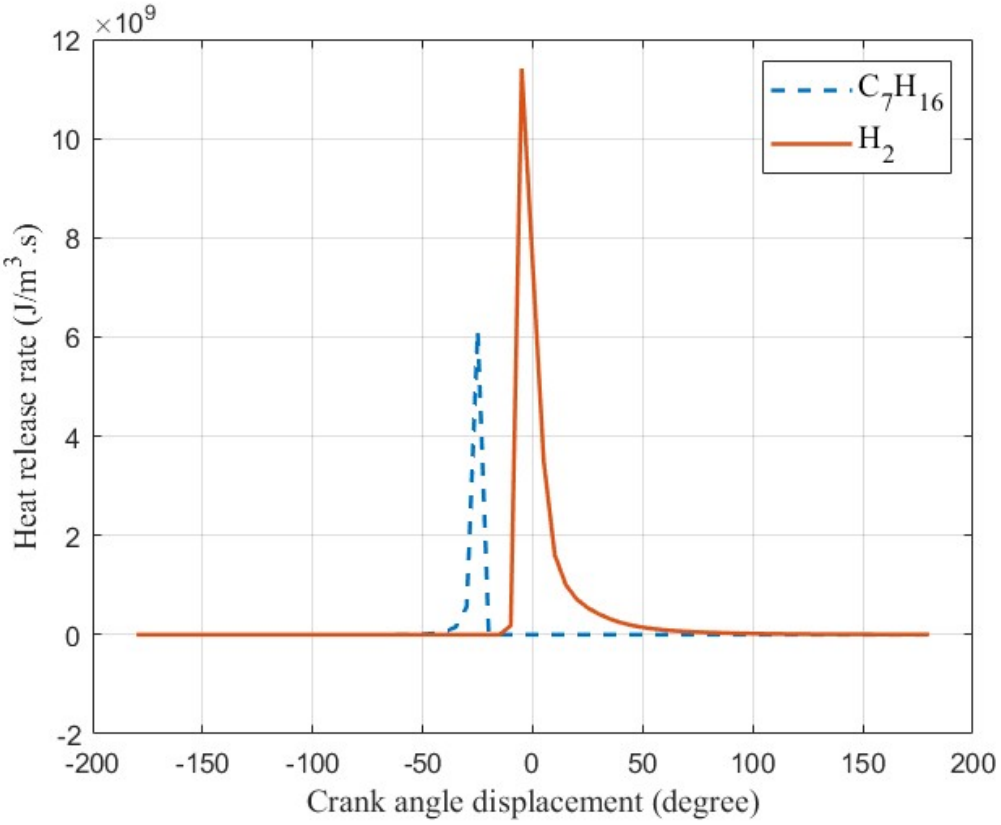

Figure 4.32: Variation of heat of reaction between two fuels at same mass flow rate

Figure 4.32 compares heat of reaction variation between two fuels hydrogen and heptane when same mass flow rate is considered. In this case,the heat release rate per unit volume for hydrogen fuel is $11.5 * 10^{09}\ Watt/m^3$ whereas the heat release rate per unit volume for heptane fuel is $6 * 10^{09}\ Watt/m^3$. Hydrogen fuel exhibits higher and shaper peaks near around TDC however, heptane fuel indicates lower heat release with early ignition.

4.6 Comparing testing parameters between hydrogen and heptane fuel at stoichiometric conditions

Table 4.1 compares performance parameters between hydrogen and heptane fuel in a HCCI engine under stoichiometric conditions. The heptane fuel shows higher indicated mean effective pressure, specific power output and thermal efficiency indicating better performance due to complete combustion of fuel mixture whereas hy-

drogen shows prominent effects with significantly lower specific fuel consumption due to higher calorific value per unit mass. Ali et. al conducted 3D CFD modeling of HCCI engine using fuel mixture H_2 & H_2O_2 and validated with syn gas fuel combustion experimental data. They observed combustion phasing, indicated mean effective pressure and thermal efficiency at varying equivalence ratios & engine speed and found thermal efficiency reaching a value of 45% with 20% volume fraction of H_2O_2 (Ali et al., 2023). Therefore, the simulation results obtained in case of hydrogen fuel in this research work is in good agreements with the prior study.

However, M.M. Hasan and his team conducted numerical study of engine parameters on combustion & performance characteristics in an n-heptane fueled HCCI engine using a zero-dimensional single zone model. A reduced n-heptane chemical reaction mechanism consisting 770 elementary reactions was considered to solve the chemical reaction during combustion. The simulation showed good results when comparing with the published experimental results. They analyzed the maximum load increased successfully with increasing the intake air pressure and found the maximum load value of 11.27 bar of IMEP at 200 KPa and 333 K intake air pressure and temperature respectively (Hasan et al., 2018). The discrepancies in the results for the heptane fuel is due to complete combustion because of single step reaction mechanism considered in this research study.

Table 4.1: Comparison of performance parameters for hydrogen and heptane fuel at stoichiometric conditions

S.No.	Parameter	Hydrogen	Heptane
1	Indicated mean effective pressure	7.16 bar	17.2 bar
2	Indicated power	5.012 kW	12 kW
3	Specific indicated output	8951 kW/m^3	21493 kW/m^3
4	Specific fuel consumption	0.07236 kg/kWh	0.1188 kg/kWh
5	Indicated thermal efficiency	42%	69%

4.7 Comparing testing parameters between hydrogen and heptane fuel at same mass flow rate

Table 4.2 compares performance parameters between hydrogen and heptane fuel combustion when consider at the same mass rate supply. At the same mass flow rate, hydrogen gas shows significant engine performances as compared to heptane fuel in terms of IMEP, indicated power, specific output and specific fuel consumption. This highlights hydrogen as a potential fuel especially when the supply of the fuel is limited which demonstrates better fuel efficiency by mass. However, heptane demonstrates a higher thermal efficiency which converts large fraction of chemical energy into useful work. Despite, hydrogen's high energy content, heptane is better during combustion control as well as good compatibility with engine design.

Table 4.2: Comparison of performance parameters for hydrogen and heptane fuel at same mass flow rate

S.No.	Parameter	Hydrogen	Heptane
1	Indicated mean effective pressure	7.16 bar	3.65 bar
2	Indicated power	5.012 kW	2.55 kW
3	Specific indicated output	8951 kW/m^3	4553.6 kW/m^3
4	Specific fuel consumption	0.07236 kg/kWh	0.14167 kg/kWh
5	Indicated thermal efficiency	42%	58%

CHAPTER FIVE: CONCLUSIONS AND RECOMMENDATIONS

5.1 Conclusions

The present computational study aims to provide an understanding of a compression-ignition premixed combustion of hydrogen fuel in an internal combustion engine to establish hydrogen gas as a potential fuel towards carbon neutrality. The premixed hydrogen fuel is auto-ignited during the end of compression stroke and the variation of thermodynamic properties with CAD is observed. Similarly, the comparison of thermodynamic properties between hydrogen and heptane fuel is observed keeping the initial conditions unchanged except the inlet temperature. In addition, the testing parameters of both the fuel is calculated based on computational work and compares against each other. The key observations and findings are presented below:

1. The mean in-cylinder pressure and temperature variation for premixed hydrogen fuel at stoichiometric condition is plotted against CAD. The peak mean in-cylinder pressure and temperature value of 37 bar and 2450 K respectively is obtained primarily because of reaction occurring between reacting species. Similarly, with the reaction progression, large amount of heat is released in the narrow range as the ignition starts at multiple points within the combustion chamber known as heat of reaction. Furthermore, the heat of reaction depends on how the reaction progresses which ultimately depends upon how quickly the mass-fraction of reactants convert into products. Similarly, intermediate species are formed and consumed during the reaction propagation. In turn, the heat of reaction affects temperature as higher temperature drives reaction step forward through acting on reaction rates and equilibrium composition. In addition, the actual PV diagram of premixed hydrogen fuel obtained close to the ideal cycle of HCCI engine because of higher laminar flame speed.

2. For varying ϕ_e, ranging between 0.7 to 1.3, the mean in-cylinder pressure and temperature variation is plotted. For ϕ_e is equal to 1.3, the peak mean pressure and temperature is maximum because at higher mass-fraction of H_2, the rate of reaction increases proportionally. Also, with increase in mass-fraction, the frequent collisions of the species increases due to decrease in mean free path. However, the heat of reaction decreases with increase in ϕ_e after ϕ_e equals to 1 because more

fuel is available resulting in incomplete combustion as most of the O_2 is utilized.

3. With increase in rpm, the ignition delay increases i.e. shift towards right because shorter residence time is available for the reacting species. However, the peak mean in-cylinder pressure and temperature increases at higher rpm because of faster combustion resulting in rapid energy release. Also, the exhaust temperature in the system increases because less time is available for heat transfer through the walls.

4. On comparison between heptane and hydrogen fuel, the peak mean pressure and temperature of heptane fuel is significantly high in comparison to hydrogen fuel because of one-step reaction mechanism consider as well as complete combustion in case of heptane fuel. In addition, single-step reaction mechanism oversimplifies the complex chemical and physical process involved and does not take into account radical formation and recombination. Furthermore, single step reaction does not include chain branching reactions step as a result ignition delay and flame propagation prediction become inaccurate. Similarly, the PV diagram in case of heptane fuel experience negative work done around TDC which results in efficiency drop due to early start of combustion causing the piston to bear increased cylinder pressure on the upward stroke towards TDC. Moreover, the heat of reaction of heptane fuel is higher in comparison to hydrogen fuel because of instantaneous combustion, intermediate species are absent. Also inaccurate modeling of flame propagation, ignition delay and pollutant formation due to single reaction mechanism of heptane fuel, it over predicts heat release rate.

5. On comparing the testing parameters between hydrogen and heptane fuel at stoichiometric mixture such as indicated mean effective pressure, indicated power, specific indicated output, specific fuel consumption and indicated thermal efficiency, heptane fuel has higher values than hydrogen fuel because of peak mean in-cylinder pressure resulting due to oversimplifies reaction mechanism consideration in case of heptane fuel. Similarly, the testing parameters between hydrogen and heptane fuel are tested at the same mass flow rate (considering hydrogen mass flow rate), the testing parameters show good result with hydrogen fuel except indicated thermal efficiency because of highly dilute fuel concentrations for heptane

fuel. Although, the indicated power of hydrogen fuel is higher than heptane fuel at the same mass flow rate, the indicated thermal efficiency of heptane fuel is higher because of lower LHV of heptane fuel which converts large fraction of chemical energy into useful work. For the same power output, hydrogen fuel can be a better option than heptane fuel which can lead to fuel economy and long driving range.

5.2 Recommendations

Although, this study provides valuable insights of the combustion characteristics of premixed hydrogen fuel in HCCI engine, there are few recommendations drawn based on the literature review and the experience gained by the author while performing simulation of premixed hydrogen fuel in an internal combustion engine. Some of the recommendation are listed below:

1. This study uses a single step reaction mechanism for heptane fuel which limits the complex chemical and physical process involved during combustion. This reaction mechanism does not consider radical formation and recombination. As a result, future work should incorporate detailed reaction mechanism of heptane fuel such as capture complex chemical phenomena including formation and consumption of intermediate species.
2. Since, this study make use of premixed hydrogen fuel in internal combustion engine, future work should incorporate hydrogen direct injection strategies including spray development, radial penetration, sensitivity to turbulence and choked flow condition. For this study, implementation of a cloud properties setup for gaseous hydrogen injection in OpenFOAM to provide realistic insights into non-premixed combustion.
3. For validating simulation results, experimental study is crucial. Future work should investigate experimental study on comparison of mean pressure, temperature, heat release and emissions on hydrogen fueled internal engine.
4. This study treats hydrogen and heptane as standalone fuels. To evaluate efficiency gain and emission reductions, future work should investigate exploring dual fuel combustion concepts.

REFERENCES

Heywood, J. (2018). Internal combustion engine fundamentals.

Khaliq, A., Trivedi, S. K., & Dincer, I. (2011). Investigation of a wet ethanol operated hcci engine based on first and second law analyses. *Applied thermal engineering*, *31*(10), 1621–1629.

Armaroli, N., & Balzani, V. (2011). The hydrogen issue. *ChemSusChem*, *4*(1), 21–36.

Algayyim, S. J. M., Saleh, K., Wandel, A. P., Fattah, I. M. R., Yusaf, T., & Alrazen, H. A. (2024). Influence of natural gas and hydrogen properties on internal combustion engine performance, combustion, and emissions: A review. *Fuel*, *362*, 130844. https://doi.org/https://doi.org/10.1016/j.fuel.2023.130844

Fayaz, H., Saidur, R., Razali, N., Anuar, F. S., Saleman, A., & Islam, M. (2012). An overview of hydrogen as a vehicle fuel. *Renewable and Sustainable Energy Reviews*, *16*(8), 5511–5528.

Durbin, D. J., & Malardier-Jugroot, C. (2013). Review of hydrogen storage techniques for on board vehicle applications. *International journal of hydrogen energy*, *38*(34), 14595–14617.

Kumar, N., Lee, S.-Y., & Park, S.-J. (2024). Advancements in hydrogen storage technologies: A comprehensive review of materials, methods, and economic policy. *Nano Today*, *56*, 102302.

Alnaeli, M., Alnajideen, M., Navaratne, R., Shi, H., Czyzewski, P., Wang, P., Eckart, S., Alsaegh, A., Alnasif, A., Mashruk, S., Et al. (2023). High-temperature materials for complex components in ammonia/hydrogen gas turbines: A critical review. *Energies*, *16*(19), 6973.

Li, W., Cao, R., Xu, L., & Qiao, L. (2021). The role of hydrogen in the corrosion and cracking of steels-a review. *Corrosion Communications*, *4*, 23–32.

Baykara, S. Z. (2018). Hydrogen: A brief overview on its sources, production and environmental impact. *International Journal of Hydrogen Energy*, *43*(23), 10605–10614.

Boretti, A., & Banik, B. K. (2021). Advances in hydrogen production from natural gas reforming. *Advanced Energy and Sustainability Research*, *2*(11), 2100097.

Freni, S., Calogero, G., & Cavallaro, S. (2000). Hydrogen production from methane through catalytic partial oxidation reactions. *Journal of Power Sources*, *87*(1-2), 28–38.

Oni, A., Anaya, K., Giwa, T., Di Lullo, G., & Kumar, A. (2022). Comparative assessment of blue hydrogen from steam methane reforming, autothermal reforming, and natural gas decomposition technologies for natural gas-producing regions. *Energy Conversion and Management*, *254*, 115245.

Sebbahi, S., Assila, A., Belghiti, A. A., Laasri, S., Kaya, S., Rachidi, S., Hajjaji, A., Et al. (2024). A comprehensive review of recent advances in alkaline water electrolysis for hydrogen production. *International Journal of Hydrogen Energy*, *82*, 583–599.

Rațiu, S. (2003). The history of the internal combustion engine. *Ann. Fac. Eng. Hunedoara*, *1*, 145–148.

Fairbanks, J. W. (2004). Engine maturity, efficiency, and potential improvements, In *Diesel engine emission reduction conference (coronado, california, 2004)*.

Schöffel, K. (2005). Hydrogen-the energy carrier for the future, In *Workshop-environmental issues in theory and practice (porsgrunn, norway, 2005)*.

Erren, R. (1939). Der erren-wasserstoffmotor. *Automobiltechnische Zeitschrift ATZ*, *41*, 523–524.

Plotnikov, L., & Ulman, N. (2021). Computational and analytical evaluation of the efficiency of using hydrogen as a fuel in an internal combustion engine, In *Iop conference series: Earth and environmental science*. IOP Publishing.

Das, L. (2016). Hydrogen-fueled internal combustion engines, In *Compendium of hydrogen energy*. Elsevier.

Furuhama, S. (1997). Problems of forecasting the future of advanced engines and engine characteristics of the hydrogen injection with lh {sub 2} tank and pump. *Journal of engineering for gas turbines and power*, *119*(1).

Furuhama, S., & Kobayashi, Y. (1982). A liquid hydrogen car with a two-stroke direct injection engine and lh2-pump. *International Journal of Hydrogen Energy*, *7*(10), 809–820.

Furuhama, S., Fukuma, T., & Sakai, H. (1986). Conversion of turbo-diesel passenger car into hydrogen powered car, In *Hydrogen systems*. Elsevier.

Yao, M., Zheng, Z., & Liu, H. (2009). Progress and recent trends in homogeneous charge compression ignition (hcci) engines. *Progress in energy and combustion science*, *35*(5), 398–437.

Norbeck, J., Durbin, T., Heffel, J., & Montano, M. (1996). *Hydrogen fuel for surface transportation*. SAE International.

Tsujimura, T., Mikami, S., Achiha, N., Tokunaga, Y., Senda, J., & Fujimoto, H. (2003). A study of direct injection diesel engine fueled with hydrogen. *SAE transactions*, 390–405.

Naber, J. D., & Siebers, D. L. (1998). Hydrogen combustion under diesel engine conditions. *International journal of hydrogen energy*, *23*(5), 363–371.

Stenlåås, O., Christensen, M., Egnell, R., Johansson, B., & Mauss, F. (2004). Hydrogen as homogeneous charge compression ignition engine fuel. *SAE transactions*, 1317–1326.

Caton, P., & Pruitt, J. (2009). Homogeneous charge compression ignition of hydrogen in a single-cylinder diesel engine. *International Journal of Engine Research*, *10*(1), 45–63.

Antunes, J. G., Mikalsen, R., & Roskilly, A. (2008). An investigation of hydrogen-fuelled hcci engine performance and operation. *International journal of hydrogen energy*, *33*(20), 5823–5828.

Guo, H., & Neill, W. S. (2013). The effect of hydrogen addition on combustion and emission characteristics of an n-heptane fuelled hcci engine. *International journal of hydrogen energy*, *38*(26), 11429–11437.

Pochet, M., Truedsson, I., Foucher, F., Jeanmart, H., & Contino, F. (2017). *Ammonia-hydrogen blends in homogeneous-charge compression-ignition engine* (tech. rep.). SAE Technical Paper.

Wang, Q., Zhao, Y., Wu, F., & Bai, J. (2019). Study on the combustion characteristics and ignition limits of the methane homogeneous charge compression ignition with hydrogen addition in micro-power devices. *Fuel*, *236*, 354–364.

Shi, Y., Liu, Y., Jia, X., Pei, P., Lu, Y., & Yi, L. (2014). Simulation on the combustion system work process for internal combustion engine by using kiva-3v, In *Moving integrated product development to service clouds in the global economy*. IOS Press.

Kannan, B., & Srivathsan, P. (2016). Numerical simulation of spark ignition engine using openfoam®. *Perspectives in Science*, *8*, 13–15.

Babayev, R., Andersson, A., Dalmau, A. S., Im, H. G., & Johansson, B. (2021). Computational characterization of hydrogen direct injection and nonpremixed combustion in a compression-ignition engine. *International Journal of Hydrogen Energy*, *46*(35), 18678–18696.

Boivin, P. Et al. (2011). Reduced-kinetic mechanisms for hydrogen and syngas combustion including autoignition. *PHD, Universidad Carlos III de Madrid*.

Kolambe, K., & Borse, S. (2016). Engine combustion simulation using openfoam. *International Engi–neering Research Journal (IERJ) Special*, (2016), 885–891.

Zoldak, P. S. (2005). Design of a research engine for homogeneous charge compression ignition (hcci) combustion.

Albayrak, B. (2012). Use of hydrogen-methane blends in internal combustion engines. *Hydrogen Energy—Challenges and Perspectives; InTech: London, UK*.

Fathi, M., Saray, R. K., & Checkel, M. D. (2010). Detailed approach for apparent heat release analysis in hcci engines. *Fuel*, *89*(9), 2323–2330.

Tóth-Nagy, C. (2024). Study of the negative work area in the pv diagram of an hcci engine. *Engineering Proceedings*, *79*(1), 22.

Ali, K., Amna, R., & Ali, M. I. H. (2023). Hcci engine performance using fuel mixture of h2 and h2o2. *Energy Conversion and Management*, *276*, 116588.

Hasan, M., Rahman, M., Kadirgama, K., & Ramasamy, D. (2018). Numerical study of engine parameters on combustion and performance characteristics in an n-heptane fueled hcci engine. *Applied Thermal Engineering*, *128*, 1464–1475.

APPENDICES

Appendix A: Different Testing Parameters and It's Calculations

Indicated mean effective pressure

$$P_{imp} = \frac{W_{net}}{V_s}$$

And,

$$W_{net} = \frac{P_1 V_1}{\gamma - 1}[(r^{\gamma-1} - 1)(r_p - 1)]$$

Similarly,

$$V_s = \frac{\pi}{4} * D^2 * L_s$$

Indicated power

$$IP = \frac{nP_{imp}LA_rNK * 10}{6}\ kW$$

Specific indicated output

$$SIO = \frac{IP}{V_s}$$

Specific fuel consumption

$$SFC = \frac{\dot{m}_f}{IP}$$

Indicated thermal efficiency

$$\eta_{th} = \frac{IP}{\dot{m}_f \times \text{LHV}}$$

Testing parameters for hydrogen fuel at stoichiometric ratio

$$P_{imp} = \frac{W_{net}}{V_s}$$

From PV diagram,

$$W_{net} = 401 \text{ Joule}$$

And,

$$V_s = 0.00056 \text{ m}^3$$

Now,

$$P_{imp} = 7.16 \text{ bar}$$

which gives,

$$IP = 5.012 \text{ kW}$$

$$SIO = 8951 \text{ kW/m}^3$$

Again,

$$\dot{m}_{mix} = \frac{\rho \times V_s \times N}{120} \text{ kg/s}$$

$$\rho = \frac{P}{R_{mix} T} \text{ kg/m}^3$$

$$\rho = 0.5050 \text{ kg/m}^3$$

On calculation,

$$\dot{m_{mix}} = 3.521 * 10^{-3} \text{ kg/s}$$

Now,

$$\dot{m}_{H_2} = Y_{H_2} \times \dot{m}_{mix} \quad \text{kg/s}$$

i.e.

$$\dot{m_{H_2}} = 1.0035 * 10^{-4} \text{ kg/s}$$

And,

$$SFC = 0.0721 \text{ kg/kWh}$$

$$\eta_{th} = \frac{5.012 * 1000}{1.0074 * 10^{-4} * 120 * 10^6}$$

$$\eta_{th} = 41.62\%$$

Testing parameters for heptane fuel at stoichiometric ratio

$$P_{imp} = \frac{W_{net}}{V_s}$$

From PV diagram,

$$W_{net} = 963 \text{ Joule}$$

And,

$$V_s = 0.00056 \text{ m}^3$$

Now,

$$P_{imp} = 17.2 \text{ bar}$$

which gives,

$$IP = 12 \text{ kW}$$

$$SIO = 21493 \text{ kW/m}^3$$

Again,

$$\dot{m}_{mix} = \frac{\rho \times V_s \times N}{120} \text{ kg/s}$$

$$\rho = \frac{P}{R_{mix} T} \text{ kg/m}^3$$

$$\rho = 0.91 \text{ kg/m}^3$$

And,

$$\dot{m_{mix}} = 6.37 * 10^{-3} \text{ kg/s}$$

$$\dot{m}_{C_7H_{16}} = Y_{C_7H_{16}} \times \dot{m}_{mix} \quad \text{kg/s}$$

i.e.

$$\dot{m_{C_7H_{16}}} = 3.96 * 10^{-4} \text{ kg/s}$$

Now,

$$SFC = 0.1188 \text{ kg/kWh}$$

And,

$$\eta_{th} = \frac{12 * 1000}{3.96 * 10^{-4} * 44 * 10^6}$$

$$\eta_{th} = 69\%$$

Testing parameters for heptane fuel at same mass flow rate i.e equal to mass flow of hydrogen gas

$$P_{imp} = \frac{W_{net}}{V_s}$$

which gives,

$$W_{net} = 204 \text{ Joule}$$

And,

$$V_s = 0.00056 \text{ m}^3$$

Now,

$$P_{imp} = 3.65 \text{ bar}$$

which gives,

$$IP = 2.55 \text{ kW}$$

And,

$$SIO = 4553.6 \text{ kW/m}^3$$

Again,

$$SFC = 0.14167 \text{ kg/kWh}$$

Finally,

$$\eta_{th} = \frac{2.55 * 1000}{1.0035 * 10^{-4} * 44 * 10^6}$$

$$\eta_{th} = 58\%$$

Appendix B: Miscellaneous Formula

Volume of the cylinder (V) is calculated as:

$$V_\theta = V_c + A * [l + a - S_\theta]$$

$$S_\theta = a\cos(\theta) + \sqrt{l^2 - a^2 \sin^2\theta}$$

Molecular weight (MW_{mix}) of the mixture is calculated as:

$$MW_{mix} = \frac{1}{\sum_{s=1}^{N} \frac{Y_s}{MW_s}}$$

Density (ρ_{mix}) of the mixture is calculated as:

$$\rho_{mix} = \frac{P}{\frac{R_u}{MW_{mix}} * T}$$

Appendix C: Letter of Paper Acceptance at IOEGC

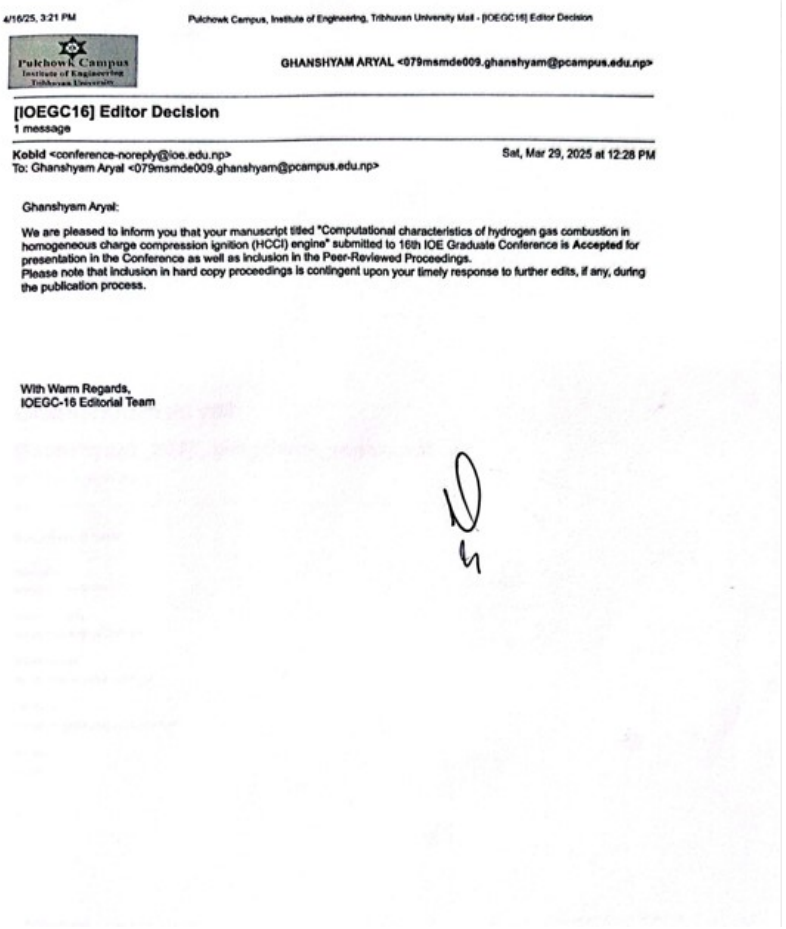

4/16/25, 3:21 PM Pulchowk Campus, Institute of Engineering, Tribhuvan University Mail - [IOEGC16] Editor Decision

Pulchowk Campus
Institute of Engineering
Tribhuvan University

GHANSHYAM ARYAL <079msmde009.ghanshyam@pcampus.edu.np>

[IOEGC16] Editor Decision
1 message

Kobid <conference-noreply@ioe.edu.np> Sat, Mar 29, 2025 at 12:28 PM
To: Ghanshyam Aryal <079msmde009.ghanshyam@pcampus.edu.np>

Ghanshyam Aryal:

We are pleased to inform you that your manuscript titled "Computational characteristics of hydrogen gas combustion in homogeneous charge compression ignition (HCCI) engine" submitted to 16th IOE Graduate Conference is **Accepted** for presentation in the Conference as well as inclusion in the Peer-Reviewed Proceedings.
Please note that inclusion in hard copy proceedings is contingent upon your timely response to further edits, if any, during the publication process.

With Warm Regards,
IOEGC-16 Editorial Team

Appendix D: Similarity Report

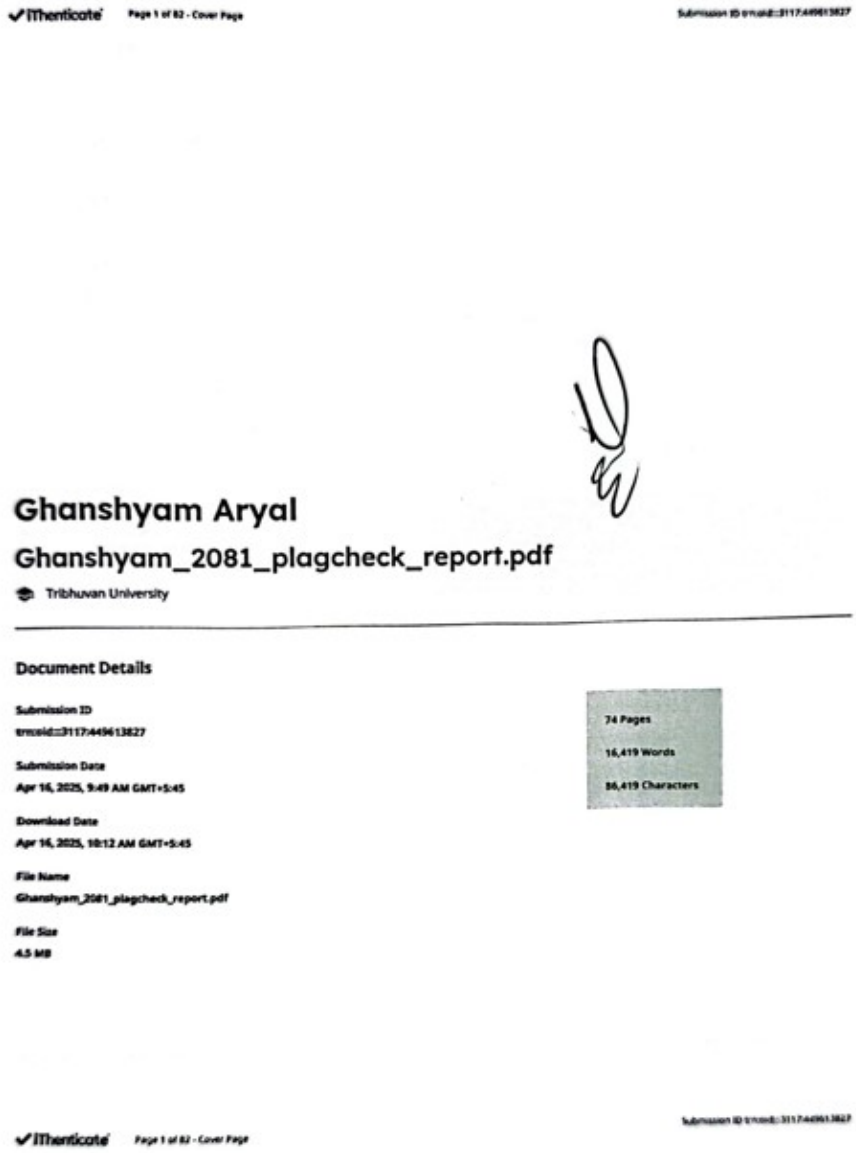

iThenticate Page 1 of 82 - Cover Page

Submission ID trn:oid:::3117:449613827

Ghanshyam Aryal

Ghanshyam_2081_plagcheck_report.pdf

Tribhuvan University

Document Details

Submission ID
trn:oid:::3117:449613827

Submission Date
Apr 16, 2025, 9:49 AM GMT+5:45

Download Date
Apr 16, 2025, 10:12 AM GMT+5:45

File Name
Ghanshyam_2081_plagcheck_report.pdf

File Size
4.5 MB

74 Pages

16,419 Words

86,419 Characters

iThenticate Page 1 of 82 - Cover Page

Submission ID trn:oid:::3117:449613827

15% Overall Similarity

The combined total of all matches, including overlapping sources, for each database.

Filtered from the Report

- Bibliography
- Quoted Text
- Cited Text
- Small Matches (less than 8 words)

Exclusions

- 3 Excluded Matches

Match Groups

- 186 Not Cited or Quoted 15%
  Matches with neither in-text citation nor quotation marks
- 0 Missing Quotations 0%
  Matches that are still very similar to source material
- 0 Missing Citation 0%
  Matches that have quotation marks, but no in-text citation
- 0 Cited and Quoted 0%
  Matches with in-text citation present, but no quotation marks

Top Sources

12% Internet sources
10% Publications
0% Submitted works (Student Papers)

Integrity Flags

1 Integrity Flag for Review

- Replaced Characters
  75 suspect characters on 16 pages
  Letters are swapped with similar characters from another alphabet.

Our system's algorithms look deeply at a document for any inconsistencies that would set it apart from a normal submission. If we notice something strange, we flag it for you to review.

A Flag is not necessarily an indicator of a problem. However, we'd recommend you focus your attention there for further review.

Match Groups

- 186 Not Cited or Quoted 15%
  Matches with neither in-text citation nor quotation marks
- 0 Missing Quotations 0%
  Matches that are still very similar to source material
- 0 Missing Citation 0%
  Matches that have quotation marks, but no in-text citation
- 0 Cited and Quoted 0%
  Matches with in-text citation present, but no quotation marks

Top Sources

12% Internet sources
10% Publications
0% Submitted works (Student Papers)

Top Sources

The sources with the highest number of matches within the submission. Overlapping sources will not be displayed.

1	Internet	
dokumen.pub		1%
2	Internet	
research.usq.edu.au		1%
3	Publication	
Sattar Jabbar Murad Algayyim, Khalid Saleh, Andrew P. Wandel, Islam Md Rizwan...		1%
4	Internet	
moam.info		<1%
5	Internet	
archive.org		<1%
6	Internet	
ae-plus.com		<1%
7	Internet	
ebin.pub		<1%
8	Internet	
www.mdpi.com		<1%
9	Publication	
Hongsheng Guo, W. Stuart Neill. "The effect of hydrogen addition on combustion ...		<1%
10	Internet	
www.mikalsen.eu		<1%

iThenticate Page 3 of 82 - Integrity Overview Submission ID trn:oid:::3117:449613827